THESE

Présentée à

L'Université des Sciences et Technologies de Lille

Pour obtenir le titre de
DOCTEUR EN CHIMIE
Spécialité: Sciences de la Matière, du Rayonnement et de l'Environnement

par

Fangli JING

Catalyseurs innovants à base de polyoxométalate de type Keggin pour l'oxydation sélective de l'isobutane en acide méthacrylique

Soutenance le 21 septembre 2012 devant la commission d'examen :

Président du Jury
M. Franck Dumeignil, Professeur, Université Lille1 (France)
Rapporteurs
M. Fabrizio Cavani, Professeur associé, Université de Bologne (Italie)
M. Emmanuel Cadot, Professeur, Université de Versailles Saint-Quentin (France)
Examinateur
M. Jean-Marc Millet, Directeur de recherche CNRS, Institut de Recherche sur la Catalyse et l'Environnement de Lyon (France)
Directeur
Mme. Elisabeth Bordes-Richard, Professeur, Ecole Nationale Supérieure de Chimie de Lille (France)
Co-directeur
M. Sébastien Paul, Professeur, Ecole Centrale de Lille (France)

THESIS

Université des Sciences et Technologies de Lille

For obtaining a title of
DOCTOR IN CHEMISTRY
Spécialité: Sciences de la Matière, du Rayonnement et de l'Environnement

by

Fangli JING

Innovative Keggin-type polyoxometalate-based catalysts for the selective oxidation of isobutane into methacrylic acid

---

Defended on the 21st of September 2012

President of Jury
Mr. Franck Dumeignil, Professor, Université Lille 1 (France)
Reviewers
Mr. Fabrizio Cavani, Associate Professor, Université de Bologna (Italy)
Mr. Emmanuel Cadot, Professor, Université de Versailles Saint-Quentin (France)
Examiner
Mr. Jean-Marc Millet, CNRS Research Director, Institut de Recherche sur la Catalyse et l'Environnement de Lyon (France)
Director
Mme. Elisabeth Bordes-Richard, Professor, Ecole Nationale Supérieure de Chimie de Lille (France)
Co-director
Mr. Sébastien Paul, Professor, Ecole Centrale de Lille (France)

Acknowledgement

Firstly, I want to thank Mrs. Elisabeth Bordes-Richard and Mr. Sébastien Paul for their kind guidance, offering the challenging subject and enthusiastic help whatever on the research work or daily life. More importantly, I am deeply affected by their scientific method and attitude.

I also would like to thank Mr. Benjamin Katryniok for the help, valuable discussion and advice. The other members of VALBIO group especially Mr. Franck Dumeignil and Mr. Mickaël Capron are acknowledged for their useful advices.

Many thanks to *Unité de Catalyse et Chimie du Solide* (UCCS, UMR 8181) of *Université des Sciences Technologies de Lille* (USTL) and *Ecole Centale de Lille* (ECLille) for affording a good scientific environment and experimental platform. It is impossible to complete the work without the help of the whole team. I wish to thank all the technicians for their contribution, especially Mr. Olivier Gardoll, Mr. Arnaud Beaurain and Mr. Gérard Cambien.

I am grateful to *Chinese Scholarship Council* (CSC) for the financial support during my stay in France, as well as Mr. Xiaotao Zhang, Ms. Yaping Qiang and the other staffs from *Education Service of Embassy of China* for the kind attention.

Moreover, thanks to Mr. Fabrizio Cavani and Mr. Emmanuel Cadot for accepting the role of referees for my thesis, and Mr. Jean-Marc Millet for accepting the role of examiner.

Thanks to the colleagues and friends of UCCS for a memorable experience: Jorge Miguel Beiramar, Amit Sharma, P. R. Naren, Jingping Hong, Wenhao Fang, Yihao Wu, Jingjuan Wang, Yong Miao, Lei Zhang and Xinyu Lu. Finally I express my special thanks to my family including my parents, my young brother Fangwei Jing and my wife Yuanyuan Zhang for their enduring support throughout the graduate school.

Content

Abstract

A novel catalytic route for the production of methacrolein (MAC) and methacrylic acid (MAA) starting from isobutane (IBAN) was studied. Keggin-type heteropolycompounds proved to be good candidates to catalyse the reaction because of their tuneable acid and redox properties. However the low surface and low thermal stability of the bulk heteropolycompounds limit their application. Therefore, different silica-based materials presenting high surface areas were chosen to play the role of supports for the active phase $(NH_4)_3HPMo_{11}VO_{40}$ (APMV). The caesium salt $Cs_3PMo_{12}O_{40}$ (CPM) was selected as support as well. The nature of the support significantly influenced the catalytic properties. Thermal decomposition of the active phase always took place under the reaction conditions but to a different extent depending on the nature of the support used. The CPM support led to a limited deactivation compared to silica-supported catalysts. It was shown that a well-balanced combination of appropriate textural and acidic properties, which are well represented by the notion of surface acid site density, is necessary to get an active catalyst. The optimization of this characteristic was further studied on CPM-supported catalysts. The deactivation was limited but still occurred on the long term. Ammonium cations decomposition and caesium cations mobility from the bulk to the surface proved to play an important role in the deactivation process under stream. At higher temperature simple unselective oxides are formed and also play a role on the activity and selectivity decrease. The method of preparation of the catalyst can strongly influence on the textural, acid and redox properties and therefore on the catalytic performances. An active catalyst must present a multilayer stack of acid active phase dispersed on the CPM support to present a minimal surface area of 15-20 m^2/g and limit the diffusion of caesium cations to the surface. Moreover it must present also good redox properties to orientate the evolution of the intermediates formed toward methacrolein and methacrylic acid. The vanadium atom substituted in the primary structure of the Keggin anion plays an important role in this step. The best catalytic performances were obtained at 340 ^{o}C with a contact time of 7.2 s using the 40APMV/CPM sample. An isobutane conversion of 20.2% and a yield of 8.6% into MAA+MAC were achieved.

Résumé

Une nouvelle voie de synthèse de méthacroléine (MAC) et d'acide méthacrylique (MAA) à partir d'isobutane a été étudiée. Les hétéropolycomposés de type Keggin sont de bons candidats pour catalyser cette réaction en raison de leurs propriétés acido-basiques et redox ajustables. Cependant leur faible aire spécifique et leur mauvaise stabilité thermique empêchent leur utilisation en l'état. Ainsi, différentes silices présentant des aires spécifiques élevées ainsi que le sel $Cs_3PMo_{12}O_{40}$ (CPM) ont été testés en tant que support de la phase active $(NH_4)_3HPMo_{11}VO_{40}$ (APMV). La nature du support influence fortement les propriétés catalytiques. Une décomposition thermique de la phase active existe toujours mais son ampleur est fortement dépendante de la nature du support. Ainsi le support CPM permet de limiter cette désactivation en comparaison des silices. Il a été montré qu'une combinaison équilibrée des propriétés acido-basiques et texturale, bien représentées par la notion de densité de sites acides en surface, est nécessaire pour l'obtention d'un catalyseur actif. L'optimisation de ce critère a été étudiée sur les catalyseurs supportés sur CPM. La désactivation a été limitée mais est toujours présente sur le long terme. La décomposition des ions ammonium et la mobilité des ions césium du cœur du catalyseur vers la surface jouent un rôle important dans le processus de désactivation de ces catalyseurs sous flux réactionnel. A plus haute température la formation d'oxydes simples non sélectifs jouent également un rôle dans la décroissance de l'activité et de la sélectivité. La méthode de préparation des catalyseurs peut fortement influer sur leurs propriétés texturales, acides et redox et donc sur les performances catalytiques obtenues. Un catalyseur actif doit présenter un minimum de surface spécifique (de l'ordre de 15-20 m^2/g) et pouvoir limiter la diffusion des ions césium vers la surface. De plus, il doit présenter les propriétés redox nécessaires à l'orientation de l'intermédiaire formé en surface vers la méthacroléine ou l'acide méthacrylique. Dans cette étape l'insertion de vanadium dans la structure primaire joue un rôle essentiel. Les meilleures performances catalytiques ont été obtenues à 340 °C avec un temps de contact de 7,2 s sur le catalyseur 40APMV/CPM. La conversion de l'isobutane est alors de 20.2% et le rendement en produits d'intérêt de 8.6%.
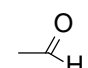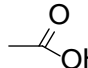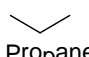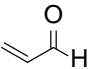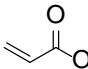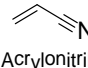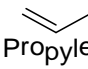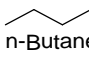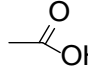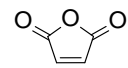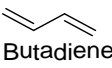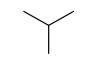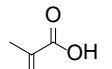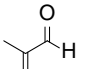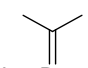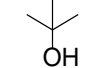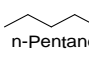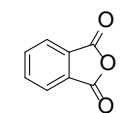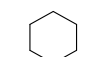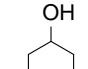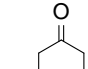
1 Introduction

1.1 General information on alkane oxidation

Selective oxidation is an important chemical process in modern chemical industry. Many chemical products and fine chemistry intermediates are actually synthesized via a process that includes an oxidation step. The most important applications of oxidation reactions are surely the activation of hydrocarbons. Hydrocarbons are generally issued from coal, oil and natural gas. They are still the main feedstock of the chemical industry, even though large efforts are more and more done to increase the use of compounds issued from biomass instead of them. Therefore, the transformation of saturated, as well as non-saturated (i.e. aromatic, olefinic and acetylenic) hydrocarbons constitutes an extremely important field of research. Whereas the latter are already widely used as starting material in chemical industry, the alkanes strongly suffer from their high chemical inertness. Therefore, it is necessary to develop novel chemical routes for catalytically activating the low cost alkane materials to more valuable products, such as alcohols, ketones, acids and anhydrides. The main oxidation transformation processes of light alkanes (C_1-C_6) are listed in Table 1-1. Several of them are already transposed to the industrial scale, such as the oxidation of ethane to acetic acid (SABIC), propane to acrylic acid (BASF), *n*-butane to maleic anhydride (several companies), or the oxidation of cyclohexane to cyclohexanol and cyclohexanone (several companies). Nevertheless, most of them are still in the state of development and research at the lab-scale.

Table 1-1 Commercial, pilot stage or "under-study" oxidation reactions of light alkanes (C_1-C_6)

Raw material	Product	Catalyst	Development stage
CH_4 ⟶ Methane	CH_3OH Methanol	$FePO_4$ [1]	Pilot
	$CO+H_2$ Syngas	Ni/Al_2O_3 [2]	Pilot
	$H_2C=CH_2$ Ethylene	Sr/La_2O_3 [3]	Pilot
	HCHO Formaldehyde	FeMoO [4]	Industrial

Alkane	Product	Catalyst	Status
H_3C-CH_3 Ethane	$H_2C=CH_2$ Ethylene	HPMo$_{12}$/SiO$_2$ [5]	Research
	Acetaldehyde	K$_2$MoO$_4$ [6]	Research
	Acetic acid	MoVNbO [7]	Research
Propane	Acrolein / Acrylic acid	MoVSbTeO [8]	Research
	Acrylonitrile	MoVSbWO [9]	Research
	Propylene	NiMo$_4$/SiO$_2$ [10]	Research
n-Butane	Acetic acid	VMoPO [11]	Industrial
	Maleic anhydride	VPO [12]	Industrial
	Butadiene	Mg$_4$V$_2$Mo$_2$O$_x$ [13]	Industrial
iso-Butane	Methacrylic acid / Methacrolein	Keggin POM [14]	Research
	iso-Butene	VSbO [15]	Research
	t-Butyl alcohol	Fe complex [16]	Research
n-Pentane	Phthalic anhydride	VPO [17]	Research
Cyclohexane	Cyclohexanol / Cyclohexanone	CoAlPO-5 [18]	Research

From Table 1-1, it can be seen that important intermediates such as unsaturated aldehydes, anhydrides and carboxylic acids can be obtained from alkanes. These intermediates are well known starting materials for the synthesis of more valuable (fine) chemicals. For example,

acrylic and methacrylic acids are widely used to synthesize the corresponding esters which are needed to produce commercially important polymers and co-polymers.

In between, methacrylic acid is the precursor of methyl methacrylate (MMA), which is further used for the production of poly methyl methacrylate (PMMA), better known under one of its commercial name Plexiglas[®] [19]. As estimated by Mitsubishi Rayon, the global demand increases constantly by 5-6% annually [20], the trend is shown in Figure 1-1. Since 2010, the demand for optical PMMA has significantly increased in Asia for applications in the new segment of liquid crystal display (LCD) & other electronic equipment and in automotive and mobile phone industries. The great demand also caused the price of bulk methyl methacrylate to increase by 10% [21]. Moreover, Figure 1-1 shows that the worldwide demand will overpass the global supply capacity in 2015. Therefore an increase of the production of PMMA will be necessary in a near future.
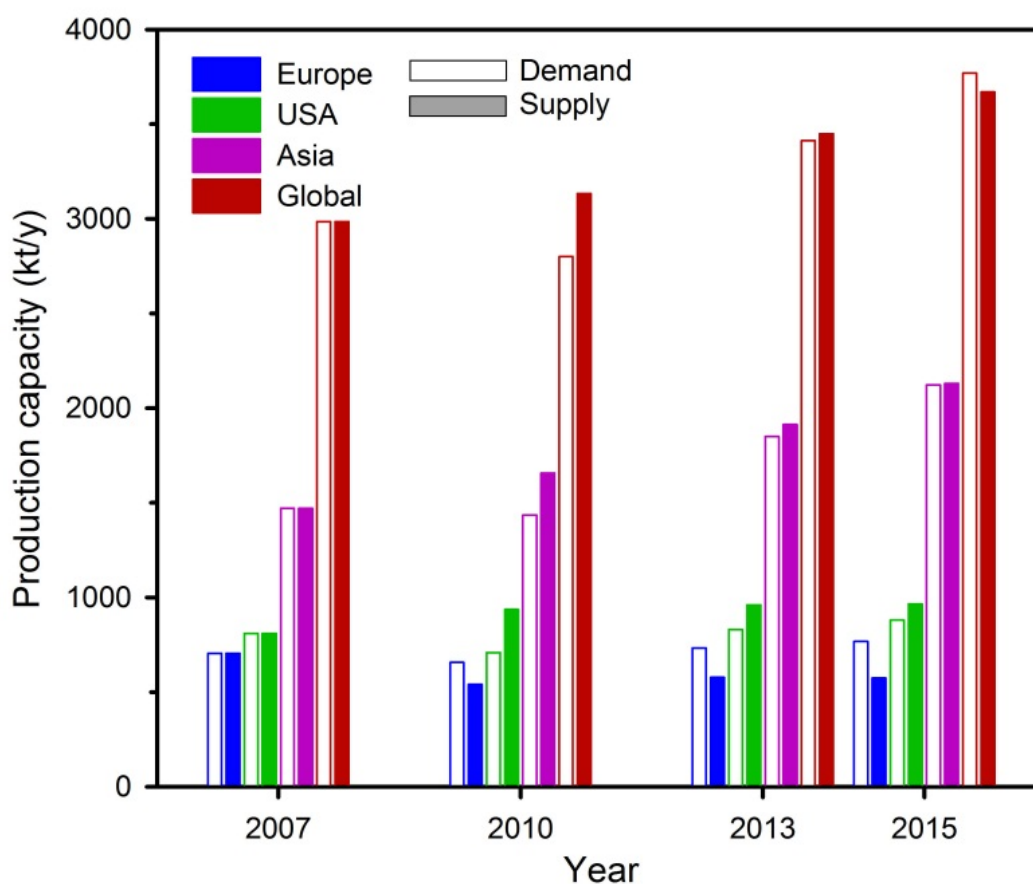
Figure 1-1 Trends of demand and supply of MMA in future estimated by Mitsubishi Rayon [20]

1.2 Manufacturing process of methyl methacrylate and methacrylic acid

1.2.1 ACH route

As noted above, the methyl methacrylate is an important industrial chemical. The industrial process for its production is traditionally based on the acetone-cyanohydrin (ACH) route [22]. The corresponding reactions are described as follows:
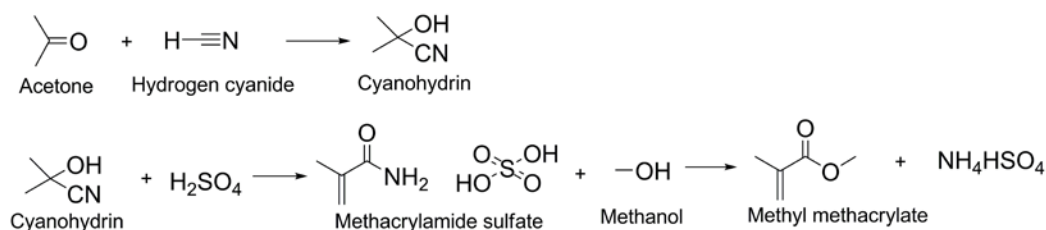
Scheme 1-1 Traditional ACH route for the production of methyl methacrylate

The route developed and commercialized in the 1930s consists of 3 steps (Scheme 1-1): Starting from acetone and hydrogen cyanide, the cyanohydrin is generated. The latter is then reacted with excess of concentrated sulfuric acid to form the methacrylamide sulfate. In the final step, the generated methacrylamide sulfate is treated with an aqueous methanol solution in excess in order to hydrolyzed and esterify the amide. A mixture of methyl methacrylate and methacrylic acid is obtained, and stoichiometric amounts of ammonium bisulfate are co-produced.

Obviously, the traditional industrial process exposed several drawbacks to which is paid more and more attention due to safety and environmental aspects. Firstly, the use of high toxic (and expensive) hydrogen cyanide is one of the main drawbacks of this process. Secondly, the excess amount of concentrated sulfuric acid, which plays the role of catalyst as well as solvent during the hydrolysis of amide, generates large quantity of ammonium bisulfate, which is contaminated by the organic compounds and can thus not be reused [23, 24]. The disposal of the co-product is costly as severe limitations also apply now for landfills.

1.2.2 Improved ACH route

A new improved ACH route was developed and industrialized by Mitsubishi Gas Chemicals (Scheme 1-2): the cyanohydrine is firstly hydrated to 2-hydroxy isobutylamide in the presence of MnO_2 as catalyst. In the next step, the amide is reacted with methylformate in presence of CaO as catalyst to produce the methyl ester (methyl 2-hydroxyisubutyrate) whereby formamide is co-produced. The latter can be dehydrolyzed to give HCN, which is then recycled in the ACH process [25, 26]. On the other hand, the dehydration of the ester yields MMA. The process was further improved by the same company (see the dashed line in Scheme 1-2) whereby 2-hydroxy isobutylamide is hydrolyzed in aqueous methanol to form ammonia and methyl 2-hydroxyisobutyrate. The ammonia can be used to synthesize HCN by reacting with methanol and oxygen [26]. The advantages of the *in situ* generation of HCN raw material and of the suppression of the excess concentrated sulfuric acid are that it allows avoiding the production of ammonium bisulfate.
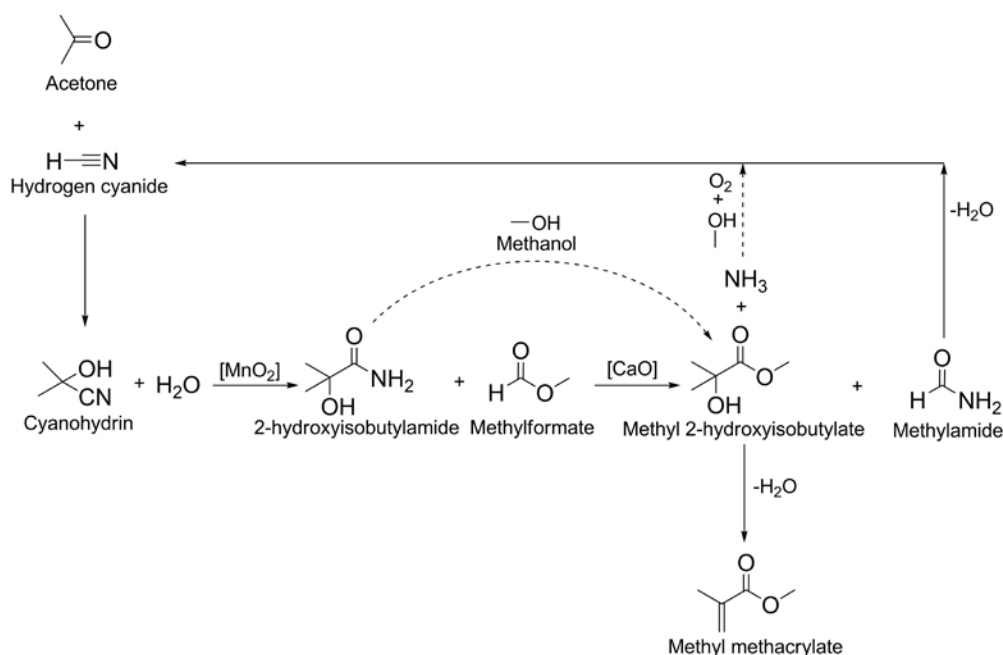
Scheme 1-2 Improved ACH route for the production of methyl methacrylate

1.2.3 Ethylene route

Ethylene is the simplest olefin without branched carbon atoms. In order to prepare methacrylic acid with 4 carbon atoms, increasing the length of the hydrocarbon chain is the first step. The Koch reaction provided a known pathway to produce carboxylic acid by reacting olefins with CO and an alcohol or water in the presence of a strong acid such as sulfuric acid or hydrogen fluoride [27]. In early stage of development, a large number of catalysts based on Ir, Pt, *etc.*, were used for this reaction. Unfortunately, the use of noble metal as catalysts is costly and this aspect makes these approaches economically unattractive. Even when complex catalysts consisting in BF_3 and methanol or water were used for preparing the carboxylic acid ester or carboxylic acid, the complicated preparation of catalyst, the multi-step reaction processes and the strict reaction conditions became the main drawbacks [27, 28]. However, BASF developed a route starting from ethylene. The methacrylic acid was synthesized *via* the successive processes of propionaldehyde and methacrolein, which was catalysed by a secondary amine. The prepared methacrolein was further oxidized to generate methacrylic acid [29].

Another reaction route starting from ethylene is well known as the Lucite "Alpha" process, which involves the combined carbonylation and esterification of ethylene to methyl propionate. Methyl methacrylate was obtained through gas condensation of methyl propionate and formaldehyde under anhydrous conditions. The carbonylation of ethylene step is catalysed by a Pd complex catalyst with high efficiency [30, 31]. The condensation step was performed over Cs_2O/SiO_2 catalyst with a maximum single pass reactivity of 30%. The catalyst lifetime may be an issue [32]. Similarly, methacrylic acid could be obtained by reacting formaldehyde with propionic acid using SnO_2-based/SiO_2 catalyst [33, 34]. The reaction routes starting from ethylene are gathered in Scheme 1-3.
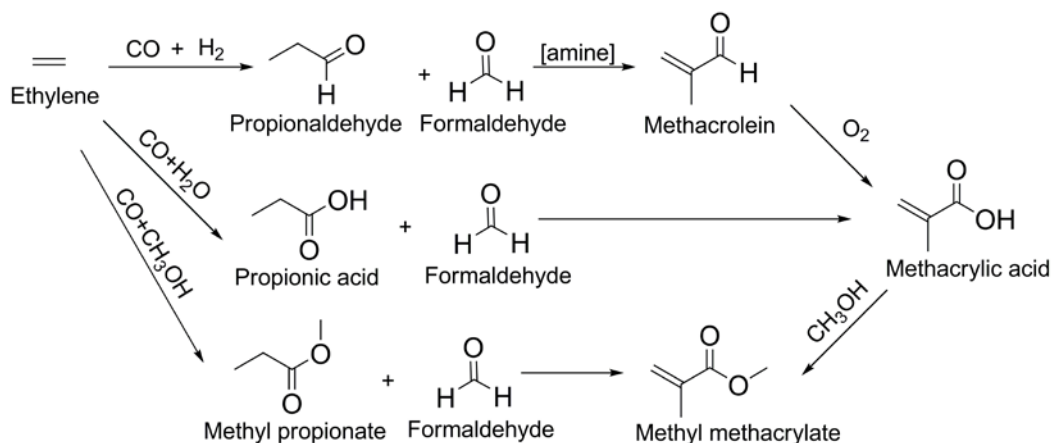
Scheme 1-3 Reaction routes starting from ethylene for the production of methyl methacrylate

1.2.4 Propylene route

The oxidation of propylene to methacrylic acid follows a similar process as the oxidation of ethylene (Scheme 1-4). Firstly, the isobutyraldehyde was synthesized by carbonylation and hydrogenation of propylene with a mixture of H_2 and CO. The synthesized product was oxidized to isobutyric acid, which could be further dehydrogenated to methacrylic acid. During the process for preparing methacrylic acid, two main problems had to be faced: one was the yield of the oxidative dehydrogenation reaction of isobutyric acid and the other one was the catalyst life time. The isobutyric acid can also be synthesized directly by reacting propylene with CO and H_2O over noble metal catalyst [28, 35].
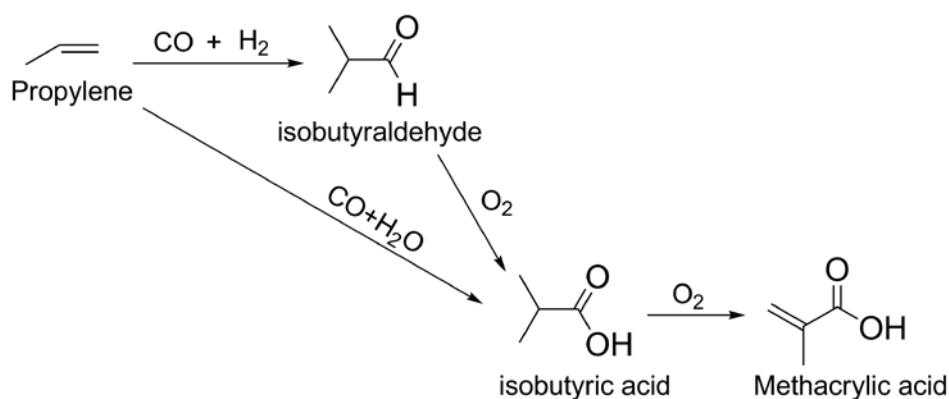
Scheme 1-4 Reaction routes starting from propylene for the production of methacrylic acid

The oxidative dehydrogenation of isobutyric acid itself has been thoroughly studied for *ca.* twenty years [36-39]. The process was developed up to the pilot scale but never came to the commercial scale. The main problem was the necessity to add a lot of steam to isobutyric acid to maintain the high activity and the stability of the heteropolymolybdic acid catalyst, which strongly increased the cost of the process.

1.2.5 Isobutene and tertiary butyl alcohol route

Starting from isobutene, there are at least three methods to prepare methacrylic acid, including the direct oxidation and indirect oxidation (ammoxidation) *via tert*-butanol and methacrylonitrile as presented in Scheme 1-5. The first one consists in a 3-step reaction *via tert*-butanol and methacrolein. The *tert*-butanol was obtained by reacting isobutene-containing hydrocarbons mixture with water over a solid acid catalyst [40, 41]. Etzkorn *et al.* improved the process by the use of essentially inert anhydrous diluted gases to replace steam in the reaction stream [42]. Abe *et al.* [43] carried out a 2-step reaction using two different catalysts and two successive multi-tubular reactors with combined heat exchangers during direct oxidation of isobutene or *tert*-butanol. Firstly the raw materials isobutene or *tert*-butanol was reacted with molecular oxygen to produce methacrolein in the first reactor containing a BiMo mixed metal oxides catalyst. In the following step the as-prepared methacrolein was oxidized to methacrylic acid by vapour phase reaction in using Keggin type Mo-P heteropolyacid or its metal salts catalysts. Arntz *et al.* [44] disclosed a process for preparing methacrolein from isobutene over a mixed metal oxides containing Mo-Bi-Fe-Ni-K-O and yielding up to 83% in methacrolein and methacrylic acid. Benyahia *et al.* [45] prepared multi-components Mo-based catalyst to investigate the kinetics of selective oxidation of isobutene to methacrolein, and pointed out that the reaction proceeded *via* a redox model, in which the catalyst reduction was the rate determining step and non-dissociated oxygen was involved in the re-oxidation step. Weng *et al.* [46, 47] studied the use of mixed tin and antimony oxides in order to improve the selectivity and yield of desired products compared to the pure oxides.

Another reaction pathway is the ammoxidation of isobutene to methacrylonitrile in the presence of sulfuric acid and successive hydrolysis of the latter to methacrylic acid. The silica supported BiMoO catalysts were found to be effective for the ammoxidation of propylene and isobutene. Furthermore, the addition of the other elements such as Ce, Fe and K was found to improve the catalytic performances and catalyst life time. The high conversion of isobutene and high yield to methacrylonitrile made BiMo based catalysts applicable in industrial application [48, 49].
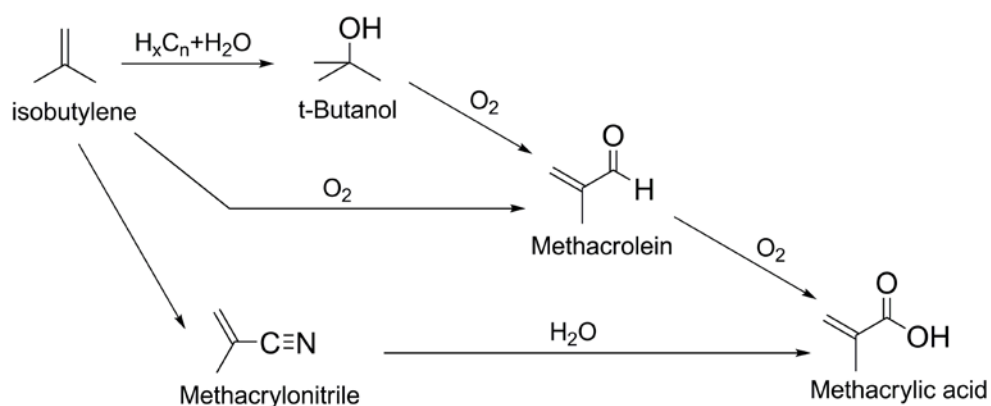
Scheme 1-5 Reaction pathways starting from isobutene for methacrylic acid product

1.2.6 Isobutane route

Although the above mentioned commercialized processes contribute mostly for the production of methyl methacrylate, some drawbacks are also obvious, such as multi-step reaction, use of toxic raw materials, large amount of by-products, separation and purification of the products and expensive catalyst, *etc*. Taking the example of the ACH route, the drawbacks are non-disputable. The use of high toxic raw material hydrogen cyanide and a large amount of co-produced NH_4HSO_4 make the process environmentally unfriendly, not in accordance with the development of modern and sustainable chemical industry. Thus, more and more efforts are necessary to improve or even replace the ACH technology and develop a more environmentally friendly and economical industrial process. Although some positive results were obtained by transformation of light hydrocarbons such as ethylene, propylene and

isobutene into methacrylic acid [24, 50, 51], the harsh reaction conditions and the necessity of at least two reaction steps restricted their industrial application.

On the other hand, the selective oxidation of isobutane was shown to be possible in only one step when using the appropriate catalyst. The detailed reaction network could be described as follows:
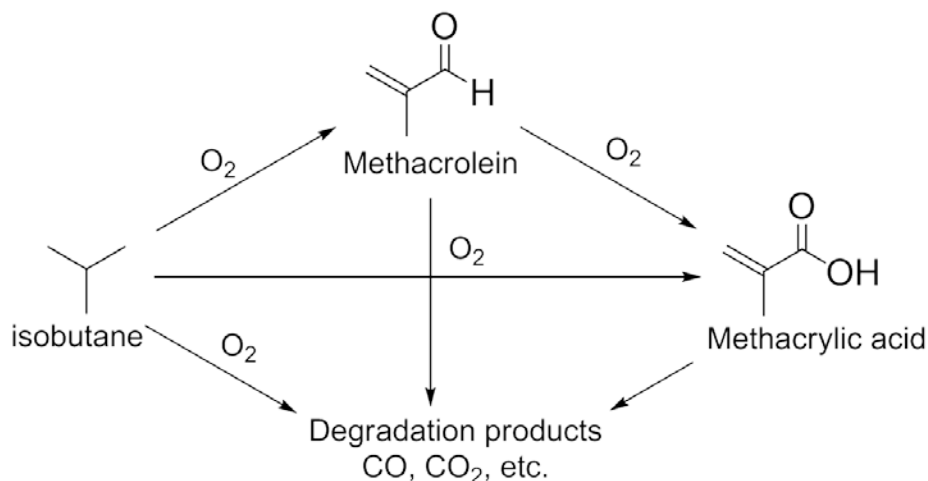
Scheme 1-6 Selective oxidation of isobutane into methacrylic acid

From the reaction scheme, the advantages of oxidation of isobutane are rather eye-catching: (i) the lower cost of the main raw materials, (ii) the lower impact on the environment, (iii) the simplicity of the one-step process, and (iv) the lower amount of the co- or by-products [51]. Those are the reasons why this route attracts more and more researchers' interest.

Methacrolein is an important intermediate as guessed from the reaction. Therefore, a highly efficient oxidation process to produce methacrylic acid becomes significant in determining the final productivity. The direct vapour phase oxidation of methacrolein is the simplest way to produce methacrylic acid scheme (Scheme 1-7), the key factor for the process being the development of highly efficient catalysts. A large number of scientific articles and patents was published where most catalysts were based on Keggin-type heteropolyacids or salts. Krabetz *et al.* [52] developed a complex mixed oxide catalyst containing P-Mo-V-Nb-Cs-O for the oxidation of methacrolein to methacrylic acid. The highest

performance reported was 81.7% conversion and 82.3% selectivity (corresponding to a yield of 67.2%), but the activity decreased during 1010 h of time-on-stream. Naitou *et al.* [53] prepared (NH_4^+) P-Mo-V-O mixed oxides using a less sophisticated method, which led to an increased MAA yield up to 72.4%. Novel heteropolyacid catalysts based on similar compositions were also studied. During catalyst preparation, the ratio of nitric acid to molybdenum and the amount of ammonia had significant effect on pore size distribution [54]. The metal elements K, Cs and certain transition metal were introduced into the P-Mo-V based heteropolyacid catalyst in order to optimize the catalytic performances. Finally it was shown that the nature of the metal precursor also affected the performance significantly [55, 56].
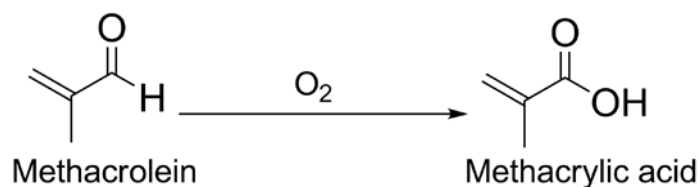
Scheme 1-7 Oxidation of methacrolein to methacrylic acid

1.3 Catalysts for selective oxidation of isobutane

As just shown, the oxidation of isobutane requires active and selective catalysts which are complex, multicomponent mixed oxides. Therefore it is worthwhile to describe their composition, structure and preparation methods. Both unsupported and supported catalysts were studied.

1.3.1 Bulk heteropolycompounds catalysts

1.3.1.1 <u>Several important concepts</u>

Heteropolyacids and their derivatives are called "heteropolycompounds" (HPC). Heteropolyacids are the protonated form of heteropolyanions, which typically include three types, (i) Keggin-type polyanion, for example $PMo_{12}O_{40}^{3-}$ (see Figure 1-2), (ii) Dawson-type

polyanion such as $P_2W_{18}O_{62}^{6-}$, (iii) Anderson polyanion like $PW_6O_{24}^{7-}$. Several polyanions like Lindqvist $Mo_6O_{19}^{2-}$ anion also exist [57, 58]. Among them, the Keggin-type HPCs are most commonly used in catalysis due to their good thermal stability and easy synthesis.

The typical Keggin-type anion structure of $PMo_{12}O_{40}^{3-}$ heteropolymolybdate is shown in Figure 1-2. The heteroatom-oxygen tetrahedral group PO_4 is located in the centre, caged by 12 edge-sharing and corner-sharing octahedral MoO_6 units. They are arranged in four Mo_3O_{13} groups, connecting the central tetrahedral by the shared central oxygen (O_a). Each Mo_3O_{13} group contains 3 edge-sharing octahedral MoO_6 and is linked one another by corner-sharing oxygen (O_c).
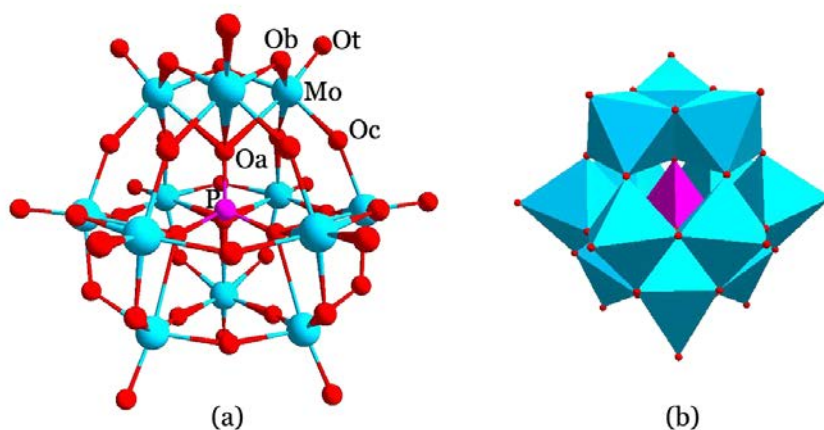
Figure 1-2 Typical Keggin anion $PMo_{12}O_{40}^{3-}$ showing the four distinct O species: central (O_a), terminal (O_t), edge-sharing bridge (O_b) and corner-sharing bridge (O_c). (a: ball and stick, b: polyhedral)

The structure of HPCs is hierarchical and composed of primary, secondary and tertiary structures, as shown in Figure 1-3 [59]. The Keggin "ball-type" structure of heteropolyanions like $[PMo_{12}O_{40}]^{3-}$ is the primary structure, and the secondary structure is the three-dimensional arrangement of heteropolyanions with cations, water of crystallization and eventually other molecules (alcohols, ethers, *etc*.). The secondary structure makes the HPCs difference by varying the cations and heteropolyanions, which results in different properties. At a larger scale, the secondary structures are assembled to generate the tertiary structure, giving the solid particles and their related properties such as particle size, surface area and pore structure. Obviously, the tertiary structure has also a significant effect on the catalytic function of HPCs.

The use of heteropolyacids in catalysis has seen a rapid development since the 1970s because of two important and controllable properties: acidity and redox characters [60]. All heteropolyacids are rather strong acids, even much stronger than mineral acids and other conventional solid acids [61, 62]. The moving surface charge density throughout the large heteropolyanions leads to the weak interaction between the protons and anions, which makes the dissociation much easier, allowing even complete dissociation. The acidity can be modified *via* the composition of HPC (number of protons, nature of the heteroatom). The acidic character is the key parameter for the activation of the C-H bond in the oxidation of paraffins. Furthermore, it also facilitates the desorption of the acid products from the active sites. The redox property is the other important property of HPCs when oxidation (or reduction) of organic reactants is concerned. It is mostly affected by the metal atoms in the primary structure (mainly Mo and V), and the cations (e.g. Cu, Fe…). For the heteropolymolybdates, the replacement of one or more Mo by V in the primary structure was found to significantly improve the redox property because of the V reducibility which is stronger than that of Mo.
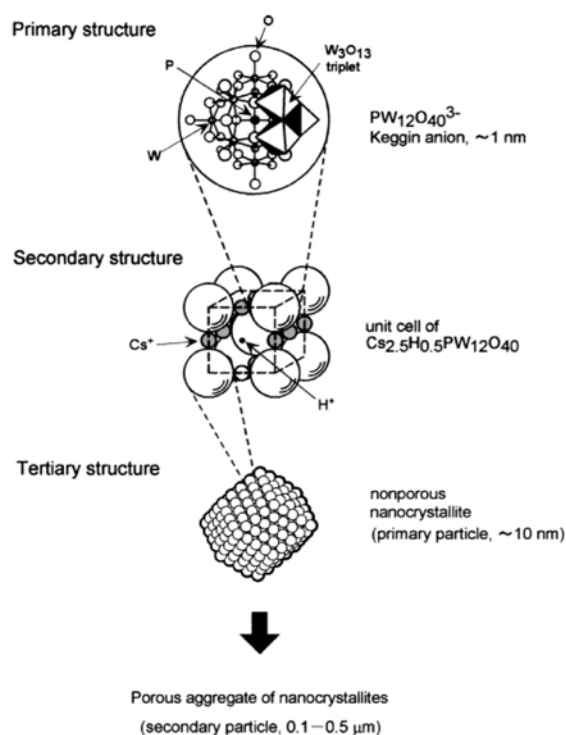
Figure 1-3 Primary, secondary and tertiary structure of HPC [57].

Three different types of mechanisms for the solid heteropolycompounds were proposed by Mizuno and Misono including the surface type catalysis, bulk type-I and bulk type-II (Figure 1-4) [23]. The surface type mechanism is the most widely observed (or at least postulated) in heterogeneous catalysis. The reaction takes place on the external surface and internal surface (in the pores) of the catalyst. For bulk type-I reaction mechanism, the reactant molecule can diffuse into the lattice of the solid. This necessitates that the diffusion rate is significantly higher than the reaction rate (in other words, the chemical regime), so that the reaction can take place inside the solid. The product molecules then diffuse from inside the catalyst to its surface and further to the gas phase. This type of mechanism is also referred as pseudo-liquid phase. On the other hand, oxidation reactions at high temperature generally proceed according to the bulk type-II mechanism. It combines the features of the surface type catalysis and bulk type-I mechanism because the whole bulk solid takes part in the reaction. Furthermore, it exhibits a rapid migration of the redox carriers such as protons and electrons [57, 59, 63].
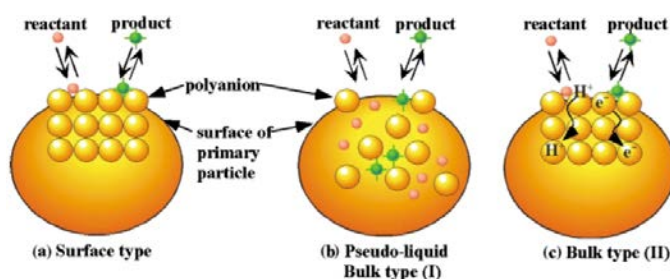
Figure 1-4 Three types of catalysis processes over the heteropolycompounds [57]

1.3.1.2 Keggin-type P-Mo and P-Mo-V based heteropolycompounds as catalysts

It is well known that the bulk heteropolyacid such as $H_3PMo_{12}O_{40}$ exhibits generally poor catalytic activity for oxidation of isobutane. Notably the low surface area (less than 10 m^2/g) may be a probable reason [64]. A lot of works were focused on the modification of this catalyst to increase the surface area and thereby the catalytic performance. The first choice is generally the salification of the heteropolyacid by introduction of cations. By introduction of large counter-cations such as NH_4^+, K^+ or Cs^+ into the secondary structure the small H^+ is

replaced. This substitution has profound effects on the tertiary structure, resulting in the formation of micro- and mesopores whereby the surface area increases [65]. Similar textural features were found for the V-contained heteropolyacid, $H_4PMo_{11}VO_{40}$. However, introducing large cations into $H_3PMo_{12}O_{40}$ affects the catalytic activity for the oxidation of isobutane only to a small extent. On the other hand, the selectivities to methacrolein and methacrylic acid were improved considerably. The Asahi company [66] developed a series of modified catalysts based on P-Mo and P-Mo-V heteropolyacids. Only little change in the conversion of isobutane was observed, but the selectivities to the desired products over the metal-doped P-Mo were much higher than those of pure heteropolyacids. Notably the V-doped samples exhibited increased catalytic performances.

As described above, the acidic and redox properties are two important factors also for the selective oxidation of isobutane, which can be influenced *via* the metal-addenda atoms in the primary structure, the cations and the amount of protons. Thus it may explain the beneficial effect of the introduction of V into the primary Mo-based structure. Some selected catalytic results are gathered in Table 1-2.

Table 1-2 Reported catalytic performance over different Keggin-type heteropolycompounds-based catalysts in oxidation of isobutane (Iban)

Catalyst	Feed, v/v% Iban/O_2/Inert/H_2O	Reaction temp., ^oC	Catalytic performance				Ref.
			Conv. Iban%	Sel.MAA% [a]	Sel. MAC% [b]	Yield (MAC+MAA), %	
$H_3PMo_{12}O_{40}$	26/13/49/12	340	4.1	3.9	12.2	0.66	[67]
$(NH_4)_3PMo_{12}O_{40}$	26/13/49/12	340	3.8	33.3	20.9	2.06	[67]
$Cs_{2.5}H_{0.5}PMo_{12}O_{40}$	17/33/50/0	340	16	24	7	4.96	[23]
$Cs_2HPMo_{12}O_{40}$	33.4/17.2/49.4/0	340	7	12	14	1.82	[68]
$Cs_2Fe_{0.2}H_{0.4}PMo_{12}O_{40}$	33.4/17.2/49.4/0	340	6.8	24	17	2.79	[68]
$Fe_{0.85}H_{0.45}PMo_{12}O_{40}$	33.4/17.2/49.4/0	340	4	9	27	1.44	[68]
$Cs_{1.5}(NH_4)_2Fe_{0.5}PMo_{12}O_{40}$	25/25/35/15	360	12	17	4	2.52	[69]
$Cs_{1.5}(NH_4)_2PMo_{11.5}Fe_{0.5}O_{39.5}$	25/25/35/15	360	12	9.8	3	1.54	[69]
$Cs_{2.5}Fe_{0.08}H_{0.26}PMo_{12}O_{40}$	33/13/54/0	340	15	-	30	4.50	[70]
$K(NH_4)_{0.5}Fe_{1.5}PMo_{12}O_{40}$	26/13/49/12	350	10.8	3.5	1.0	0.49	[71]
Sb-doped $H_3PMo_{12}O_{40}$	26/13/49/12	350	8	13	2	1.20	[72]
$Te_{0.6}H_{1.8}PMo_{12}O_{40}$	27/13.5/49.5/10	355	6.3	27	22	3.09	[73, 74]
$Cs_2Te_{0.2}H_xPMo_{12}O_{40}$	27/13.5/49.5/10	352	10	55	13	6.80	[73]
$Cs_{2.5}Ni_{0.08}H_{0.34}PMo_{12}O_{40}$	17/33/50/0	340	24	28	5	7.92	[23]
$H_4PMo_{11}VO_{40}$	26/13/49/12	340	2.5	25	38.9	1.60	[67]
$Cs_{2.5}Ni_{0.08}H_{1.34}PMo_{11}VO_{40}$	17/33/50/0	340	31	29	4	10.23	[22]
$(NH_4)_3HPMo_{11}VO_{40}$	26/13/49/12	340	2.3	49.4	32.2	1.88	[67]
$Cs_{1.15}(NH_4)_{1.85}HPMo_{11}VO_{40}$	26/13/49/12	340	6.0	45.3	15.3	3.64	[67]
$Cs_{1.3}(NH_4)_{2.2}H_{0.5}PMo_{11}VO_{40}$	26/13/49/12	350	3.1	40.5	29.0	2.15	[14]
$Mo_{12}V_{0.5}P_{1.5}As_{0.4}Cu_{0.3}Cs_{1.4}O_x$	25/25/35/15	360	17	20	3	3.91	[75, 76]
$H_xFe_{1.2}PMo11VAs_{0.3}O_y$	29/29/42/0	370	23.9	69.8	4.1	17.66	[77]
$Cs_2Te_{0.3}V_{0.1}H_xPMo_{12}O_{40}$	27/13.5/49.5/10	350	16.1	54	11	10.47	[73]

[a] MAA=methacrylic acid and [b] MAC=methacrolein

1.3.1.3 <u>The role of V in Keggin-type P-Mo-V based catalysts</u>

Paul *et al*. [14] investigated the reaction kinetics of isobutane oxidation over phosphomolybdate catalysts. The classical Mars & van Krevelen redox mechanism applies to all the steps of the isobutane oxidation. The paraffin is adsorbed and activated under acidic sites promotion, giving a reduced catalyst surface, which is then re-oxidised by the oxygen of the gas phase. Vanadium in $PMo_{11}VO_{40}$ is generally at its highest oxidation state (V^{5+}), resulting in an increased redox potential as compared with $PMo_{12}O_{40}$. Mizuno *et al*. [78] pointed out that a partially reduced catalyst exerted important effects on the catalytic performance. Inmuaru *et al*. [79] focused their work on the vanadium species and its redox behaviour in the same reaction. The results suggested that the relative rate constants of methacrolein and methacrylic acid degradation into acetic acid and/or carbon oxides were much lower compared to those of catalysts without V. The existence of V species may facilitate the reduction and re-oxidation process by promoting the transformation of adsorbed oxygen into lattice oxygen O^{2-}. The latter is known to be more selective to methacrylic acid than electrophilic specie like O_2^- and O^- responsible for degradation. The role of vanadium is also the matter of intense discussions, as it is generally claimed that V is not located in the primary structure, but in the secondary structure under the operating conditions. Nevertheless, Brückner *et al*. [80] demonstrated that most of V species in as-synthesized V-contained heteropolyacid were V^{5+} and part of the Keggin anions, whereas only small amount of V sites existed in the void of the crystal structure as hydrated vanadium oxides. The partial migration of V from Keggin to the secondary structure resulted in the formation of defects, but with little or no significant influence on the crystal structure.

1.3.1.4 <u>Other modifications in addenda atoms and counter-cations</u>

Besides vanadium which is the most used to modify the properties of P-Mo-O HPC, iron was also proposed and was shown to exhibit good catalytic performance in the selective oxidation of isobutane. $PMo_{11}FeO_{39}{}^{4-}$ is usually prepared by reacting Fe salt with $PMo_{12}O_{40}{}^{3-}$ heteropolyanion. The stability of the Keggin structure became strongly modified. Knapp *et al*.

[69] prepared the Cs^+/NH_4^+ salt of Fe-doped P-Mo-O heteropolyacid and studied the nature of Fe species. A similar phenomenon like for $PMo_{11}VO_{40}$ was observed, where Fe could be released from the Keggin structure to the extra-framework under the reaction conditions. It seemed that the counter-cation had a significant effects on the stability of Fe-doped Keggin anions. Compared to the ammonium salt, the caesium salt could enhance the thermal stability, by increasing the temperature of the Fe release from the Keggin structure. The catalytic performance for selective oxidation of light alkane was enhanced by adding Fe into caesium acidic salt of $P-Mo_{12}$ acid, which coincided with the conclusions of Mizuno [70, 81]. The stability of the ammonium salt was found lower. The interaction between Fe^{3+} and NH_4^+ favoured Fe^{3+} release from Keggin units, leading to the elimination of NH_4^+ at lower temperature than for $P-Mo_{12}$ compounds. As a result, the high unstable lacunary compound $PMo_{11}O_{39}^{7-}$ formed which was easily rearranged as $PMo_{12}O_{40}^{3-}$ under reaction conditions. In this case, the introduction of Fe into the ammonium salt of heteropolyacid as catalyst had a negative effect on the catalytic performances. The amount of Fe in Keggin units and its redistribution during the reaction also affected the catalytic performances as shown by Etienne *et al*. [82]. The selectivity for methacrylic acid decreased as the increased Fe content, which resulted from the strong Lewis acid character of the metal. In fact, the presence of Fe generated iron-III-oxide [68, 69, 82], a well-known Lewis-acid, which may directly catalyse the consecutive combustion of the desired products.

Generally, the Cs^+ and/or NH_4^+ proton-substituted heteropolyacids were used in the oxidation of isobutane. Nevertheless, transition metals were also studied as counter-cations [22, 54, 63, 68, 76, 78, 83-87]. The addition of transition metals may enhance the re-oxidation of the catalyst. A series of catalyst containing Fe, Cu, Co, Mn and Ni in heteropolycompounds were prepared and the catalytic performances for light alkanes oxidation were studied [22, 63, 78, 88]. The results displayed that the optimum ratio between the caesium and transition metal cations was 2.5:0.08. For the selective oxidation of isobutane using $Cs_{2.5}Ni_{0.08}H_{1.34}PMo_{11}VO_{40}$ as catalyst, the selectivity of desired products could be improved. At the same time, the Cs^+ at this content could be effective in suppressing the elimination of V from the Keggin structure.

1.3.2 Supported P-Mo based heteropolycompounds catalysts

1.3.2.1 <u>Examples of catalytic reactions requiring acidity and redox properties</u>

The main drawback of heteropolymolybdates is their poor stability on stream and also their low surface area. Both can be increased by deposition on a support. Several supports were tried, depending on applications. As the selective oxidation of isobutane is thought as a surface-type reaction, the surface area of catalyst plays an important role on the catalytic performance. To obtain highly dispersed surface heteropolycompounds catalysts, the use of porous materials such as silica, MCM-41, activated carbon and salt of heteropolyacids as supports for the active phase was widely studied [64, 89]. Benadji *et al*. [90] prepared a catalyst with homogeneous dispersion of $H_4PMo_{11}VO_{40}$ on mesomaterials such as hexagonal mesoporous silicate (HMS) by an impregnation method and utilized it to catalyse the selective oxidation of propylene. The results showed that the supported samples performed better to produce the desired compounds compared than the bulk HPA. Additionally, the thermal stability was improved as well after supporting. Kim *et al*. [91] synthesized $H_3PW_{12}O_{40}/SiO_2$ nanoparticles by a micro-emulsion method and pointed out that the surface area and the acidity were significantly dependent on the particle size. In the probe reaction of ethanol oxidation by H_2O_2, both ethanol conversion and acetaldehyde selectivity were higher for the supported samples than with the bulk HPA sample. For the $H_{3+n}PV_nMo_{12-n}O_{40}/K_3PMo_{12}O_{40}$ (n = 0-3) system, the supported heteropolyacids displayed much stronger acidity than those of unsupported acid [92, 93], which was correlated to the degree of hydration. The interaction between the dispersed acid and the support led not only to the improvement of its acidity and redox properties, but also to the enhancement of structural thermal stability. For the supported catalyst, the active phases heteropolyacid were stabilized by the support. Furthermore, as the activity was determined mainly by the adsorption rates and the stability of the secondary structure, thus, supported acids showed better catalytic performances in oxidation of methanol, acrolein and alkanes to aldehyde or acids [37, 94].

1.3.2.2 Incorporation of HPCs into mesoporous materials

From the viewpoint of the catalyst design, it is important that the catalytic properties could be controlled at atomic or molecular level. As the development of nanomaterial techniques moves forward, preparing catalyst with high, uniform and monolayer dispersion of active sites should become possible. Mesoporous silicas are utilized widely as catalyst support because of the unique pore structure, and of the associated textural properties including high surface area and large pore volume. Several kinds of heteropolyacids supported on different silica materials were used in various selective oxidation reactions. For the preparation of silica-supported caesium and/or ammonium salt of heteropolyacids, various preparation methods including multi-impregnation, gas phase reaction with ammonia, hydrothermal synthesis and urea impregnation method are reported [95]. They were widely used for other oxidation reactions, like methacrolein to methacrylic acid [96, 97], propylene oxidation to acetaldehyde/acrolein [90], isobutyric acid to methacrylic acid [98, 99], toluene oxidation to benzaldehyde [100], as well as in reactions needing mostly acid sites like alkylation [101, 102], hydroisomerization of *n*-heptane [103], dehydration of glycerol to acrolein [104, 105], etc. More applications of supported heteropolycompounds as catalysts were listed in Table 1-3, including catalytic gas and liquid phase reactions.

The preparation technique is another important aspect in affecting the catalytic properties. Usually when mesoporous materials with regular structure are used as support, the controllable texture, particle size and active phase dispersion *etc*. are controlled finely in order to gain the best catalytic performances. The caesium and ammonium salts are not soluble in water because of low solvation energy, thus it is impossible to prepare caesium or ammonium salt-supported heteropolyacid by a co-impregnation method. A multi-step impregnation is usually used to prepare supported heteropolycompounds catalysts. The support is generally impregnated with the counter-cation precursor (i.e. Cs_2CO_3) in the first step. The second step consists then in the addition of the heteropolyacid to the as-impregnated support [106]. This method provided a way to prepare highly dispersed catalyst. The use of other supports such as

CeO mainly took into account the capacity of storing and releasing oxygen for the redox process under reaction conditions.

Ballarini *et al.* [107] tried to introduce the heteropolyanions directly during the gel formation in order to disperse the considerable reaction heat and prevent the products from oxidative degrading to CO_2. Nevertheless, the obtained samples displayed lower thermal stability compared to the bulk one. The catalyst showed low activity in the oxidation of isobutane. The heteroatom P was replaced by Si during the gel formation, whereby the structure and redox properties were modified. The decomposition of the heteropolycompound and the combustion of desired products were responsible for the decrease in catalytic performance.

Chemical immobilization supplies another way to prepare a catalyst with monolayer dispersion of the active phase. The surface of the mesoporous silica was functionalized with $-NH_2$ next to the silanol groups by reacting with acidic heteropolyanions. Such functionalized surface supplied anchoring sites for specific catalyst, whereby high dispersion of the active phase could be obtained [108, 109]. Two possible procedures are shown in Figure 1-5 and Figure 1-6, surface modified meso-structured cellular foam and mesoporous carbon are the bases, respectively.
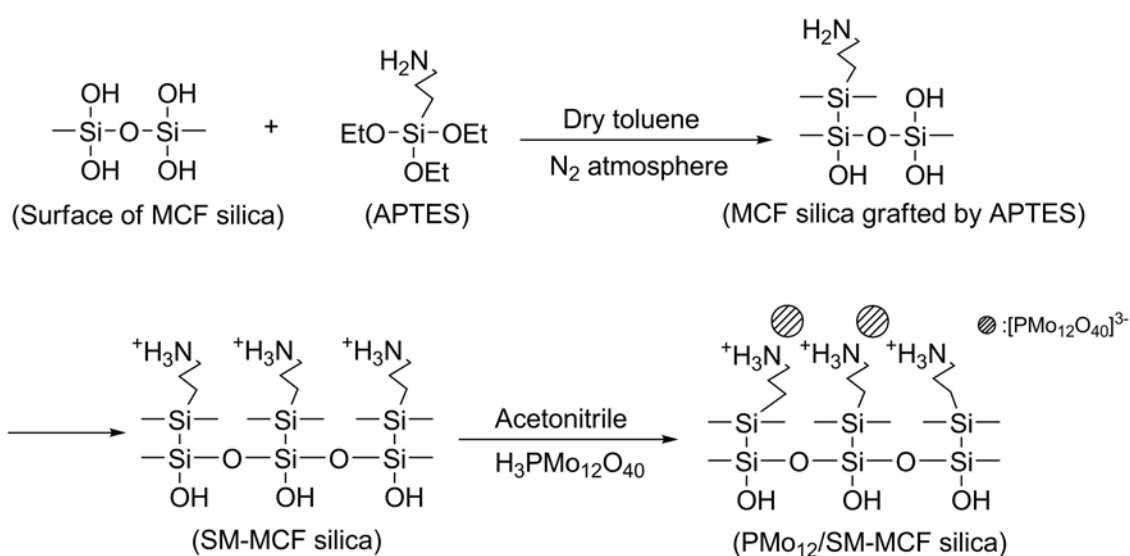
Figure 1-5 Procedure of surface modification of MCF with APTES and immobilization of heteropolyacid on the surface of functionalized MCF [108]
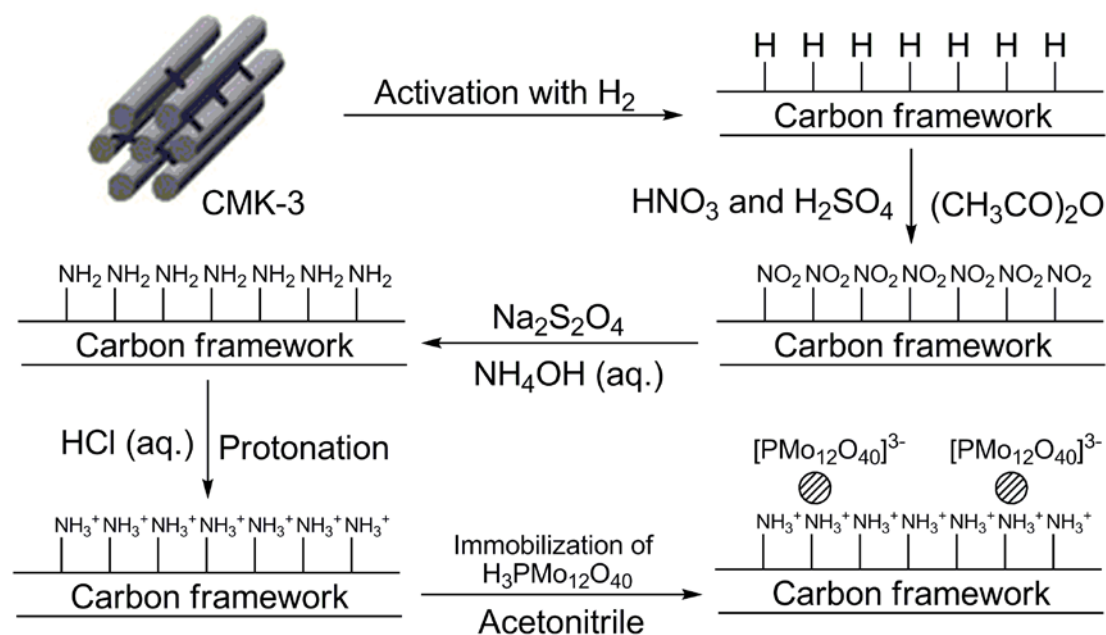
Figure 1-6 Procedure of surface modification of mesoporous carbon (MC) and immobilization of heteropolyacid on the surface of functionalized MC [110]

Table 1-3 Applications of supported heteropolycompounds catalysts for different reactions

Catalyst	Preparation method	Catalyzed reaction	Ref.
Gas-solid phase reaction			
$H_3PMo_{12}O_{40}$/TUD-1	Impregnation	Hydro-isomerization of n-heptane	[103]
$H_3PMo_{12}O_{40}$/APTES/MCF	Grafting-impregnation	Ethanol conversion	[108]
$H_3PMo_{12}O_{40}$/SiO$_2$	Impregnation	Dehydration of glycerol to acrolein	[105]
$H_3PW_{12}O_{40}$/ZrO$_2$	Impregnation	Dehydration of glycerol to acrolein	[111]
$H_3PMo_{12}O_{40}$/SiO$_2$ $H_3PW_{12}O_{40}$/SiO$_2$ $H_4SiW_{12}O_{40}$/SiO$_2$	Impregnation	Dehydration of glycerol to acrolein	[104]
$H_3PW_{12}O_{40}$/(APTES)/SiO$_2$ $H_3PW_{12}O_{40}$/(APTES)/MCM-41	Grafting-impregnation	Dehydration of isopropanol	[109]
$H_3PW_{12}O_{40}$/Cs/SiO$_2$ $H_3PW_{12}O_{40}$/Cs/MCM-41	2-step impregnation	Isomerization of n-butane	[112]
$H_3PW_{12}O_{40}$/SBA-15	Impregnation	*tert*-Butylation of phenol	[113]
$H_3PW_{12}O_{40}$/SBA-15	Impregnation, direct doped in SBA-15	Isomerization of n-decane	[114]
$H_3PMo_{12}O_{40}$/polystyrene	Impregnation	Methacrolein to methacrylic acid	[97]
$H_4PMo_{11}VO_{40}$/SiO$_2$	Impregnation	Methacrolein to methacrylic	[96]

		acid	
$H_5PMo_{10}V_2O_{40}$/N-MC	Grafting	Methacrolein to methacrylic acid	[115]
$H_4PMo_{10}VO_{40}$/HMS	Impregnation	Oxidation of propylene	[90]
$H_{3+x}PMo_{12-x}V_xO_{40}$/TiO$_2$	Impregnation	Total oxidation of chlorobenzene	[116]
$(NH_4)_4PMo_{11}VO_{40}$/CeO$_2$	In situ synthesis	Ammoxidation of 2-methylpyrazine	[117]
Liquid phase reaction			
$H_4PMo_{11}VO_{40}$/Nb$_2$O$_5$	Impregnation	Oxidation of toluene	[100]
$Cs_{2.5}H_{0.5}PWO_{40}$/SiO$_2$ (meso)	2-step Impregnation	Alkylation of 1,3,5-trimethylbenzene	[106]
$Cs_{2.5}H_{0.5}PWO_{40}$/SBA-15	2-step impregnation	MTBE synthesis	[118]
$Cs_{2.5}H_{0.5}PWO_{40}$/HMS	2-step Impregnation	Mono-alkylation of biphenyl	[102]
$Cs_xH_{3-x}PWO_{40}$/Y	2-step Impregnation	Etherification of acetic acid	[119]
$K_{2.5}$/$(NH_4)_{2.5}$/$Ce_{0.83}H_{0.5}PWO_{40}$/MCM-41	2-step Impregnation	Mono-alkylation of benzene	[101]
$H_3PW_{12}O_{40}$/SBA-15	direct doped in SBA-15	Deep HDS	[120]
$H_3PW_{12}O_{40}$/SBA-15	Impregnation	Isopropylation of naphthalene	[121]
$H_3PW_{12}O_{40}$/ZrO$_2$/MCM-41	2-step impregnation	Acetylation of veratrole	[122]
$H_3PW_{12}O_{40}$/ZrO$_2$/SBA-15	2-step impregnation	Benzylation of phenol	[123]
$H_3PW_{12}O_{40}$/SBA-15	Impregnation	Dehydration of isopropane, MTBE synthesis	[124]
$H_3PW_{12}O_{40}$/Al-SBA-15			
$H_3PW_{12}O_{40}$/Al$_2$O$_3$			

1.3.3 Mixed metal oxides catalyst

Oxidation reactions over mixed metal oxides also obey the classic redox theory of Mars and van Krevelen mechanism which consists in the reduction of the catalyst by the hydrocarbons under reaction conditions and the successive re-oxidation of the thus reduced catalyst by the oxygen of the gas phase [125].

Mixed metal oxides catalysts are already widely used as catalysts in the oxidation or ammoxidation of propane [126-134] and selective oxidation of isobutane [135-143]. Comparable to the work on HPC catalysts, mixed metal oxide catalysts used in the oxidation of propane consist of Mo and V. Compared to the catalyst without V, the catalysts containing V are generally more active. The selective oxidation of propane to acrylic acid consists in the

activation of the C-H bond and subsequent insertion of oxygen. The same mechanism is necessary in the catalytic oxidation of isobutane to methacrolein and methacrylic acid. Thus, in most catalysts for the selective oxidation of isobutane, the elements V and Mo are included and even other transition metals are used as a dopant. Usually, the mixed metal oxides do not have a special structure like heteropolycompounds which exhibit the Keggin structure. They rather exhibit mixed crystalline phases or surface amorphous phases. As far as the preparation technique is concerned, the mixed metal oxides are generally obtained by a high temperature thermal treatment. Therefore the prepared catalysts could exhibit good thermal stability. This is definitely an advantage compared with the heteropolycompounds catalysts.

Some catalytic performances for the selective oxidation of isobutane into methacrolein and methacrylic acid over mixed metal oxides are listed in Table 1-4. Mo-V based mixed metal oxides are effective catalysts. Furthermore, the doping with metal elements such as Te, Sb, Nb and Ce and/or non-metal element like P could effectively improve activity and products distribution. As generally observed for mixed metal oxide catalysts, not only the composition but also the preparation methods had important influences on the catalytic performance. By comparing catalysts with the same composition like Mo-V-Te, Mo-V-Te-Sb and Mo-V-Te-Ce prepared with and without hydrothermal treatment, one can see that the catalysts synthesized without hydrothermal treatment displayed higher isobutane conversion. On the other hand the latter displayed higher selectivity to methacrolein and lower selectivity to isobutene whereby the selectivity in methacrylic acid was generally very low. Besides these, the preparation parameters such as calcination atmosphere [144] and temperature [142] also have considerable effects on the catalytic performance.

Table 1-4 Reported catalytic performance of mixed-metal oxides for selective oxidation of isobutane

Catalyst	Method [a]	Feedstock, v/v% Iban/O_2/Insert/H_2O	T, ^{o}C	Conv. % Iban	Sel.% MAC [b]	MAA [c]	iC_4H_8	Ref.
Re-Sb	P +HT	18/36/46/0	500	7	43	/	40	[145]
Mo-V	P	1/1/0/1	440	28.5	4	10	13	[146]
Mo-V-Sb	P	1.6/1 /2/0	440	8.7	21	/	10.8	[147]
Mo-V-Te	P	1/1/0/1	440	21.3	17	16	13	[146]
Mo-V-Te-Sb	P	1/1/0/1	470	26.2	18	13	18	[148]
Mo-V-Te-P-Sb	P	1/2/2/1	440	10.2	38	12	7	[149]
Mo-V-Te-Ce	P	1/2.5/2/2	420	22.7	20	10	5	[150]
Mo-V	P+HT	2/1/1.6/1.4	440	11.1	26.8	1.7	23.8	[140]
Mo-V-Te	P+HT	1/1/2/1	420	15.6	44.2	3.5	11.8	[151]
Mo-V-Te-Nb	P+HT	1/1/2/1	380	16.2	30.3	9.8	0.6	[139]
Mo-V-Te-Sb	P+HT	1/1/2/1	390	15.1	48.6	10.3	1.3	[152]
Mo-V-Te-Ce	P+HT							[153]

[a] P=precipitation, HT=hydrothermal, [b] MAC=methacrolein, [c] MAA=methacrylic acid

1.4 Reaction conditions and mechanism

The reaction conditions such as feed composition, reaction temperature and contact time are the main factors which affect the catalytic performances. At the same time the ratio of hydrocarbons and oxygen have also a significant effect. Under oxygen-rich conditions, the introduction of Fe and Ni can increase the yield in the desired products while the introduction of Cu did not show any beneficial effect. On the other hand, under oxygen-poor conditions, the Cu promoter could improve the catalytic performance [88]. The kinetic study carried out by Paul *et al*. [14] showed the phenomenon of surface saturation by studying isobutane reaction rate *vs.* the hydrocarbon and oxygen concentrations. As aforementioned, the Mars and van Krevelen mechanism can be adapted to all steps of isobutane oxidation, meaning thus that hydrocarbon reacted with oxidized sites. After the partial reduction of active site by isobutane, the adsorbed intermediate further reacted with surface lattice oxygen to form the target products. Thereafter, the reduced catalytic sites was re-oxidized by gaseous oxygen. This kinetic model, also known as classic redox mechanism, is described in Figure 1-7.

It is well known that appropriate concentration of water in isobutane feed has a positive effect on the selectivity to methacrylic acid [73]. Furthermore, water is actually one of the products in this reaction. Some results suggested that water may influence not only the quantity of active sites but also their intrinsic properties [73].
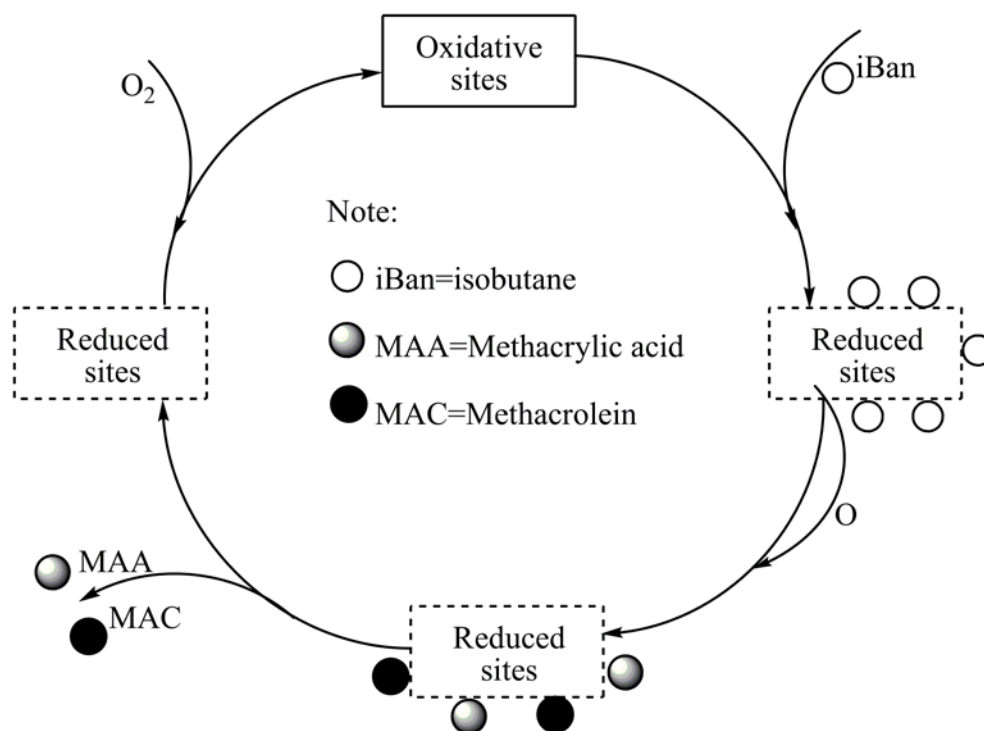
Figure 1-7 The redox mechanism for isobutane oxidation reaction [14, 24]

As far as the reaction mechanism is concerned, Busca *et al*. [154] proposed the mechanism shown in Figure 1-8 using $K(NH_4)_2PMo_{12}O_{40}$ as catalyst. The mechanism involved the initial abstraction of H⁻ species at tertiary C atom of isobutane, which was considered as the rate-determining step of the reaction. This species could evolve towards the formation of absorbed isobutene as a result of oxidative dehydrogenation reaction, which was known to be promoted by acidic surface. The produced alkoxide was then converted to an allylic alkoxy species which react to give the common intermediate dioxyalkylidene species where the primary carbon atom was connected to the catalyst surface *via* two C-O-Mo bridges. Starting from the intermediate, two parallel reactions may occurred: one for the formation of

methacrolein and the other one for the formation of methacrylic acid. A similar reaction mechanism was also suggested by Huynh *et al*. [73].
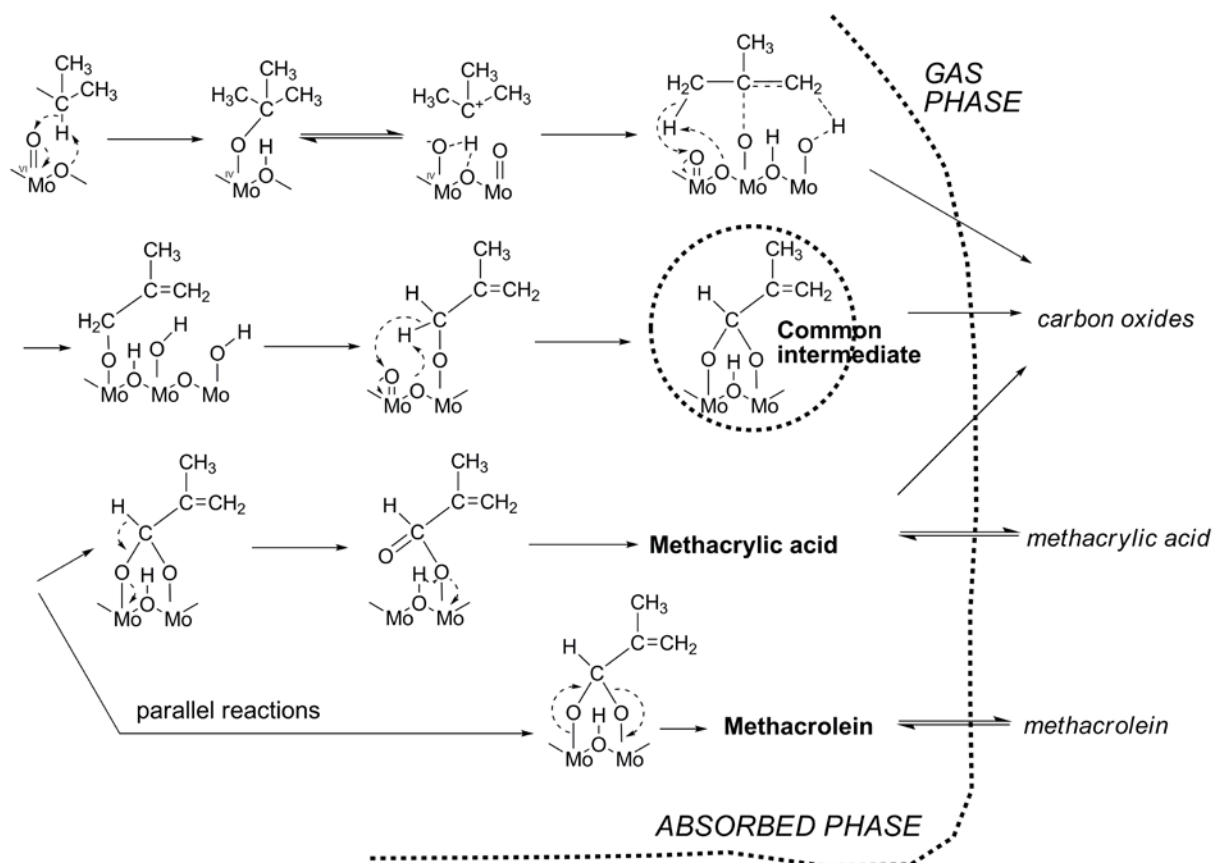
Figure 1-8 Mechanism of oxidation of isobutane to methacrylic acid over Keggin-type polyoxometalate proposed by Busca [154].

By comparing the reaction networks proposed by Paul *et al*. and Busca *et al*., it can be found that the former suggested a direct pathway from isobutane to methacrylic acid and an indirect pathway *via* methacrolein, while the later proposed the probable formation of isobutene and two parallel reaction of isobutane to methacrolein and methacrylic acid. Furthermore no consecutive reaction of methacrolein to methacrylic acid was involved. In exploring the reaction mechanism of isobutane oxidation, various literature is available [73, 75, 155]. The results revealed that the isobutene was firstly formed, but it was not detected during the experiments. The phenomenon is ascribed to its fast conversion as it is known that the oxidation of isobutene is 500 times faster than its formation.

1.5 Our work on the catalytic oxidation of isobutane

As we have seen in the previous paragraphs, the selective oxidation of isobutane, as a shortcut for the production of methacrolein and methacrylic acid has already attracted significant research interests. Starting from isobutane to form methacrolein and methacrylic acid, the activation of C-H, the oxidative dehydrogenation and the oxygen insertion are necessary. Therefore the design and development of catalytic systems must be focused on the optimization of these parameters. For the bulk catalysts, the research works were mainly focused on the catalyst composition, the catalyst preparation techniques and the optimization of reaction conditions.

On the other hand, the development of mesoporous materials, especially mesoporous silica, offers a new way to prepare more active catalysts with higher surface area, than that of heteropolycompounds which is rather low. Furthermore, it was found that when the heteropolyacids and their salts were supported on silica, their properties such as acidity, redox, thermal stability and texture *etc.* were modified, which in turn affected the catalytic performance. Therefore, the relationship between each property such as the texture, acidity, redox and structural thermal stability would be paid more attention to optimize the catalyst design.

Both the compositions of the active phase and of the support are very important for the catalytic activity. For the supported catalysts, the preparation technique always plays a key role as another problem is faced: how to disperse homogeneously the active phases on the surface? Impregnation, precipitation, co-precipitation, deposition-precipitation and multi-step impregnation are the conventional methods for the preparation of supported catalysts but lot of work has still to be done to control these processes.

For the reaction of selective oxidation of isobutane to methacrolein and methacrylic acid, the net reaction is rather simple, but – of course – the catalytic process is more difficult than the reaction scheme, we need not only to promote the objective reaction for production of methacrolein and methacrylic acid, but also to restrict the combustion reaction of the reactant

and of the desired compounds simultaneously. Heteropolycompounds and especially phosphomolybdic acids have weak thermal stability. They easily decompose under the reaction conditions. On the other hand, the activity of the isobutane oxidation increases, while the selectivity of the expected products decreases with the reaction temperature. Therefore, it becomes a challenge to prepare such a catalyst with good structural stability and high catalytic performance.

In this work, we will be first focussed on the preparation of high specific surface area catalysts by dispersing the active phase on various supports, including silica-based materials (commercial SiO_2 and prepared SBA-15), surface modified SBA-15 (ZrO_2/SBA-15) and salt of heteropolyacid ($Cs_3PMo_{12}O_{40}$), to obtain catalysts with different surface area. The influences of the support on textural properties, structure, acidity and redox will be investigated systematically. The correlation between the catalytic performance and the physical-chemical properties of the prepared catalysts will be established to find the most determining factors for selective oxidation reaction. Afterwards, the best catalyst obtained will be optimized in composition. At this step the work will be concentrated on the active phase such as the surface chemical state and element distribution, interaction with support, acidity and reducibility. The long-term reaction will be also studied. At last, we will design and prepare the catalyst with different methods to explore the possible factors leading to deactivation of catalyst and their influences on the products distribution.

References

[1]   Y. Wang, K. Otsuka, J. Catal. 155 (1995) 256.

[2]   Y. Zhang, W. Chu, W. Cao, C. Luo, X. Wen, Plasma Chem. Plasma Process. 20 (2000) 137.

[3]   A. Marafee, C. Liu, G. Xu, R. Mallinson, L. Lobban, Ind. Eng. Chem. Res. 36 (1997) 632.

[4]   J. H. Lunsford, Catal. Today 63 (2000) 165.

[5]   S. S. Hong, J. B. Moffat, Appl. Catal. A: Gen 109 (1994) 117.

[6]   A. Erdöhelyi, K. Fodor, F. Solymosi, J. Catal. 166 (1997) 244.

[7]   M. Roussel, S. Barama, A. Löfberg, S. Al-Sayari, K. Karim, Catal. Today 141 (2009) 288.

[8]   M. Hatano, A. Kayo (1991) US 5049692

[9]   A. T. Guttmann, R. K. Grasselli, J. F. Brazdil (1988) US 4746641

[10]   D. L. Stern, R. K. Grasselli, J. Catal. 167 (1997) 550.

[11]   M. P. Hughes (1975) US 3907833

[12]   G. J. Hutchings, Appl. Catal. 72 (1991) 1.

[13]   D. L. Stern, J. N. Michaels, L. DeCaul, R. K. Grasselli, Appl. Catal. A: Gen 153 (1997) 21.

[14]   S. Paul, V. LeCourtois, D. Vanhove, Ind. Eng. Chem. Res. 36 (1997) 3391.

[15]   V. P. Vislovskiy, N. T. Shamilov, A. M. Sardarly, V. Y. Bychkov, M. Y. Sinev, Chem. Eng. J. 95 (2003) 37.

[16]   J. E. Lyons, P. E. Ellis, Catal. Lett. 8 (1991) 45.

[17]   F. Cavani, A. Colombo, F. Trifiro, M. T. Sananes Schulz, J. C. Volta, Catal. Lett. 43 (1997) 241.

[18]   R. Raja, G. Sankar, J. M. Thomas, J. Am. Chem. Soc. 121 (1999) 11926.

[19]   http://www.rohmhaas.com/history/ourstory/innovation_plexiglastriumphs.htm.

[20]   M. Moukawa, Chemical World 7 (2010) 50.

[21]   http://www.icis.com/v2/chemicals/9076048/methyl-methacrylate/pricing.html.

[22]   N. Mizuno, H. Yahiro, J. Phys. Chem. B 102 (1998) 437.

[23]   N. Mizuno, M. Tateishi, M. Iwamoto, J. Catal. 163 (1996) 87.

[24]   F. Cavani, F. Trifiro, Catal. Today 51 (1999) 561.

[25]   K. Nagai, Appl. Catal. A: Gen 221 (2001) 367.

[26]   K. Kida (2000) US 6075162

[27]   G. M. Kramer, W. Weissman, H. C. Brown, R. Pettit (1985) US 4518798

[28]   J. A. Jung, J. Peress (1981) US 4256913

[29]   F. Merger, H. J. Foerster (1983) US 4408079

[30]   E. Drent, P. H. M. Budzelaar, Chem. Rev. 96 (1996) 663.

[31]   E. Drent, J. A. M. Van Broekhoven, M. J. Doyle, J. Organomet. Chem. 417 (1991) 235.

[32]   O. H. Bailey, R. A. Montag, J. S. Yoo, Appl. Catal. A: Gen 88 (1992) 163.

[33]   R. A. Montag, S. T. McKenna (1989) US 4801571

[34]   R. A. Montag, S. T. Mckenna (1990) EP 0400692

[35]   F. A. Pesa, T. A. Haase (1984) US 4469886

[36]   M. Akimoto, H. Ikeda, A. Okabe, E. Echigoya, J. Catal. 89 (1984) 196.

[37]   K. Brückman, J. M. Tatibou T, M. Che, E. Serwicka, J. Haber, J. Catal. 139 (1993) 455.

[38]   V. Ernst, Y. Barbaux, P. Courtine, Catal. Today 1 (1987) 167.

[39]   G. B. McGarvey, J. B. Moffat, J. Catal. 132 (1991) 100.

[40]   B. Scholz, F. Nierlich, D. Reusch, S. Fernandez, A. Beckmann (2007) US 7179948

[41]   S. Fernandez, J. Sauer, G. Stochniol, D. Maschmeyer, W. Buschken (2006) US 7002050

[42]   W. G. Etzkorn, G. G. Harkreader (1992) US 5155262

[43]   T. Abe, M. Manabe, K. Deguchi, H. Uhara, Y. Aoki (1990) US 4954650

[44]   D. Arntz, G. Prescher, J. Heilos (1984) US 4442308

[45]   F. Benyahia, A. M. Mearns, Appl. Catal. 70 (1991) 149.

[46]   L. T. Weng, B. Yasse, J. Ladrière, P. Ruiz, B. Delmon, J. Catal. 132 (1991) 343.

[47]   L. T. Weng, P. Patrono, E. Sham, P. Ruiz, B. Delmon, J. Catal. 132 (1991) 360.

[48]   K. Aoki (1998) US 5780664

[49]   H. Midorikawa, K. Someya, K. Aoki, O. Nagano (1997) US 5658842

[50]   T. Okuhara, N. Mizuno, M. Misono, Appl. Catal. A: Gen 222 (2001) 63.

[51]   F. Cavani, R. Mezzogori, A. Pigamo, F. Trifiro, E. Etienne, Catal. Today 71 (2001) 97.

[52]   R. Krabetz, F. Merger, M. Schwarzmann (1984) US 4487962

[53]   H. Naitou, T. Karasuda (2009) US 7625834

[54]   S. A. Stevenson, W. Liang, J. W. Kauffman, L. Cai, A. McGuffey (2010) US 7732367

[55]   G.-h. Hwang, M.-H. Kim, H.-k. Noh, W.-h. Lee, M.-s. Kim (2010) US 2010/0069230 A1

[56]   A. Sudo, T. Kurakami, T. Kojima, S. Hayashimoto, Y. Kobayashi (2009) US 2009/0036707 A1

[57]   M. Misono, Chem. Commun. 2001 (2001) 1141.

[58]   E. Coronado, C. J. Gomez-Garcia, Chem. Rev. 98 (1998) 273.

[59]   N. Mizuno, M. Misono, Chem. Rev. 98 (1998) 199.

[60]   N. Mizuno, M. Misono, Curr. Opin. Solid State Mater. Sci. 2 (1997) 84.

[61]   A. M. Alsalme, P. V. Wiper, Y. Z. Khimyak, E. F. Kozhevnikova, I. V. Kozhevnikov, J. Catal. 276 (2010) 181.

[62]   G. M. Maksimov, Russ. Chem. Rev. 64 (1995) 445.

[63]   N. Mizuno, D. Suh, Appl. Catal. A: Gen 146 (1996) 249.

[64]   I. V. Kozhevnikov, K. R. Kloetstra, A. Sinnema, H. W. Zandbergen, H. Van Bekkum, J. Mol. Catal. A: Chem. 114 (1996) 287.

[65]   T. Okuhara, N. Mizuno, M. Misono, Adv. Catal. 41 (1996) 113.

[66]   S. Yamamatsu, T. Yamaguchi (1993) US 5191116

[67]   M. Sultan, S. Paul, M. Fournier, D. Vanhove, Appl. Catal. A: Gen 259 (2004) 141.

[68]   M. Langpape, J. Millet, Appl. Catal. A: Gen 200 (2000) 89.

[69]   C. Knapp, T. Ui, K. Nagai, N. Mizuno, Catal. Today 71 (2001) 111.

[70]   J. S. Min, N. Mizuno, Catal. Today 66 (2001) 47.

[71]   F. Cavani, E. Etienne, M. Favaro, A. Galli, F. Trifiro, Catal. Lett. 32 (1995) 215.

[72]   F. Cavani, R. Mezzogori, A. Pigamo, F. Trifiro, Top. Catal. 23 (2003) 119.

[73]   Q. Huynh, Y. Schuurman, R. Delichere, S. Loridant, J. M. M. Millet, J. Catal. 261 (2009) 166.

[74]   Q. Huynh, A. Selmi, G. Corbel, P. Lacorre, J. Millet, J. Catal. 266 (2009) 64.

[75]   G. P. Schindler, T. Ui, K. Nagai, Appl. Catal. A: Gen 206 (2001) 183.

[76]   G. P. Schindler, C. Knapp, T. Ui, K. Nagai, Top. Catal. 22 (2003) 117.

[77]   Q. Deng, S. L. Jiang, T. J. Cai, Z. S. Peng, Z. J. Fang, J. Mol. Catal. A: Chem. 229 (2005) 165.

[78]   N. Mizuno, D. J. Suh, W. Han, T. Kudo, J. Mol. Catal. A: Chem. 114 (1996) 309.

[79]   K. Inumaru, A. Ono, H. Kubo, M. Misono, J. Chem. Soc., Faraday Trans. 94 (1998) 1765.

[80]   A. Brückner, G. Scholz, D. Heidemann, M. Schneider, D. Herein, J. Catal. 245 (2007) 369.

[81]   N. Mizuno, J. S. Min, A. Taguchi, Chem. Mater. 16 (2004) 2819.

[82]   E. Etienne, F. Cavani, R. Mezzogori, F. Trifiro, G. Calestani, Appl. Catal. A: Gen 256 (2003) 275.

[83]   H. Kasuga, K. Nakatani, E. Shiraishi (2003) US 6624326

[84]   S. Berndt, K. J. MÜLler-Engel, G.-P. Schindler, F. Rosowski, J. Petzoldt (2005) US 6933407

[85]   S. Watanabe, H. Yoshioka, J. Izumi (1999) US 5856259

[86]   K. Nagai, Y. Nagaoka, N. Ishii (1997) EP 0495504 B1

[87]   U. Kortz, S. S. Mal (2010) US 7645907

[88]   N. Mizuno, W. C. Han, T. Kudo, J. Catal. 178 (1998) 391.

[89]   P. Y. Gayraud, N. Essayem, J. C. Védrine, Catal. Lett. 56 (1998) 35.

[90]   S. Benadji, P. Eloy, A. Léonard, B. L. Su, K. Bachari, Microporous Mesoporous Mater. 130 (2010) 103.

[91]   H.-J. Kim, Y.-G. Shul, H. Han, Appl. Catal. A: Gen 299 (2006) 46.

[92]   K. Brückman, J. Haber, E. Lalik, E. M. Serwicka, Catal. Lett. 1 (1988) 35.

[93]   K. Brückman, J. Haber, E. M. Serwicka, Faraday Discuss. Chem. Soc. 87 (1989) 173.

[94]   E. M. Serwicka, K. Brückman, J. Haber, E. A. Paukshtis, E. N. Yurchenko, Appl. Catal. 73 (1991) 153.

[95]   S. Soled, S. Miseo, G. McVicker, W. Gates, A. Gutierrez, Catal. Today 36 (1997) 441.

[96]   M. Kanno, T. Yasukawa, W. Ninomiya, K. Ooyachi, Y. Kamiya, J. Catal. 273 (2010) 1.

[97]   H. Kim, J. Jung, S. Yeom, K. Lee, I. Song, J. Mol. Catal. A: Chem. 248 (2006) 21.

[98]   A. Aboukaïs, D. Ghoussoub, E. Blouet-Crusson, M. Rigole, M. Guelton, Appl. Catal. A: Gen 111 (1994) 109.

[99]   T. Ilkenhans, B. Herzog, T. Braun, R. Schlogl, J. Catal. 153 (1995) 275.

[100]   K. Rao, P. Rao, P. Nagaraju, P. Prasad, N. Lingaiah, J. Mol. Catal. A: Chem. 303 (2009) 84.

[101]   Z. Zhu, W. Yang, J. Phys. Chem. C 113 (2009) 17025.

[102]   G. Yadav, G. George, Catal. Today 141 (2009) 130.

[103]   D. Liu, X. Quek, S. Hu, L. Li, H. Lim, Catal. Today 147 (2009) 51.

[104]   E. Tsukuda, S. Sato, R. Takahashi, T. Sodesawa, Catal. Commun. 8 (2007) 1349.

[105]   H. Atia, U. Armbruster, A. Martin, J. Catal. 258 (2008) 71.

[106]   S. Choi, Y. Wang, Z. Nie, J. Liu, C. Peden, Catal. Today 55 (2000) 117.

[107]   N. Ballarini, F. Candiracci, F. Cavani, H. Degrand, J. L. Dubois, Appl. Catal. A: Gen 325 (2007) 263.

[108]   H. Kim, J. Jung, P. Kim, S. Yeom, K. Lee, J. Mol. Catal. A: Chem. 259 (2006) 150.

[109]   L. Pizzio, P. Vázquez, C. Cáceres, M. Blanco, Appl. Catal. A: Gen 256 (2003) 125.

[110]   H. Kim, J. Jung, I. Song, Catal. Surv. Asia 11 (2007) 114.

[111]   S.-H. Chai, H.-P. Wang, Y. Liang, B.-Q. Xu, Appl. Catal. A: Gen 353 (2009) 213.

[112]   W. Yang, J. Billy, Y. Ben Taârit, J. C. Védrine, N. Essayem, Catal. Today 73 (2002) 153.

[113]   G. S. Kumar, M. Vishnuvarthan, M. Palanichamy, V. Murugesan, J. Mol. Catal. A: Chem. 260 (2006) 49.

[114]   B. Gagea, Y. Lorgouilloux, Y. Altintas, P. Jacobs, J. Martens, J. Catal. (2009).

[115]   H. Kim, J. C. Jung, D. R. Park, S.-H. Baeck, I. K. Song, Appl. Catal. A: Gen 320 (2007) 159.

[116]   A. Predoeva, S. Damyanova, E. M. Gaigneaux, L. Petrov, Appl. Catal. A: Gen 319 (2007) 14.

[117]   K. Mohan Reddy, N. Lingaiah, P. Rao, P. Nagaraju, P. Sai Prasad, Catal. Lett. 130 (2009) 154.

[118]   P. Madhusudhan Rao, M. V. Landau, A. Wolfson, A. M. Shapira-Tchelet, M. Herskowitz, Microporous Mesoporous Mater. 80 (2005) 43.

[119]   F. Zhang, J. Wang, C. Yuan, X. Ren, Sci. China, Ser. B: Chem 49 (2006) 140.

[120]   X.-M. Yan, J.-H. Lei, D. Liu, Y.-C. Wu, W. Liu, Mater. Res. Bull. 42 (2007) 1905.

[121]   Q.-Y. Liu, W.-L. Wu, J. Wang, X.-Q. Ren, Y.-R. Wang, Microporous Mesoporous Mater. 76 (2004) 51.

[122]   D. P. Sawant, A. Vinu, F. Lefebvre, S. B. Halligudi, J. Mol. Catal. A: Chem. 262 (2007) 98.

[123]   D. P. Sawant, A. Vinu, N. E. Jacob, F. Lefebvre, S. B. Halligudi, J. Catal. 235 (2005) 341.

[124]   P. Madhusudhan Rao, A. Wolfson, S. Kababya, S. Vega, M. V. Landau, J. Catal. 232 (2005) 210.

[125]   B. Grzybowska- Świerkosz, Top. Catal. 11 (2000) 23.

[126]   C. G. Lugmair, J. Zysk, R. K. Grasselli (2005) US 2005/0054869 A1

[127]   N. R. Shiju, V. V. Guliants, Catal. Commun. 9 (2008) 2253.

[128]   V. H. Rane, U. Rodemerck, M. Baerns, J. Chem. Technol. Biotechnol. 81 (2006) 381.

[129]   T. Ushikubo, Catal. Today 78 (2003) 79.

[130]   D. C. Chambers, N. W. Cant, Appl. Catal., B 41 (2003) 61.

[131]   P. Boizumault-Moriceau, A. Pennequin, B. Grzybowska, Y. Barbaux, Appl. Catal. A: Gen 245 (2003) 55.

[132]   A. M. Gaffney, R. Song (2010) US 7718568

[133]   M. Dieterle, H. Hibst, W. J. Popel, J. Petzoldt, K. J. Mueller-Engel (2010) US 7667073

[134]   L. E. Bogan, A. M. Gaffney, S. V. Han, M. D. Heffner, R. Song (2010) EP 1318127 B1

[135]   Y. Takita, S. Hikazudani, K. Soda, K. Nagaoka, J. Mol. Catal. A: Chem. 280 (2008) 164.

[136]   G. Mitran, I. C. Marcu, T. Yuzhakova, I. Sandulescu, J. Serb. Chem. Soc. 73 (2008) 55.

[137]   S. M. Kendell, T. C. Brown, R. C. Burns, Catal. Today 131 (2008) 526.

[138]   S. Hikazudani, K. Kikutani, K. Nagaoka, T. Inoue, Y. Takita, Appl. Catal. A: Gen 345 (2008) 65.

[139]   J. Q. Guan, Y. Yang, B. Liu, Y. Y. Ma, X. F. Yu, React. Kinet. Catal. Lett. 95 (2008) 313.

[140]   J. Q. Guan, H. Y. Xu, K. Song, B. Liu, F. P. Shang, Catal. Lett. 126 (2008) 293.

[141]   J. Q. Guan, C. Xu, Z. Q. Wang, Y. Yang, B. Liu, Catal. Lett. 124 (2008) 428.

[142]   J. Q. Guan, C. Xu, B. Liu, Y. Yang, Y. Y. Ma, Catal. Lett. 126 (2008) 301.

[143]   K. Samson, B. Grzybowska-Swierkosz, Pol. J. Chem. 81 (2007) 1345.

[144]   J. Q. Guan, K. Song, H. Y. Xu, Y. Y. Ma, X. F. Yu, React. Kinet. Catal. Lett. 95 (2008) 321.

[145]   H. C. Liu, E. M. Gaigneaux, H. Imoto, T. Shido, Y. Iwasawa, Appl. Catal. A: Gen 202 (2000) 251.

[146]   J. Q. Guan, S. B. Jing, S. J. Wu, H. Y. Xu, Z. L. Wang, React. Kinet. Catal. Lett. 90 (2007) 27.

[147]   T. Shishido, A. Inoue, T. Konishi, I. Matsuura, K. Takehira, Catal. Lett. 68 (2000) 215.

[148]   J. Q. Guan, M. J. Jia, S. B. Jing, Z. L. Wang, L. H. Xing, Catal. Lett. 108 (2006) 125.

[149]   J. Q. Guan, S. J. Wu, M. J. Jia, J. H. Huang, S. B. Jing, Catal. Commun. 8 (2007) 1219.

[150]   J. Q. Guan, S. J. Wu, H. S. Wang, S. B. Jing, G. J. Wang, J. Catal. 251 (2007) 354.

[151]   J. Q. Guan, K. Song, H. Y. Xu, Z. Q. Wang, Y. Y. Ma, Catal. Commun. 10 (2009) 528.

[152]   J. Q. Guan, H. S. Wang, K. Song, C. Xu, Z. Q. Wang, Catal. Commun. 10 (2009) 1437.

[153]   J. Q. Guan, S. J. Wu, Y. Q. Shao, Y. Y. Ma, F. P. Shang, Pol. J. Chem. 83 (2009) 605.

[154]   G. Busca, F. Cavani, E. Etienne, E. Finocchio, A. Galli, J. Mol. Catal. A: Chem. 114 (1996) 343.

[155]   L. Jalowiecki-Duhamel, A. Monnier, Y. Barbaux, G. Hecquet, Catal. Today 32 (1996) 237.

2 Experimental

2.1 Description of the experimental set-up

The catalytic reaction rig used for testing the catalysts for the selective oxidation of isobutane into methacrolein and methacrylic acid consists of three parts: the feeding zone, the reaction zone and the analysis zone. The details are depicted in Figure 2-1.

Isobutane and O_2 are necessary as reactants, but steam is also added because it is known to improve the catalytic performance. They are supplied by two individual gas cylinders (Air Liquide). A mixture of He containing 1 vol.% Kr is used as diluent, Kr serving as internal standard. The flow-rates of each gas are regulated by mass flow controllers (MFC - BROOKS). Water is introduced *via* an evaporation/saturation system. The catalytic reaction being carried out under 1 atmosphere (760 mmHg), the temperature of the saturator for keeping 10% partial pressure of water in the gas stream was calculated according to the following Antoine equation (1):

$$\lg P = 8.07131 - \frac{1730.63}{T + 233.426}$$

(1)

Where the units of pressure (P) and temperature (T) are mmHg and ^{o}C, respectively. In order to obtain 10% molar fraction (76 mmHg) of water, the theoretical required temperature is 46.2 ^{o}C.

From the feeding zone, the reactant gases arrive directly in the reactor. The latter is made of a stainless steel tube, with an inner diameter of 10 mm and a length of 140 mm. The details of the reactor with the loaded catalyst are depicted on Figure 2-2.
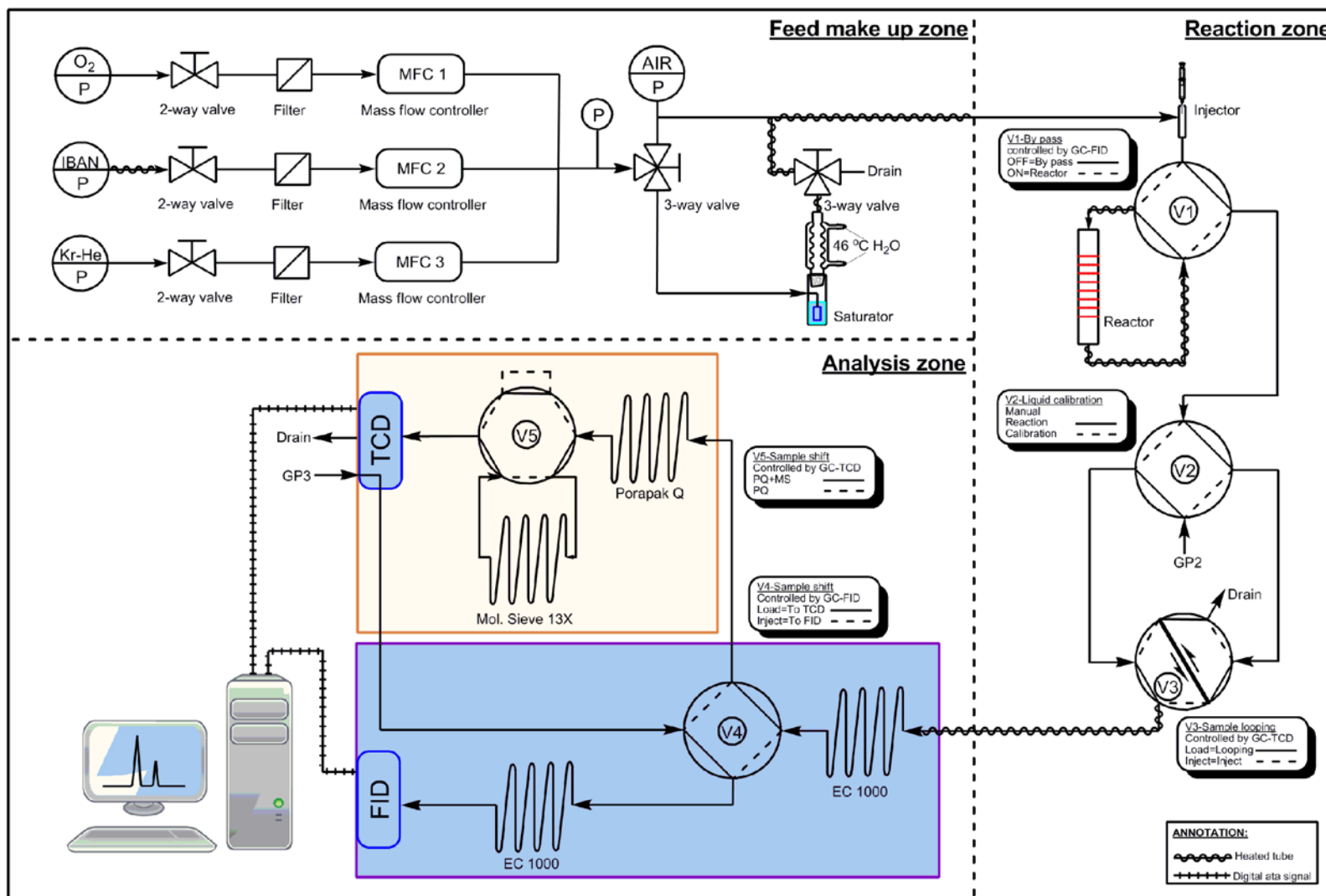
Figure 2-1 Reaction system used for selective oxidation of isobutane into methacrolein and methacrylic acid study
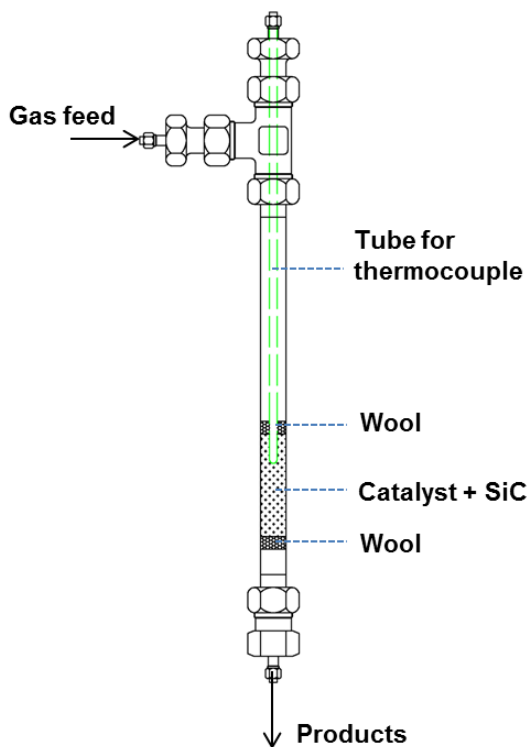
Figure 2-2 The reactor and the loaded catalyst
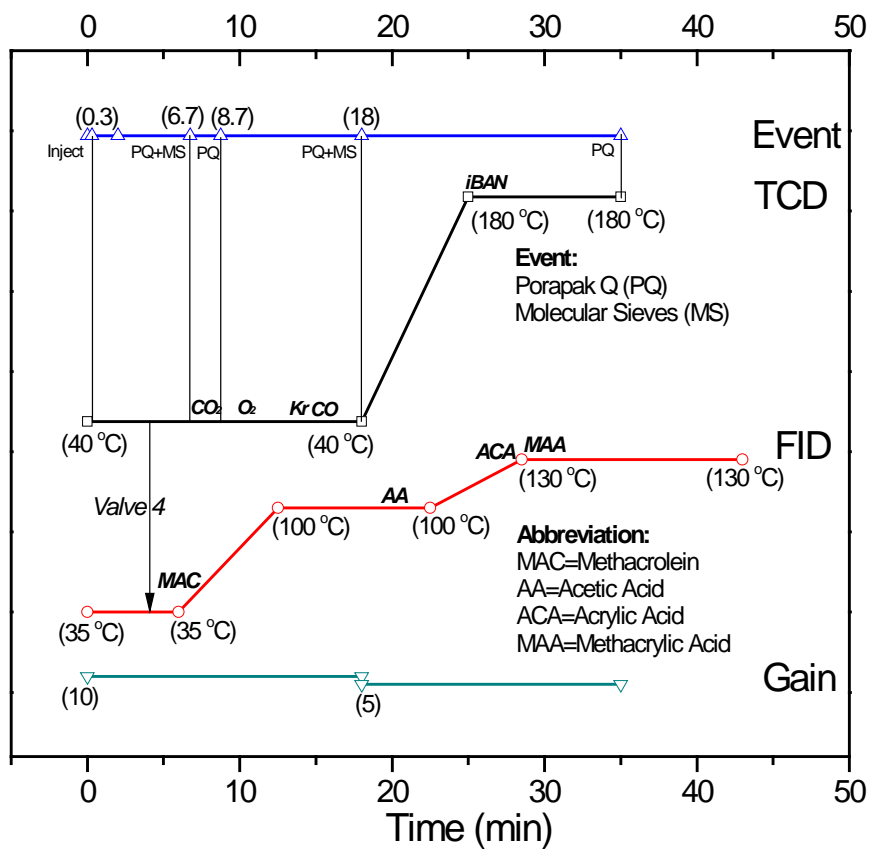
Figure 2-3 Detailed information on the analysis system used
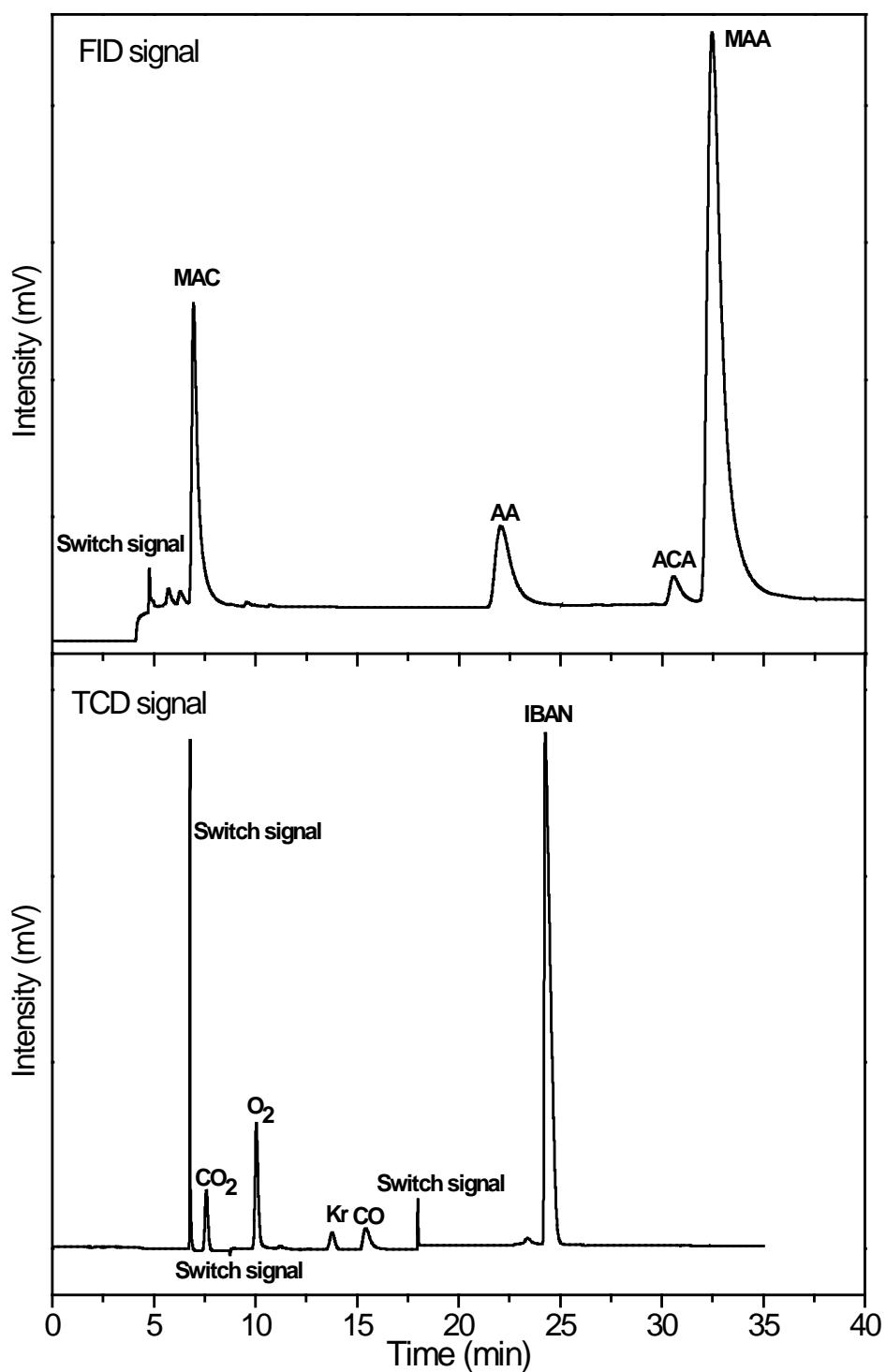
Figure 2-4 A typical analysis result over a Keggin-type heteropolycompounds catalyst using 2 combined GCs (up: response on the FID detector; down: response on the TCD detector)

The catalytic reaction is carried out at 340 $^{\circ}$C under atmospheric pressure. Downstream to the reactor the products fill a sampling loop which is connected to the analysis zone. The light

products such as CO, CO_2, the unreacted O_2, isobutane and the internal standard Kr are analysed by gas-chromatography equipped with a TCD detector (Perichrom - PR2100). The latter is installed with two types of packed columns (Porapak Q and Molecular sieves 13X) installed in series. The heavy products like methacrolein (MAC), methacrylic acid (MAA), acetic acid (AA) and acrylic acid (ACA) are analysed by gas-chromatography on a FID detector (HP 5890) equipped with a semi-capillary column (Alltech - EC1000). The detailed conditions of the two methods are listed in Figure 2-3 and a typical analysis using the two GCs is shown in Figure 2-4.

2.2 Catalytic oxidation of isobutane

2.2.1 Catalytic performance evaluation

The catalytic experiments were performed in the fixed-bed reactor described above under atmospheric pressure. The reactor was loaded with 0.8 g of catalyst diluted with equal volume of SiC (0.21 mm particle size) in order to avoid the overheating of the catalytic bed and hence to keep a better control of the reaction temperature (Figure 2-2). The reactor was heated up to reaction temperature (340 °C) at 5 °C /min heating rate in an air flow (10 mL/min STP), before being replaced by the reactants mixture which was fed at a constant total flow-rate of 10 mL/min STP (molar ratio 27% Iban; 13.5% O_2; 10% H_2O; 49.5% He), corresponding to a contact time of 4.8 s. All products – except water – were analysed on-line by gas chromatography (GC) as described above. The reaction data were obtained after 24 h under stream which corresponds to steady state conditions.

The reaction conditions were always kept the same as above unless otherwise stated.

2.2.2 Quantification of the products

The catalytic performance was evaluated by calculating the conversion of the reactants

(isobutane and oxygen), the selectivity into the different products and the carbon balance. This was done as follows:

Step 1: calculation of the corrective factor r (Kr was introduced into the feed as internal standard)

$$r = \frac{V_{out}}{V_{in}} = \frac{A_{Kr, out}}{A_{Kr, in}}$$

(2)

Where V is the volume of Kr in the mixture, and A is the area of Kr in GC analysis results.

Step 2: calculation of the conversions of the reactants (X_{Iban} and X_{O_2})

$$X_{Iban} = \frac{n \cdot C_{Iban, in}\% / 100 - r \cdot n_{Iban, out}}{n \cdot C_{Iban, in}\% / 100} \times 100\%$$

(3)

$$X_{O_2} = \frac{n \cdot C_{O2, in}\% / 100 - r \cdot n_{O2, out}}{n \cdot C_{O2, in}\% / 100} \times 100\%$$

(4)

Step 3: determination of the selectivities to each product (S_i)

$$S_i = \frac{(1/v) \cdot n_{i, out} \cdot r}{n \cdot C_{Iban, in}\% / 100 - r \cdot n_{Iban, out}} \times 100\%$$

(5)

Step 4: calculation of the carbon balance (CB)

$$CB = \frac{Q_{C, out} \cdot r}{Q_{C, in}}$$

(6)

Where n, n_{Iban}, C_{Iban}, C_{O2}, Q_C and v are the molar amount of feed, isobutane, the molar concentration of isobutane, oxygen, quantity of carbon and stoichiometric number, respectively.

2.3 Catalysts syntheses

2.3.1 Precursors

2.3.1.1 Phosphomolybdic acid $H_3PMo_{12}O_{40} \cdot xH_2O$

Phosphomolybdic acid was commercially obtained from Aldrich-Sigma. The number of

crystal water molecules was determined by thermogravimetric analysis (TGA), whose results suggested 8 molecules. The TGA-DTG curves were shown in the Annex (*cf. section 6.1.1*) on Figure 6-1.

2.3.1.2 $H_4PMo_{11}VO_{40} \cdot xH_2O$

Vanado-phosphomolybdic acid (HPMV) was prepared according to the procedure described in literature [1]. It was synthesized from stoichiometric mixtures of the metal oxides and phosphoric acid

$$22\ MoO_3 + V_2O_5 + 2\ H_3PO_4 + H_2O \rightarrow 2\ H_4PMo_{11}VO_{40} \qquad (8)$$
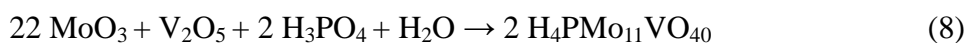
The amounts of each reactant were stoichiometrically chosen for this preparation. The details are listed in Table 2-1:

Table 2-1 Amounts of reactants used for $H_4PMo_{11}VO_{40} \cdot xH_2O$ preparation

Reactant	Mole ratio	Mole, mol	Mass, g
MoO_3	11	0.11	15.84
V_2O_5	0.5	0.005	0.909
H_3PO_4 (85 wt.%)	1	0.01	1.153
H_2O			350

In a typical synthesis procedure, 0.11 mol (15.8 g) of MoO_3 and 0.05 mol (0.91 g) of V_2O_5 were dissolved in 350 mL of deionized water and heated. Then 0.01 mol (1.2 g) of H_3PO_4 (85 wt.%) was added into the reaction mixture under reflux. The generated suspension was heated under reflux for another 6 h and left at ambient temperature until a clear solution was obtained. The resulting solution was evaporated in order to obtain about 30 mL of a concentrated solution, which was further crystallized at 4 ^{o}C for several days. The obtained orange solid was collected and dried at ambient temperature for 2 days.

The structure feature and the number of crystal water were checked by FT-IR and TGA techniques, respectively. The results were reported in Annex (*cf. section 6.1.2*).

2.3.2 Preparation of the supports

2.3.2.1 CARiACT$^{®}$ SiO$_2$

The CARiACT$^{®}$ SiO$_2$ with a specific surface area of 295 m^2/g and average pore size diameter of 15 nm was commercially obtained from Fuji Silysia Chemical Company. It presents an hexagonal structure. The textural properties were analysed by N$_2$ adsorption/desorption technique. Its isotherm and pore size distribution were depicted in Figure 6-4. The isotherm showed a typical feature of mesoporous solid but with a relative wider pore size distribution (4 nm < D < 90 nm centred at around 17 nm).

2.3.2.2 Mesoporous molecular sieve SBA-15

SBA-15 was prepared by the evaporation-induced self-assembly (EISA) process described by Brinker *et al.* [2]. Tetraethyl-orthosilicate (TEOS, Aldrich) and (EO)$_{20}$(PO)$_{70}$(EO)$_{20}$ (P123, Aldrich) were used as Si source and structuring agent, respectively. The amounts of reactants were chosen as presented in Table 2-2.

Table 2-2 Amounts of the reactants for SBA-15 preparation by EISA method

Reactant	Mole ratio	Mole, mol	Mass, g
P123 (Mw=5400)	0.018	0.00074	4
Si(OEt)$_4$ (TEOS)	1	0.040	8.32
HCl (2 M)	0.15	0.006	(3 mL)
H$_2$O	1.391	0.056	1

In a typical synthesis procedure, 2.0 g of P123 were dissolved in 40 mL of anhydrous ethanol and stirred for 3 h to obtain a clear solution. Then 4.2 g of TEOS were added drop-wise into the solution under vigorous stirring. After stirring for 3 h, 3 mL of hydrochloric acid (2 M) were added to adjust the pH to 1.5. The resulting homogeneous solution was stirred for another 24 h, before being poured into a Petri dish to undergo the EISA process. Finally, the gel obtained was calcined at 550 °C for 6 h (heating ramp of 1 °C/min) in order to remove the template.

The synthesized SBA-15 was used as a support for further catalyst preparation. Its textural properties are given in Annex (*cf. section 6.1.4*).

2.3.2.3 ZrO_2 grafted SBA-15

The SBA-15 prepared by EISA method was further modified by grafting of ZrO_2. The ZrO_2/SBA-15 support was prepared as described by Katryniok *et al.* [3] using zirconium *n*-propoxide as organic precursor of zirconia. 2.0 g of SBA-15 were slurried in 20 mL of ethanol (extra-dry, Fluka). Then 1.6 g of zirconium *n*-propoxide ($Zr[n\text{-}PrO]_4$ 70 wt.% in *n*-propanol solution, Aldrich) were added and the resulting mixture was stirred at room-temperature for 8 h. The solid was recovered, washed with ethanol, dried and calcined at 550 °C for 3 h (heating rate 1 °C/min). The surface area of obtained solid determined by N_2 adsorption/desorption technique was 512 m^2/g.

2.3.2.4 $Cs_3PMo_{12}O_{40}$ (CPM)

The preparation of the caesium salt of phosphomolybdic acid was described in reaction (3). Stoichiometric amounts of reactants were chosen as presented in Table 2-3.

$$3\ Cs_2CO_3 + 2\ H_3PMo_{12}O_{40} \rightarrow 2\ Cs_3PMo_{12}O_{40} + 3\ CO_2\uparrow + 3\ H_2O \qquad (9)$$

The CPM support was prepared by a controlled precipitation method. In a typical synthesis, the colourless aqueous solution of Cs_2CO_3 (0.1 M) was added into the yellow aqueous solution of $H_3PMo_{12}O_{40}$ (0.1 M) under vigorous stirring at 45 °C. The addition flowrate was controlled by a pump at 2 mL/min. A yellow suspension was obtained and the solid was recovered by removing the water under reduced pressure after stirring for 2 h. The samples were further dried at 70 °C for 24 h, then calcined at 350 °C under static air for 3 h with a heating ramp of 2 °C/min. Finally a dark greenish solid was obtained.

The structure was verified by FT-IR, and the textural properties were determined by N_2 adsorption/desorption measurement. Both results were gathered in Annex (*cf. section 6.1.5*).

Table 2-3 Amounts of the reactants used for $Cs_3PMo_{12}O_{40}$ (CPM) preparation by precipitation method

Reactant	Mole ratio	Mole, mol	Mass, g
Cs_2CO_3 (0.1 M)	1.5	0.0071	2.30
$H_3PMo_{12}O_{40}$ (0.1 M)	1	0.0047	9.69
H_2O for Cs_2CO_3 solution		2.61	(47.06 mL)
H_2O for $H_3PMo_{12}O_{40}$ solution		7.83	(141.2 mL)

2.3.3 Preparation of the catalysts

2.3.3.1 <u>Active phase: $(NH_4)_3HPMo_{11}VO_{40}$ (APMV)</u>

Bulk APMV was prepared by a co-precipitation method at 45 ^{o}C according to equation (10) using stoichiometric amounts (Table 2-5).

$$3\ NH_4NO_3 + H_4PMo_{11}VO_{40} \rightarrow (NH_4)_3HPMo_{11}VO_{40} + 3\ HNO_3 \qquad (10)$$

In a typical procedure, the NH_4NO_3 (0.05 M) and $H_4PMo_{11}VO_{40}$ (0.05 M) solutions were pumped (2 mL/min) into 35 mL of deionized water under stirring. After reacting for 2 h the precipitated solid was recovered by evaporating the solvent under reduced pressure at 70 ^{o}C. The sample was further dried at 70 ^{o}C for 24 h, then calcined at 350 ^{o}C (2 ^{o}C/min) for 3 h to obtain the final catalyst.

Table 2-4 Amounts of the reactants used for bulk APMV preparation by co-precipitation method

Reactant	Mole ratio	Mole, mol	Mass, g
NH_4NO_3 (0.05 M)	3	0.0011	0.26
$H_4PMo_{11}VO_{40}$ (0.05 M)	1	0.0033	2.10
H_2O for NH_4NO_3 solution		1.21	(22 mL)
H_2O for $H_4PMo_{11}VO_{40}$ solution		3.63	(66 mL)

2.3.3.2 <u>$(NH_4)_3HPMo_{11}VO_{40}$ (APMV) formed *in situ* on silica-based carriers (SiO$_2$, SBA-15 and ZrO$_2$/SBA-15)</u>

The series of silica-supported catalysts was prepared by a 2-step incipient-wetness impregnation method. The commercial CARiACT$^®$ SiO$_2$, the prepared SBA-15 and the ZrO$_2$/SBA-15 were used as supports. In the first step, an appropriate amount of aqueous solution (whose volume depended on the support) containing 1.26 g $H_4PMo_{11}VO_{40}$ to get 40

wt.% of HPMV/support was added to the 1.8 g support in case of preparation of 3 g of catalyst. After drying at ambient temperature the solid was calcined at 200 °C for 2 h under static air. In the second step the as-prepared HPMV/support solids were impregnated with NH_4NO_3 (0.16 g) solution for protons to be exchanged by ammonium ions using the same protocol as for the first step. The samples were denoted as APMV/SiO$_2$, APMV/SBA-15 and APMV/ZrO$_2$/SBA-15, respectively.

2.3.3.3 Mixed $Cs_x(NH_4)_{3-x}HPMo_{11}VO_{40}$ salts

The mixed salts $Cs_x(NH_4)_{3-x}HPMo_{11}VO_{40}$ (x = 3, 2.5, 1.7, 1.5 and 0.5) were prepared by precipitation method. In a typical procedure of $Cs_{1.7}(NH_4)_{1.3}HPMo_{11}VO_{40}$, 1.9 g of acid $H_4PMo_{11}VO_{40}$ was dissolved at 45 °C in 20 mL of deionized water to obtain a 0.05 M solution. Then the solutions of Cs_2CO_3 (0.27 g, 0.05 M) and $(NH_4)_2CO_3$ (0.06 g, 0.05 M) were added into the acidic solution by two pumps with a flow-rate of 2 mL/min under vigorous stirring. The reaction lasted 18 h and the solid was recovered by evaporating water at 70 °C under reduced pressure. After drying, the final catalyst was obtained after thermal treatment at 350 °C for 3 h. The samples were denoted as $Cs_x(NH_4)_{3-x}H$ (x = 3, 2.5, 1.7, 1.5 and 0.5).

2.3.3.4 APMV supported on CPM

The series of APMV catalysts supported on caesium-phosphomolybdic acid (APMV/CPM) with various amounts of APMV (10-50 wt.%) was prepared by deposition-precipitation method. The CPM particles were suspended in 35 mL of deionized water at 45 °C with vigorous stirring for 1 h. Then the aqueous solutions of NH_4NO_3 and $H_4PMo_{11}VO_{40}$ were pumped into the suspension simultaneously. After reacting for 2 h the solid was recovered by removing the water under reduced pressure at 70 °C, and further dried at the same temperature for another 24 h. Finally the catalysts were calcined at 350 °C for 3 h under static air. The prepared samples were denoted as xAPMV/CPM (x = 10, 20, 40 and 50), where x was the amount of active phase in wt.% .

Table 2-5 Amounts of the reactants for bulk APMV preparation by co-precipitation method

Reactant	Mole ratio	Mole, mol	Mass, g
NH_4NO_3 (0.05 M)	3	0.0011	0.26
$H_4PMo_{11}VO_{40}$ (0.05 M)	1	0.0033	2.10
H_2O for NH_4NO_3 solution		1.21	(22 mL)
H_2O for $H_4PMo_{11}VO_{40}$ solution		3.63	(66 mL)

2.4 Methods of characterisation of the catalysts

2.4.1 Thermogravimetric analysis

Thermogravimetric analysis (TGA) was performed using TA instruments (model 2960 SDT, V3.0F) to study the thermal decomposition behaviour of the fresh catalyst. The catalyst was heated from room temperature to 700 °C with a rate of 3 °C/min under air flow. A mass spectrometer was also employed for detecting the effluent gases and analysing the products of decomposition.

2.4.2 Nitrogen adsorption/desorption

The N_2 adsorption/desorption was used to characterize the textural properties of the materials. The surface area and total pore volume were measured by a Micromeritics ASAP 2010 analyser at liquid nitrogen temperature. The samples were degassed at 150 °C for 3 h prior to analysis. The specific surface area (S_{BET}) was calculated using B.E.T. method. The total pore volume (Vp) was determined using the value at relative pressure (P/P$_0$) of 0.995.

2.4.3 Fourier transformed infrared spectroscopy

Infrared spectra (FT-IR) were recorded on a Thermo Nicolet 480 apparatus equipped with a MCT detector. The samples (1 wt.%) were pressed to form KBr pellets for analysis and the

spectra were recorded from 400 to 4000 cm^{-1} with a spectral resolution of 4 cm^{-1} and 256 scans.

2.4.4 Raman spectroscopy

Raman spectra were measured on a Jobin-Yvon LabRam Infinity apparatus equipped with a CCD detector operating at liquid nitrogen temperature. A D2 filter was used to protect the catalyst structure from destruction by the laser (wavelength λ=520 nm). The Raman shift was recorded in the range of 200-1400 cm^{-1}. The homogeneity of the samples was evaluated by performing the analysis on at least 3 different locations for each sample.

2.4.5 X-ray diffraction

The crystal structure of the catalysts was revealed by X-ray diffraction (XRD) technique on a Bruker D8 Advance diffractometer, using CuKα radition (λ = 1.5506 Å) as X-ray source. A 10° < 2θ < 80° range was scanned with step of 0.02 °/s and 2 s acquisition time. The crystallite size is estimated by the Scherrer's equation:

$$L = \frac{0.89\lambda}{\beta(\theta)\cos(2\theta)}$$

(11)

where L is the crystallite size, λ is the wavelength of the radiation, θ is the Bragg diffraction angle and $\beta(\theta)$ is the full width at half maximum (FWHM) [4, 5].

The XRD measurement employing a programed-temperature was carried out on D8 Advance (Bruker AXS) under a reducible gas flow (3 v.% H_2 in N_2), the sample was heated from ambient (Amb.) to 700 ^{o}C with a heating rate of 10 ^{o}C/min.

2.4.6 X-ray photoelectron spectroscopy

Surface analyses by X-ray photoelectron spectroscopy (XPS) were carried out in a Kratos

Axis Ultra DLD apparatus equipped with a hemispherical analyser and a delay line detector (see Figure 2-5). Experiments were performed using an Al mono-chromated X-ray source (10 kV, 15 mA) with a pass energy of 40 eV (0.1eV/step) for high resolution spectra and a pass energy of 160 eV (1eV/step) for the survey spectrum in hybrid mode and slot lens mode respectively.
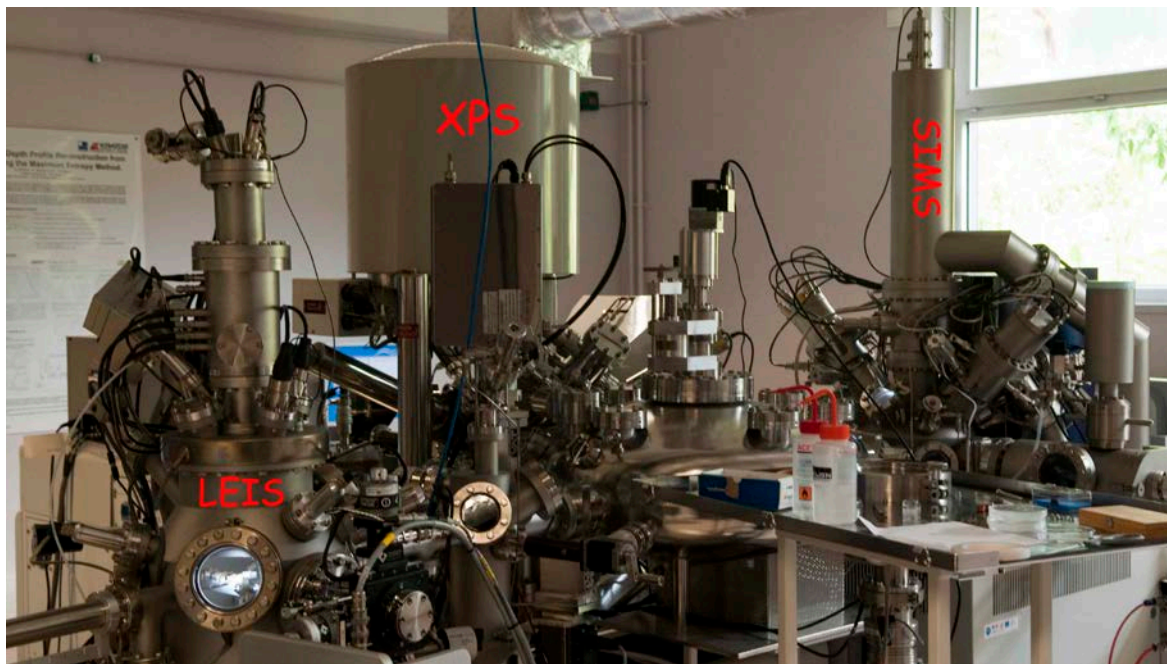
Figure 2-5 Surface analysis platform of UCCS

2.4.7 Temperature-programmed desorption of ammonia

Ammonium temperature-programmed desorption (NH_3-TPD) was employed in order to measure the amount and strength of the acidic sites of the catalysts. A typical test was done as follows: 50 mg of catalyst were pre-treated in a He flow (30 mL/min STP) at 250 °C for 2 h in order to remove the physisorbed water and the crystal water. Then the sample was cooled down to the adsorption temperature (130 °C) and NH_3 was absorbed at the surface by pulsed injections at 130 °C until saturation. The TPD profiles were monitored by a thermal conductivity detector and recorded from 130 to 700 °C at a heating rate of 10 °C/min.

2.4.8   Temperature-programmed reduction

The reducibility of the catalysts was evaluated by temperature-programmed reduction (TPR) at atmospheric pressure. 100 mg of the samples were loaded into a quartz reactor and pre-treated by a He flow (30 mL/min STP) at 100 °C for 2 h. Then helium was replaced by the reductive gas H_2/He (5 mol% H_2 in He) at the same flow-rate of 30 mL/min. The temperature of the reactor was increased linearly from 100 to 800 °C at a rate of 5 °C/min. The effluent gas was analyzed by a thermal conductivity detector (TCD).

References

[1]   T. Ressler, U. Dorn, A. Walter, S. Schwarz, A. H. P. Hahn, J. Catal. 275 (2010) 1.

[2]   C. J. Brinker, Y. Lu, A. Sellinger, H. Fan, Adv. Mater. 11 (1999) 579.

[3]   B. Katryniok, S. Paul, M. Capron, C. Lancelot, V. Bellière-Baca, Green Chem. 12 (2010) 1922.

[4]   T. Okuhara, H. Watanabe, T. Nishimura, K. Inumaru, M. Misono, Chem. Mater 12 (2000) 2230.

[5]   F. Jing, Y. Zhang, S. Luo, W. Chu, H. Zhang, J. Chem. Sci. 122 (2010) 621.

3 Textural and structural properties of the catalysts

Parts of this chapter are published in:

"Improvement of the catalytic performance of supported $(NH_4)_3HPMo_{11}VO_{40}$ catalysts in

isobutane selective oxidation", F. Jing, B. Katryniok, E. Bordes-Richard, S. Paul

Catalysis Today 2012, on-line, DOI : 10.1016/j.cattod.2012.03.028

3.1 Dispersion of the APMV active phase on various supports

3.1.1 Introduction

Keggin-type heteropolycompounds are usually used to catalyse selective oxidation reactions because of their strong and tuneable acidity and redox properties [1]. Catalytic oxidation of isobutane using Keggin-type polyoxometallates as catalyst belongs to the surface-type reaction, and in this context their low surface area becomes an obvious drawback for their application [2]. In order to get a higher surface area, the active phase $(NH_4)_3HPMo_{11}VO_{40}$ (APMV) was supported on various carriers including commercial CARiACT$^®$ SiO_2, SBA-15, ZrO_2/SBA-15 and $Cs_3PMo_{12}O_{40}$ (CPM) with an identical loading of 40 wt.%. The catalyst APMV/SiO_2, APMV/SBA-15 and APMV/ZrO_2/SBA-15 were prepared by a 2-step incipient wetness impregnation method described in Chapter 2. The APMV/CPM sample was prepared by deposition-precipitation technique in regard of the lower surface area of the support. The detailed procedure is also reported in Chapter 2. The thermal stability, textural properties, structure, crystallite phases and acidity were studied by TGA, N_2 adsorption/desorption, FT-IR and Raman, XRD and NH_3-TPD techniques. In this part we would be focused on the influence of the support on the structural and textural properties of the catalysts. Finding the key factors to establish correlations between the catalysts properties and the catalytic performance is obviously of main importance.

3.1.2 Characterization results and discussion

3.1.2.1 Evolution of the fresh catalysts during thermal treatment

Thermogravimetric analysis (TGA) was employed to monitor the thermal decomposition of the fresh bulk and supported APMV catalysts under the conditions of calcination.

For bulk APMV sample, a continuous loss of weight was observed from 50°C to 430 °C. The thermogram clearly displayed four steps (Figure 3-1). The DTG curve of APMV showed several positive peaks at *ca*. 60, 152, 386 and 424 °C respectively and one negative peak at 445 °C (Table 3-1). By analogy with what was observed in other studies for other ammonium-salified HPA like $(NH_4)_3PMo_{12}O_{40}$ and $(NH_4)_5[PMo_{11}V^{IV}O_{40}] \cdot 9H_2O$ [3], the first and second steps at *ca*. 60 and 152 °C (up to 215 °C after TG curve) were ascribed to the loss of physisorbed (or loosely bound) water and of crystal water, respectively [4]. Above 215 °C, anhydrous APMV lost weight quite continuously up to 420 °C, and regained some weight in a very short temperature range (negative DTG peak at 424 °C). Two main steps could be hypothesized for the decomposition of anhydrous APMV. The first step consisted of the release of ammonia gas (*ca*. 386 °C) produced by decomposition of the ammonium counter-cations then yielding $H_4PMo_{11}VO_{40}$ heteropolyacid, and the second step was ascribed to the elimination of acidic protons in the form of constitutional water (at about 430 °C) leading to the Keggin-type $PMo_{11}VO_{38}$ mixed oxide. The change of slope corresponding to the theoretical loss of weight (2.74%) for the first step $(NH_4)_3HPMo_{11}VO_{40} \rightarrow H_4PMo_{11}VO_{40}$ (shoulder in DTG) was at *ca*. 380 °C. As TGA was carried out in air, the final gain of weight (0.4%) corresponded to the re-oxidation of V^{4+} (theoretically 0.4%) to V^{5+} suggesting that V could be reduced by the NH_3 released. The total weight loss of 5.0% was close to the calculated theoretical value of 4.7%. Above 640 °C $PMo_{11}VO_{38}$ (PMV) was finally decomposed to the corresponding simple metal oxides, and MoO_3 began to sublimate [4].

For supported APMV samples, the same decomposition pathway was observed but the phenomena occurred at different temperatures with respect to bulk APMV. Indeed, the formation of HPMV was observed also at 286 °C for $APMV/SiO_2$, it is observed at 334 °C for APMV/SBA-15, 328 °C for $APMV/ZrO_2/SBA-15$ and at 370 °C for APMV/CPM. Therefore the protonation of APMV occurs at equal or slightly lower temperature when SiO_2-based support is used whereas it occurs at higher temperature when the CPM support is used. In other words, the CPM support stabilizes the APMV phase whereas the SiO_2-based support had no effect or a slightly negative impact on the APMV stability. In the third step, the

decomposition of the anhydrous active phase, the loss of weight increased along the CPM (1.44%) < ZrO$_2$/SBA-15 (1.95%) < SBA-15 (2.28%) < SiO$_2$ (2.77%) series of supports. In view of these results, the CPM support showed once again the best ability in stabilizing the active phase APMV.
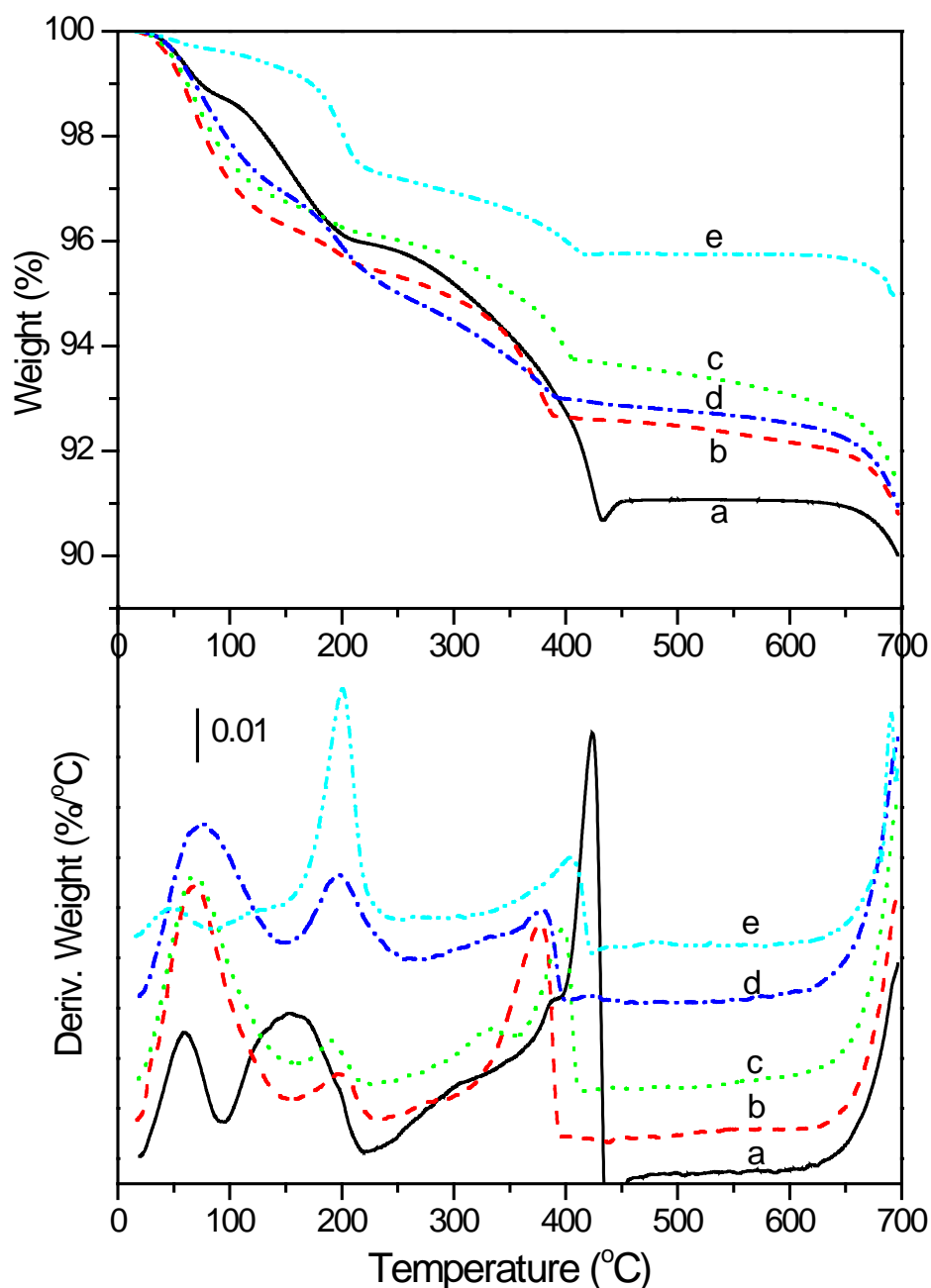
Figure 3-1 Thermogravimetric analysis of catalysts (TG, up) and (DTG, down) (a: bulk APMV, b: APMV/SiO$_2$, c: APMV/SBA-15, d: APMV/ZrO$_2$/SBA-15, e: APMV/CPM)

When APMV was supported on CPM, the crystal water was also eliminated at higher temperature 200 °C. The re-oxidation of V^{4+} to V^{5+} was still observed at *ca.* 424 °C. When 40 wt.% APMV was supported on other silica supports like SiO_2, SBA-15 or ZrO_2/SBA15, the decomposition in simple oxides of HPMV occurred at about 10-20 °C lower. Therefore, using CPM supports would be a good compromise between a correct dispersion of active species and their stabilisation.

Table 3-1 Temperature and weight loss during thermal decomposition

Sample	Loose water		Crystal water		APMV → HPMV		HPMV → MPV	
	T (°C) [a]	Δm/m	T (°C)	Δm/m	T (°C)	Δm/m	T (°C)	Δm/m
APMV	60	1.3	152	2.7	386	3.0	424	2.3
							445 [b]	0.4
APMV/SiO$_2$	69	3.7	200	0.8	286	0.7	398	2.1
APMV/SBA-15	69	3.3	190	0.6	334	1.1	397	1.2
APMV/ZrO$_2$/SBA-15	76	3.1	197	2.0	328	1.1	379	0.8 [c]
APMV/CPM	48	0.3	200	2.5	ca. 370	0.9	408	0.5
							424 [b]	0.1

[a]: DTG curve; [b]: weight gain (see text); [c]: loss for APMV → MPV step

3.1.2.2 Specific surface area and coverage

The specific surface areas of the supports and catalysts, obtained by nitrogen physisorption, are gathered in Table 3-2. As expected, the impregnation leads to a decrease of the BET surface area compared to those of the support. The surface area of the catalysts decreases along the APMV/SBA-15 > APMV/ZrO$_2$/SBA-15 > APMV/SiO$_2$ > APMV/CPM series. When comparing the experimental values with the theoretical calculated ones (*cf. section 6.2 in the Annex*), one can see that the impregnation with APMV leads to a slighter lower decrease than the predicted one when using silica supports. Therefore one can assume

that the porous structure of the support is partially blocked by APMV. Nevertheless, the difference is rather small ranging from 11 m²/g (APMV/SBA-15) to 20 m²/g (APMV/ZrO$_2$/SBA-15), whereby one still can assume a rather homogeneous distribution of APMV on the support. On the other hand, the experimental BET surface of CPM-supported catalyst is higher than predicted theoretically. This is ascribed to the deposition-precipitation method, where the APMV are hierarchically stacked and thus generated a porous multi-layer on the support surface. The corresponding catalyst thus shows an increase of its pore-volume from 0.09 mL/g for the bare CPM support to 0.11 mL/g for the APMV/CPM support (*cf. Table 6-1 in Annex section 6.2*).

The average value of the coverage of the same mass of APMV on the different supports (40 wt.%) was calculated based on a Keggin unit occupancy of 1.44 nm^2 [5]. In Table 3-2 is reported the average theoretical coverage of the support as the number of active phase layers stacking on the surface. The dispersion of the active phase is schematized in Figure 3-2. Whereas APMV/SBA-15 and APMV/ZrO$_2$/SBA-15 exhibited sub-monolayer coverage (0.5 and 0.6 respectively), a theoretical APMV monolayer was reached on CARiACT®-SiO$_2$ (1.1). As the surface area of CPM was low (22 m^2/g), APMV/CPM catalyst exhibited a multi-layer coverage (14.4 layers). This multi-layer coverage might account for the thermal stability of APMV when supported on CPM as found in TGA experiments, and could make the whole properties of the catalyst to be closer to those of bulk APMV.

Table 3-2 Specific surface area of the supported catalysts and coverage of APMV

Catalyst	$S_{BET, sup.}$, m^2/g bare support	$S_{BET, cat.}$, m^2/g catalyst	Theoretical average coverage, layer
APMV/SBA-15	632	368 [379] [a]	0.5
APMV/ZrO$_2$/SBA-15	512	287 [307] [a]	0.6
APMV/SiO$_2$	295	159 [177] [a]	1.1
APMV/CPM	22	17 [13] [a]	14.4

[a] values in brackets are calculated theoretically according to the methodology described in the Annex (*cf. section 6.2*)
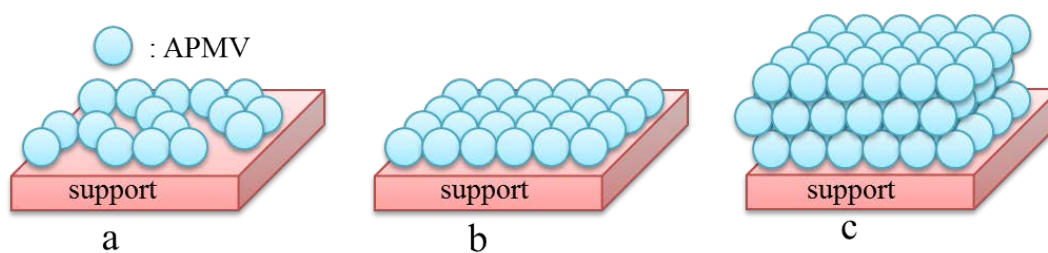
Figure 3-2 Schematics of dispersion of APMV active phase on the support
(a: partial covering, b: monolayer, c: multilayer)

3.1.2.3 Structural analysis by FT-IR and Raman spectroscopies

The presence of the APMV structure was checked using the FT-IR technique. All samples exhibited the characteristic Keggin bands at 1062, 963, 865 and 798 cm^{-1} (Table 3-3), which were attributed to the asymmetric stretching of P-O bond of PO$_4$ tetrahedron, the asymmetric stretching of peripheral Mo=O bond and the Mo-O-Mo stretching mode of inter- and intra-octahedral bridges of tri-metallic group, respectively [6, 7]. It is known from literature that vanadium substituted phosphomolybdic acid generally exhibits a characteristic splitting shoulder peak at about 1080 cm^{-1} resulting from the decrease of the oxo-anion symmetry [8]. This was not observed for our samples. The reason could be the formation of non-substituted phosphomolybdic acid (H$_3$PMo$_{12}$O$_{40}$) during the catalyst preparation or the elimination of V from the Keggin unit during the calcination step at 350 °C, as proposed by Sultan *et al*. [6]. The latter hypothesis was notably confirmed by the presence of a shoulder at about 1035 cm^{-1} which was attributed to isolated vanadium oxide (VO$_x$) [9], suggesting the migration of vanadium from the primary to the secondary structure during calcination. Finally, the presence of ammonium cations was confirmed by its characteristic band at 1414 cm^{-1} for bulk APMV and at 1416 cm^{-1} for supported APMV [10].
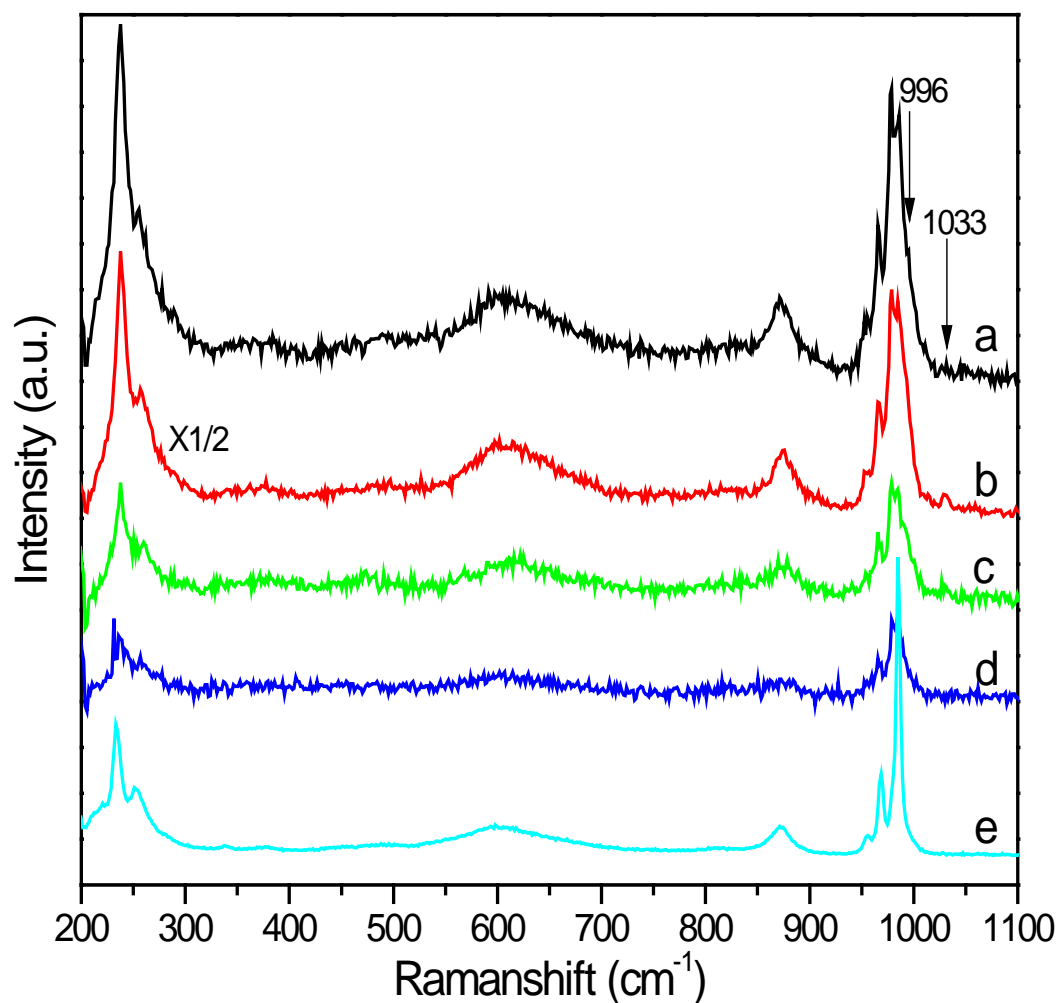
Figure 3-3 Raman spectra of bulk APMV and of the supported APMV
(a: bulk APMV, b: APMV/SBA-15, c: APMV/ZrO$_2$/SBA-15, d: APMV/SiO$_2$, e: APMV/CPM)

Table 3-3 Characteristic vibration FT-IR bands of supported catalysts

Catalyst	Wavenumber, cm^{-1}				
	v_{as} N-H	v_{as} P-O$_a$	v_{as} Mo=O$_d$	v_{as} Mo-O$_b$-Mo	v_{as} Mo-O$_c$-Mo
APMV/SBA-15	1416	1062	963(1036)	865	798
APMV/ZrO$_2$/SBA-15	masked	1062	963 (broad)	865	798
APMV/SiO$_2$	1416	1062	963 (1035)	866	798
APMV/CPM	1416	1062	969 (1035)	868	798
APMV	1414	1062	963 (1035)	865	788

Raman spectra of the calcined solids (Figure 3-3) confirmed the integrity of the APMV

structure, as shown by the well-known bands assigned to the following vibrations: v(Mo=O$_d$)

at 985 and 967 cm^{-1}, v(P-O) at 956 cm^{-1}, v(Mo-O-Mo) at 873 and 600 cm^{-1} and δ(Mo-O-Mo) at 256 and 237 cm^{-1} [11], respectively. Furthermore, the characteristic shoulders at 996 cm^{-1} and 1033 cm^{-1} were assigned to the formation of MoO_3 and vanadic species, respectively [9, 12]. Although this finding suggested the decomposition of APMV heteropolyanion and its structural reorganization, the extent of decomposition was very limited according to the intensity of the corresponding peaks and quite null in the case of APMV/CPM catalyst. The combined FT-IR and Raman results showed that a slight partial decomposition of active phase could take place during the catalyst thermal treatment. This decomposition was more pronounced for the bulk APMV and silica-based supported APMV as compared to the CPM supported samples – as already suggested by TGA measurements.

3.1.2.4 Evolution of the crystalline phases observed by temperature-programmed XRD technique in reductive conditions

The reduction of the catalysts by hydrogen was monitored by temperature-programmed XRD from room temperature up to 700 °C (Figure 3-4). At room temperature (Figure 3-4d) the catalysts exhibited the characteristic pattern of APMV with diffraction peaks at $2\theta = 10.6°$, 18.5°, 24.1°, 26.1°, 30.6°, 36.0° and 39.3° [13, 14]. Additionally, weak reflections at 28.5° and 34.4° were detected for APMV, APMV/SiO_2 and APMV/SBA-15 and could be assigned to orthorhombic MoO_3 [10]. Therefore in these cases it can be concluded that APMV had already been partially decomposed during the catalyst preparation. In the pattern of the APMV/CPM sample, the characteristic peaks of the Keggin-type structure were strong. This observation was related to the CPM support which – of course – also exhibited Keggin structure.
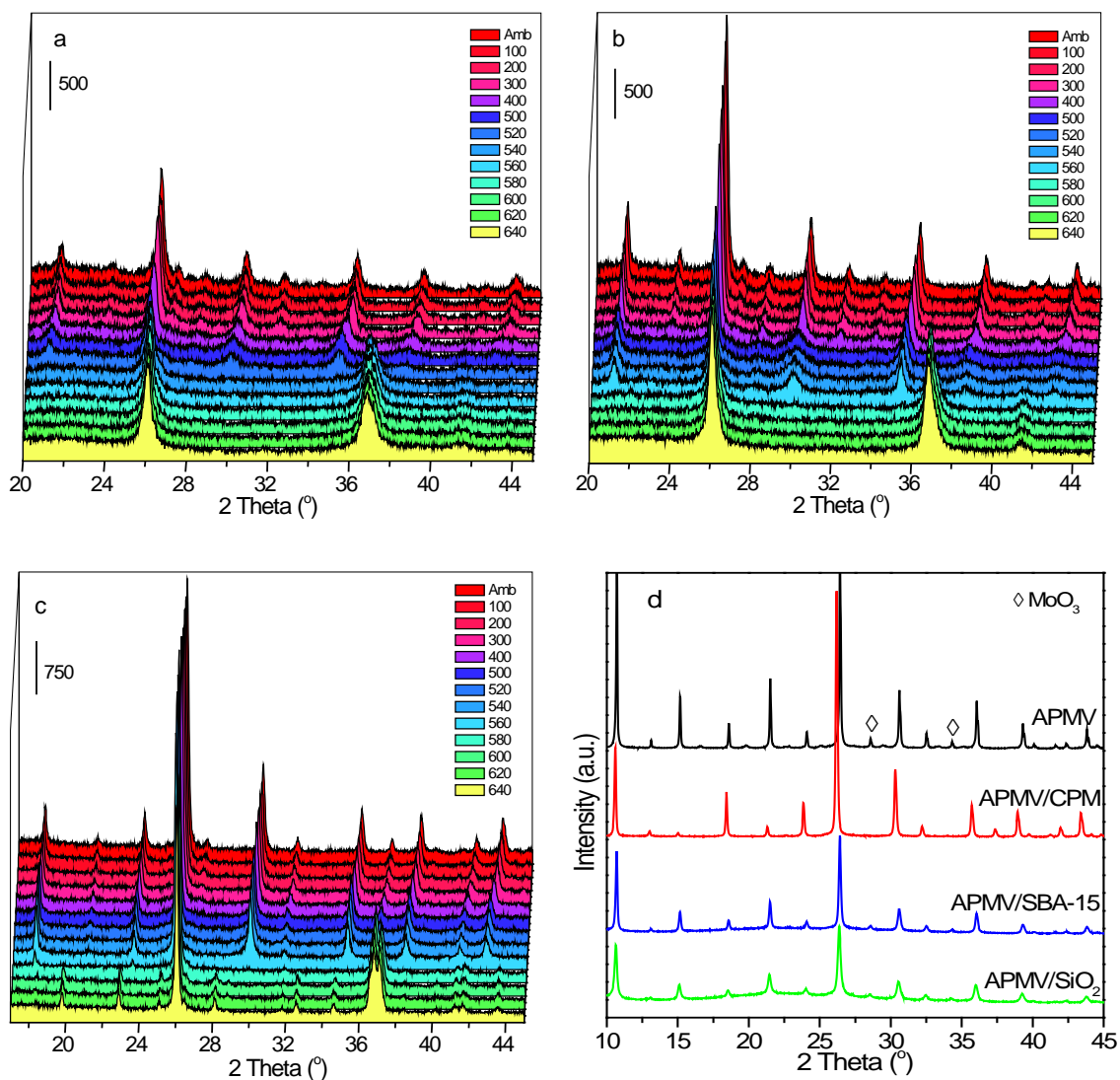
Figure 3-4 Structural evolution of the catalysts determined by XRD in reductive atmosphere
(a: APMV/SiO$_2$, b: APMV/SBA-15, c: APMV/CPM, d: XRD patterns of obtained at room temperature)

In order to discriminate the lines belonging to CPM from those belonging to the active phase we have further focused on the two diffraction peaks at $2\theta = 15.1°$ and $21.5°$ which are characteristic of APMV, and on the peak at $2\theta = 37.2°$ which is characteristic of CPM structure. As the temperature increased, the structure of the catalysts changed. For APMV/SiO$_2$ (Figure 3-4a), the intensity of the aforementioned diffraction lines decreased successively and finally disappeared at about 540 °C, thus suggesting a continuous decomposition of APMV with increasing temperature. At the same time two new diffraction peaks appeared at 36.5° and 36.7° which were assigned to MoO$_2$. The formation of MoO$_2$ could be explained by the reduction of the decomposition product MoO$_3$. A similar continuous

decomposition process was observed with APMV/SBA-15 (Figure 3-4b), but the temperature of degradation was shifted to 560 °C. The same behaviour was stated for APMV/CPM (Figure 3-4c). The decomposition occurred at 580 °C but additional diffraction lines at $2\theta = 24.2°$, 27.2° and 31.7°, besides those of MoO_2, were ascribed to the formation of caesium oxide originating from the decomposition of CPM support. These XRD experiments showed that the temperature of complete decomposition of APMV in reducing atmosphere depended on the support and followed the order APMV/SiO_2 (540 °C) < APMV/SBA-15 (560 °C) < APMV/CPM (580 °C). According to the above results, the CPM support showed once again a stronger capacity in stabilizing the active phase, which confirmed the results obtained by the FT-IR and Raman spectroscopies (*cf. section 3.1.2.3*) and TGA analysis (*cf. section 3.1.2.1*).

3.1.2.5   Nature and strength of the acid sites

The amount of acidic sites was determined by NH_3-TPD measurement. The desorption temperature profiles were plotted in Figure 3-5 and the quantitative calculation for the NH_3 uptake were collected in Table 3-4. No desorption peak could be found over the CPM support, suggesting the total absence of acidic sites. For the three silica-supported catalysts, at least four NH_3 desorption steps were observed. They were ascribed to weak acidic sites (100-300 °C), medium acidic sites (300-450 °C), strong acidic sites (450-560 °C) and super strong acidic sites (560-700 °C). As part of the released ammonia could originate from the decomposition of APMV active phases at temperatures higher than 350 °C, the amount of released ammonia from the active phases were corrected by these values, obtained from the TG analyses (calculations detailed in Annex *section 6.3*). Data in Table 3-4 showed that the total acidity increased along SBA-15 (0.87 mmol/$g_{cat.}$) < ZrO_2/SBA-15 (1.22) < SiO_2 (1.54) < CPM (1.80). When calculating the density of acidic sites on the surface, the highest value, 105.6 µmol/m^2_{cat}, was obtained for APMV/CPM catalyst, which was explained by its low specific surface area (17 m²/g). The catalysts differed mainly by the amount of strong and very strong acidic sites. Strong sites were mainly (80%) found on APMV/SiO_2, at variance of

APMV/SBA-15 (ca. 77% medium and strong sites). No strong or very strong sites were detected for APMV/ZrO$_2$/SBA-15 as no ammonia was desorbed at temperatures higher than 500 °C, while for APMV/CPM the strong and super strong sites were predominant with 49% and 36%, respectively. Therefore, as expected, the distribution of the acid sites on the active phase was significantly influenced by the properties of the support. However the highest number of acidic sites was not found for the silica-supported catalysts but for the one supported on Cs$_3$PMo$_{12}$O$_{40}$.
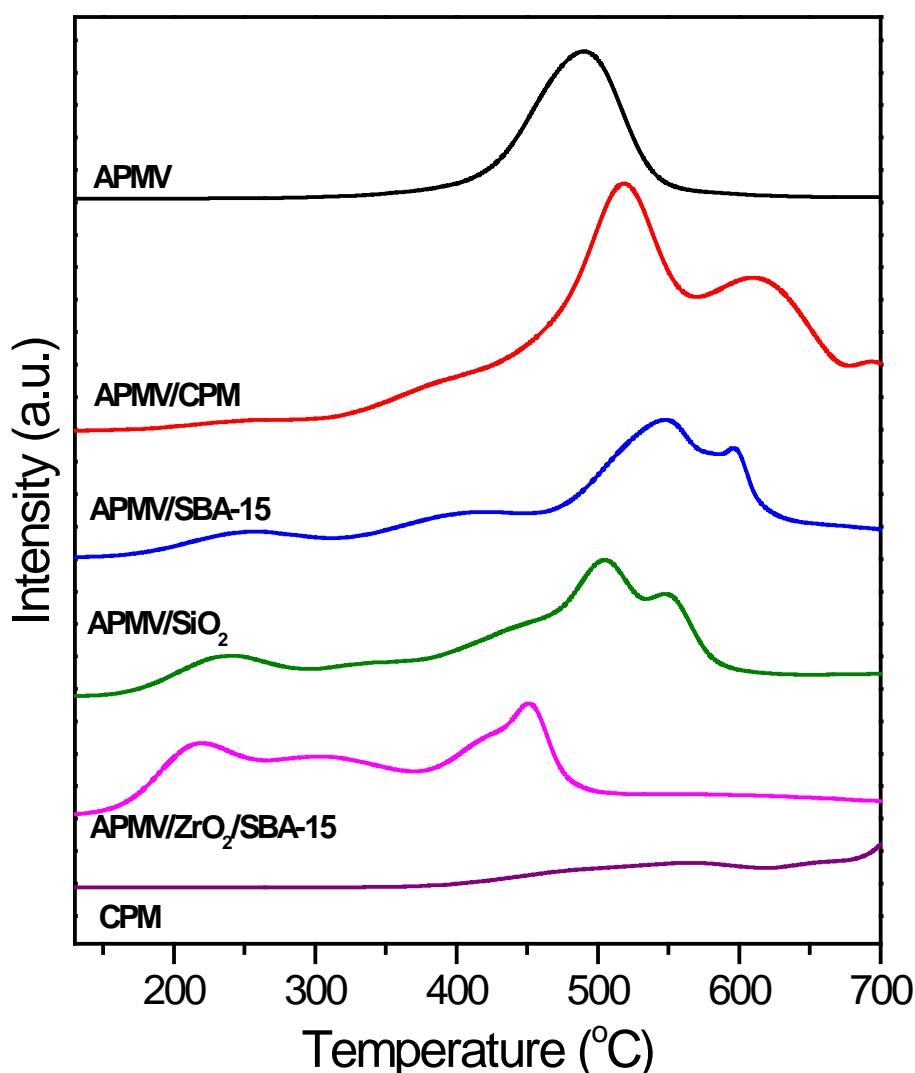

Figure 3-5 NH$_3$-TPD profiles of the supported catalysts

Table 3-4 Amount of acidic sites and distribution of acid strength

Catalyst	Acidity, NH$_3$ uptake, μmol/m^2 cat. (mmol/g cat.)				Total acidity μmol/m^2 (mmol/g)
	130-300°C weak	300-450°C medium	450-560°C strong	560-700°C very strong	
APMV	-	-	550 (2.2)	-	550 (2.2)
APMV/CPM	2.9 (0.05)	12.4 (0.21)	52.4 (0.89)	38.2 (0.65)	105.9 (1.80)
APMV/SiO$_2$	1.1 (0.17)	0. 9 (0.14)	7.76 (1.23)	-	9.7 (1.54)
APMV/ZrO$_2$/SBA-15	2.1 (0.6)	2.2 (0.62)	-	-	4.3 (1.22)
APMV/SBA-15	0.4 (0.16)	1.0 (0.35)	0.9 (0.32)	0.1 (0.03)	2.4 (0.87)
CPM	-	-	trace	trace	trace

3.1.3 Conclusions

Supporting APMV by a carrier was supposed not only to disperse but also to stabilize the active phase and of course at the end to enhance its catalytic properties. However, the influence of supporting APMV on carriers differing by their chemical nature (silicas *vs.* Keggin-type salt) and their textural properties (mesoporous *vs.* microporous) was found to be plural. As a matter of fact, as shown by physicochemical analyses, the thermal stability of the active phase was strongly affected by the coverage. Sub-multilayers – as observed for SBA-15 and commercial CARIACT$^®$ SiO$_2$ were found rather unfavourable to stability. Multilayer dispersion on CPM support resulted in surface properties much closer to those of bulk APMV but with an improved thermal stability. Therefore, as often found in selective oxidation of hydrocarbons to highly oxidized products (e.g., anhydrides or carboxylic acids), a given thickness of the active phase layers, which preserved its surface as well as its bulk structure and thus ensures its easy re-oxidation at each catalytic cycle, was necessary. Moreover, the surface acid density and distribution of acid strength that will play a strong role on the catalytic activity whereas the latter was strongly affected by the type of support used. One would have expected that the strong and very strong sites, would have been observed with silicas and not when APMV was supported on the CPM support. XRD, FT-IR and Raman spectroscopies suggested that APMV was decomposed to a more or less great extent

depending on the carrier. In the worse cases, particles of unselective metal oxides such as MoO_3 and VO_x were observed. As TGA and XRD suggested that the decomposition of APMV when supported on CPM was limited, these strong acid sites could be related to the presence of $H_4PMo_{11}VO_{40}$ at the steady state.

3.2 Influence of the APMV loading on CPM support

3.2.1 Introduction

In the previous part, we have shown that the protonated ammonium salt of 11-molybdo-1-vanadophosphoric acid, $(NH_4)_3HPMo_{11}VO_{40}$ (APMV) could be dispersed on different supports such as SiO_2, SBA-15, ZrO_2/SBA-15 and $Cs_3PMo_{12}O_{40}$ (CPM). Compared with silica-supported catalysts which were poorly stable, two main effects were observed upon supporting APMV on CPM support: (i) the resulting multilayer dispersion limited the thermal decomposition of the active phases, and (ii) the acidity of surface species was much stronger. To confirm these findings and optimize the properties of APMV/CPM catalyst, a series of catalysts with 10-50 wt.% loading of APMV on CPM was prepared. Their physicochemical properties, their reactivity in reducing atmosphere, and catalytic performances in the isobutane oxidation (see Chapter 4) were studied. The used catalysts were characterized as well in order to get more information about the changes that occured under stream.

3.2.2 Characterization: Results and discussion

3.2.2.1 Thermal decomposition behaviours of the fresh solids

TGA measurements were used to study the thermal decomposition behaviours of the fresh catalysts. Like for the other supported catalysts (*cf. section 3.1.2.1*), a five-step weight loss process was observed over the full temperature range between 50 and 700 °C (Figure 3-6). It consisted of i) the removal of physisorbed water at low temperature (<100 °C), ii) the removal of crystal water between 100 and 250 °C to give anhydrous APMV, iii) the elimination of

ammonium cations forming NH_3 in the range from 230 to 380 °C, iv) the loss of residual protons at around 430 °C to generate the Keggin-type mixed oxides and v) the decomposition of the HPA to the corresponding simple oxides [4, 17]. The details of the process was described in Scheme 3-1, and the quantification for each step was listed in Table 3-5. Hereby one can state that the corresponding temperatures were depending on the catalysts: whereas bare APMV lost its crystalline water at 152 °C, this temperature was significantly increased after supporting on CPM. In fact, for the catalysts 20APMV/CPM and 40APMV/CPM the loss of the crystalline water was observed at 180 and 200 °C, respectively.

The successive removal of ammonium and residual protons took place in the region from 250 to 450 °C as presented in the DTG curves, which implied that the active phase started to decompose under calcination and reaction conditions. It can be assumed that the amount of APMV loaded on the support played a significant role on this process: the lower the content of APMV, the easier the decomposition should occur. However, as shown in Table 3-5, the temperature of ammonium cations loss dropped down to around 370 °C for 40APMV/CPM from 395 °C for the bulk APMV and it became undetectable for the sample 20APMV/CPM. The results were therefore not so clear. It had to be noted moreover that for the lowest amount of APMV loaded on CPM the TGA analysis was within its limits of accuracy.

Similar results as referred in (*cf. section* 3.1.2.1) were observed for the re-oxidation of V^{4+} to V^{5+}, causing the increase of the mass from TG curve. As a consequence, negative peaks were recorded. This was not the case for 20APMV/CPM once again because of the low loading and the detection limits of the TGA.

As the reaction temperature and the ammonia-release temperature were quite close one may speculate whether the active phase was APMV or vanado-phosphomolybdic acid ($H_4PMo_{11}VO_{40}$) when using bare APMV as catalyst. Gathering both degradation processes for the bulk APMV, a total weight loss of 5.0% was obtained from the TG-DTG analysis, which was very close to the calculated theoretical value of 4.8%. The last weight-loss observed at higher temperature (T > 640 °C) was assigned to the final decomposition of the Keggin-type P-Mo-V mixed oxides into the corresponding metal oxides (Scheme 3-1).

$$(NH_4)_3HPMo_{11}VO_{40} \xrightarrow[-3\ NH_3]{380°C} \left[H_4PMo_{11}VO_{40} \right] \xrightarrow[-2\ H_2O]{430°C} PMo_{11}VO_{38} \xrightarrow{>640°C} \begin{array}{l} VO_x \\ MoO_x \\ PO_x \end{array}$$
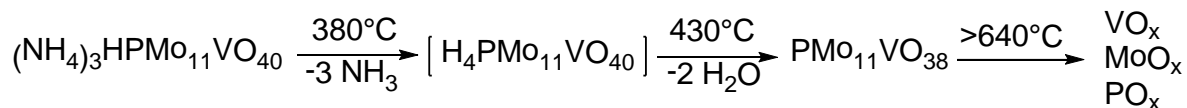
Scheme 3-1 Thermal decomposition process of APMV

Table 3-5 Temperature and weight loss during the thermal decomposition

Sample	Physisorbed water		Crystal water		APMV → HPMV		HPMV → MPV	
	T (°C) [a]	Δm/m	T (°C)	Δm/m	T (°C)	Δm/m	T (°C)	Δm/m
APMV	60	1.3	152	2.7	386	3.0	424	2.3
							445 [b]	0.4
40APMV/CPM	49	0.3	200	2.5	ca. 370	0.9	408	0.5
							424 [b]	0.1
20APMV/CPM	-	-	180	1.3	nd	nd	ca. 400	0.9 [c]

[a]: DTG curve; [b]: weight gain (see text); [c]: loss for APMV → MPV step
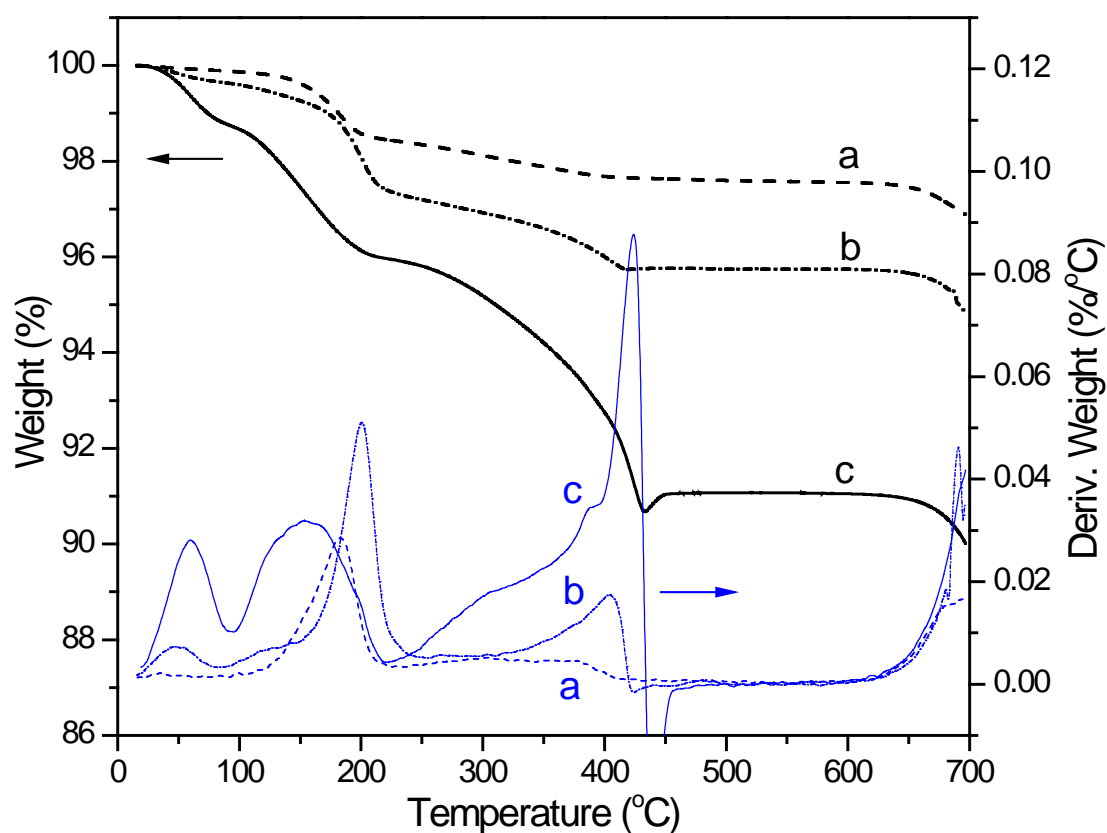

Figure 3-6 TG (black lines) and DTG (grey lines) curves of the fresh samples
(a: 20APMV/CPM, b: 40APMV/CPM and c: bulk APMV)

3.2.2.2 Surface areas and pore volumes of xAPMV/CPM

The surface areas and the total pore volumes of xAPMV/CPM catalysts were gathered in Table 3-6. The specific surface decreased when the amount of APMV increased, from 24 m²/g for x = 10 to 12 m²/g for 50APMV/CPM. As the pore volume decreased also in the same order from 0.12 cm³/g for 10APMV/CPM to 0.08 cm³/g for 50APMV/CPM, this can be ascribed to the subsequent filling of the porous network.

The CPM supported catalysts were also analysed after the catalytic experiment. (Table 3-6). The surface area and pore volume generally decreased when compared to calcined catalysts. The decrease trend depended on the amount of APMV, half of the porous volume being lost for x = 40 and 50 after catalytic experiment, but no more than 25% of porous volume for x = 10 and 20. This can be explained by the formation of larger particles due to sintering, as it will be observed also by XRD in the next paragraph (*cf. section 3.2.2.3*), but the influence of loading meant that sintering could be attributed to APMV whereas CPM should have remained rather unchanged.

Table 3-6 Surface area and pore volume of catalysts with different APMV amounts on CPM

Catalyst	S_{BET}, m²/g		Variation, %	V_p, cm³/g		Variation, %
	Calcined	Spent	$\Delta S_{BET}/S_{BET}$	Calcined	Spent	$\Delta V_p/V_p$
CPM	22	-	-	0.15	-	-
10APMV/CPM	24	17	29	0.12	0.09	25
20APMV/CPM	19	14	26	0.11	0.09	18
40APMV/CPM	17	12	29	0.10	0.05	50
50APMV/CPM	12	11	8	0.08	0.04	50
Calcined APMV	4	2	50	0.02	0.004	80
Calcined HPMV	3	1	67	0.01	0.003	70

3.2.2.3 Crystal phases analysis of the samples before and after catalytic reaction

In the XRD patterns of bulk APMV and APMV/CPM (Figure 3-7), the characteristic reflections of the Keggin-type heteropolycompounds were clearly identified at 2θ=10.6°,

26.4° and 36.0° which were attributed to the (110), (222) and (332) planes for bulk APMV, respectively [14]. The pattern of APMV was first presented by Sultan *et al.* [6]. In addition to the slightly shifted lines cited above, two reflection peaks at $2\theta = 15.1°$ and $21.4°$ are characteristic of APMV. In the case of the CPM supported catalysts, the corresponding reflections (110), (222) and (332) planes were at $2\theta = 10.5°$, $26.1°$ and $35.6°$, values which were closer from those of CPM, while the characteristic lines of APMV shifted to $2\theta = 15.0°$ and $21.2°$. The intensity of these lines decreased with the decreasing amount of APMV (x ≥ 20). Furthermore, the slight shift of the strongest reflections from the plane (222) could be clearly observed upon varying the APMV loading (Figure 3-7, insert). Apart the two characteristic APMV lines, it was not possible to distinguish between the lines of CPM and those of APMV without a detailed Rietveld structural refinement. Unfortunately, as far as we know, the crystal structure of (hydrated) APMV has not been resolved. As said before, the two very characteristic reflection peaks at $2\theta = 15.1°$ and $21.4°$ in bulk APMV were also slightly shifted to $2\theta = 15.0°$ and $21.2°$ for CPM supported catalysts. Their intensity decreased with the amount of active phase but was still detectable down to x = 20. On the other hand, the catalyst 10APMV/CPM no longer exhibited these characteristic peaks of APMV, which may either be due to the low amount of the active phase (10 wt.%) or be due to the decomposition during the calcination. The patterns of supported samples were generally shifted to lower reflection angles, which indicated the increase in *d*-spacing of crystallites.

In addition, the cubic cell parameter *a* was calculated and listed in Table 3-7. It was seen to decrease upon x increase, from 11.8273 Å for 10APMV/CPM to 11.8057 Å for 50APMV/CPM (except 10APMV/CPM, $a = 11.8273$ Å). As $a = 11.8632$ Å for bare CPM support, this trend could be explained by the partial replacement of ammonium of APMV by caesium cations, the ionic radius of which is bigger. Such an exchange could proceed during the preparation of APMV/CPM upon addition of NH_4NO_3 and $H_4PMo_{11}VO_{40}$ to the suspension of CPM particles. Though not exactly by the same process, Marchal-Roch *et al.* [19, 20] synthesized mixed ammonium-caesium $Cs^+_x(NH_4)_{3-x}PMo_{12}O_{40}$ salt by cationic exchange between $CsNO_3$ solution and solid $(NH_4)_3PMo_{12}O_{40}$ during incipient wetness

impregnation. During calcination, the evolution of water and of ammonium at higher temperatures, could as well play a role. In the case of 40APMV/CPM, TG showed that ammonia evolved as $NH_3 + \frac{1}{2} H_2O$ at 350 °C, which offered the possibility to the solid to restructure by generating a mixed ammonium/caesium $H[Cs_x(NH_4^+)_{1-x}]_3PVMo_{11}O_{40}$ salt, or even a compound of the $[Cs_y(NH_4)_{1-y}]_{3-2x}[V^{4+}O]_xPMo_{12}O_{40}$ kind. The caesium-ammonium exchange in the case of $[PMo_{12}O_{40}]$ [19] has not been demonstrated in the same way for vanadium-contained heteropoly-vanadate but certainly the process was complicated by the ability of V to go out from the Keggin unit. Therefore, the replacement of NH_4^+ cations by Cs^+ which exhibited bigger ionic radius could explain the XRD patterns shift of the supported samples.

Table 3-7 Calculated cell parameter for cubic crystals and crystallite size for the fresh and spent catalysts

Catalyst	Cell parameter a, Å			Crystalline size, nm		
	Before reaction	After reaction	Δ, %	Before reaction	After reaction	Δ, %
CPM	11.8632	-	-	-	-	-
10APMV/CPM	11.8273	11.8177	-0.08	49.1	53.1	8.1
20APMV/CPM	11.8472	11.8206	-0.22	55.4	58.3	5.2
40APMV/CPM	11.8155	11.8126	-0.02	62.5	68.5	9.7
50APMV/CPM	11.8057	11.8065	0.01	61.3	64.2	4.7
APMV	11.7113	11.6805	-0.26	>100.0	>100.0	-

The similar shift phenomena were also observed for the spent catalysts (Figure 3-8). After reaction, the Keggin feature of the catalysts was kept well for the all samples, and the characteristic reflections of the active phase APMV (at $2\theta =15.2$ and 21.4^o) were still clear except for the samples containing 10 wt.% active phase. When compared with those of fresh catalysts, the mean crystallite size of the heteropolycompounds estimated with Scherrer equation using (110), (222) and (332) diffraction peaks increased for spent catalysts (Table 3-7). Therefore it could be concluded that APMV crystallites aggregated during reaction. In turn, this sintering effect was responsible for the decrease in the specific surface area and porous volume (*cf. section 3.2.2.2*).

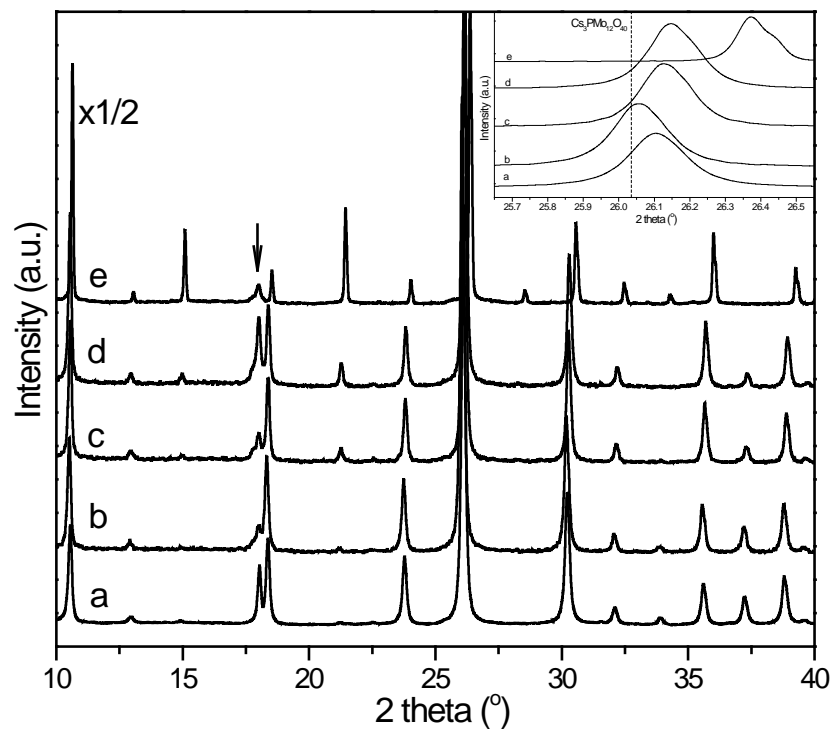Figure 3-7 XRD patterns of the catalysts before experiment

(a: 10APMV/CPM, b: 20APMV/CPM, c: 40APMV/CPM, d: 50APMV/CPM, e: bulk APMV).

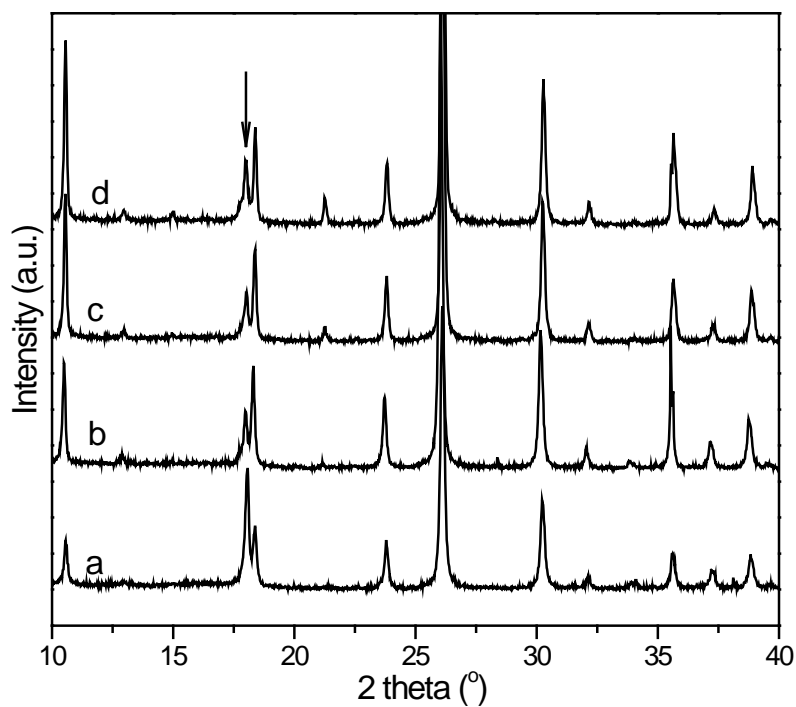The diffraction peaks indicated by arrow were from the Teflon holder.

Figure 3-8 XRD: patterns of the catalysts after experiment

(a: 10APMV/CPM, b: 20APMV/CPM, c: 40APMV/CPM and d: 50APMV/CPM).

The diffraction peaks indicated by arrow were from the Teflon holder.

3.2.2.4 FT-IR and Raman techniques

The FT-IR spectra of APMV/CPM supported catalysts were recorded before and after catalytic experiments and the bands were listed in Table 3-8. The IR spectrum of bulk APMV was also added for comparison. All the catalysts exhibited the typical bands of the Keggin-structure at 1062, 969, 868 and 798 cm^{-1}, which can be attributed to v_{as} P-O of PO_4 tetrahedron, v_{as} Mo=O band, v Mo-O_b-Mo and v Mo-O_c-Mo, respectively [8]. From literature it is known that the substitution of Mo by a V atom induces the oxo-anion symmetry giving rise to a band at about 1080 cm^{-1}. Nevertheless, this signal was not observed, which may be explained by (i) the low amount of vanadium in the final (supported) catalysts or (ii) the elimination of vanadium from the primary structure (Keggin) and its migration to the secondary structure [6, 9]. Some evidences for the last mentioned explanation were found as the spectra exhibited a shoulder peak at 1035 cm^{-1} which was attributed to isolated vanadium oxide ($V^{5+}O_x$) [9]. This seemed further plausible as the according signal increased proportionally with the amount of APMV.

The band at 1416 cm^{-1} for the supported catalysts was assigned to the characteristic vibration of N-H [6, 21]. This band was only observed for catalysts containing more than 20 wt.% APMV. For 10APMV/CPM and 20APMV/CPM samples, the absence of this v_{as} N-H can be explained either by the low amount of APMV or the total decomposition by release of ammonia as mentioned in section 3.2.2.1. This result supported our hypothesis that CPM-supported APMV catalysts were more stable when the amount of APMV loaded was increased. After test the intensity of the N-H vibration band decreased (not shown). The presence of hotspots during the reaction can easily explained a partial decomposition of APMV. In the case of 10APMV/CPM the absence of the v_{as} N-H due to the decomposition of APMV was in good agreement with the results from XRD (*cf. section 3.2.2.3*) and the observed absence of catalytic activity in the catalytic experiment reaction (*cf. Chapter 4*).

Finally it was interesting to note that all bands attributed to v_{as} N-H, v_{as} Mo=O_d, v_{as}

Mo-O_b-Mo and v_{as} Mo-O_c-Mo were shifted to higher wavenumbers when APMV was supported on CPM, thus suggesting a strong interaction between the active phase and the support. After reaction, no evident change could be observed, only the vibration Mo-O_b-Mo band shifted to lower wavenumber by 1-3 cm^{-1} which was within the accuracy of the technique (4 cm^{-1}).

Table 3-8 FT-IR characteristic vibration for the catalysts before and after catalytic reaction

Catalyst	State	Wavenumber, cm^{-1}				
		v_{as} N-H	v_{as} P-O_a	v_{as} Mo-O_d	v_{as} Mo-O_b-Mo	v_{as} Mo-O_c-Mo
10APMV/CPM	B.R.	-	1062	969	866	798
	A.R.	-	1062	969	865	798
20APMV/CPM	B.R	-	1062	969 (1035)	866	798
	A.R.	-	1062	969 (weaker)	865	798
40APMV/CPM	B.R.	1416	1062	969 (1035)	868	798
	A.R.	1416	1062	969 (1036)	865	798
50APMV/CPM	B.R.	1416	1062	969 (1035)	868	798
	A.R.	1416	1062	969 (1036)	865	798
APMV	B.R.	1414	1062	963 (1035)	865	788
	A.R.	1414	1062	963 (1035)	865	788

Here B.R. =Before reaction, A.R. =After reaction

Raman spectra for APMV/CPM samples before and after reaction were reported on Figure 3-9. All Raman spectra exhibited the Keggin feature bands at 983, 967, 956, 871 and 600 cm^{-1}, which were assigned to v_s Mo=O_d, v_{as} Mo=O_d, v_{as} P-O, v_{as} Mo-O_b-Mo and v_{as} Mo-O_c-Mo, respectively [22]. However, additional peaks at 660 and 813 cm^{-1} were found in the spectra of spent catalyst and were ascribed to MoO_3 [5]. However, the cross section of Raman diffusion of MoO_3 was very high as compared to that of other molecular solids so that tiny amounts can be detected. Let us recall that no MoO_3 could be detected by XRD (*cf. section 3.2.2.3*).
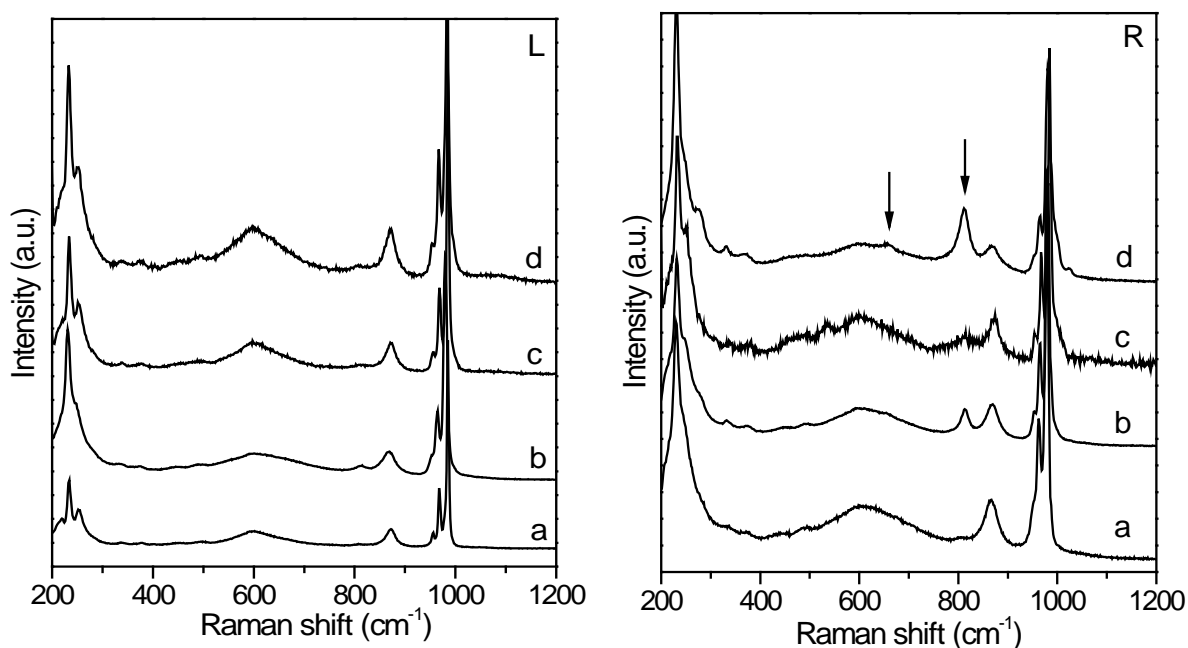
Figure 3-9 Raman spectra for the catalysts before reaction (left) and after reaction (right)
(a: 10APMV/CPM, b: 20APMV/CPM, c: 40APMV/CPM and d: 50APMV/CPM)
Arrows: peaks attributed to MoO_3

3.2.2.5 Surface analysis by XPS

The composition and the oxidation state of the elements in the near surface of the calcined and used samples were analysed by XPS technique (Table 3-9). The peaks of O1s, P2p, $Mo3d_{5/2}$ and $Cs3d_{5/2}$ at binding energy (B.E.) 531, 134, 233 and 724 eV were assigned to O^{2-}, P^{5+}, Mo^{6+} and Cs^+ ions, respectively. The nitrogen peak appeared as a shoulder to 399 eV peak which belonged to $Mo3p_{3/2}$, at *ca.* 402.5 eV after decomposition, depending on the samples. The $V2p_{3/2}$ and N1s spectra were reported in Figure 3-10 and Figure 3-11, respectively. The BE values of the related elements were gathered in Table 3-9.

The composition determined by the atomic ratio is worth analysing. Indeed, whatever for the calcined or spent catalysts, the V/P ratio was found less than the theoretical value of 1. The variability of V/P ratio indicated a redistribution of the V element on the catalysts surface after the reaction. However, the distribution did not follow a clear trend. Nevertheless, the decrease may be caused by the migration of V from the surface to the bulk during the thermal treatment and/or reaction: indeed it was known from literature that vanadium can be

eliminated from the primary Keggin-structure under reaction conditions, thus resulting in an increased mobility of the V species [23, 24].

Table 3-9 Surface analysis results for the samples before and after reaction

Catalyst	Binding Energy (BE), eV				Molar ratio		Atomic ratio
	$Mo_{3d(5/2)}$	$V_{2p(3/2)}$ (V^{5+}/V^{4+})	$Cs_{3d(5/2)}$	N_{1s}	V^{5+}/V^{4+}	N/Mo	Cs/Mo/V/P/N
Before reaction							
10APMV/CPM	233.3	518.1/516.9	724.4	403.8*	22/78	2/98	2.8/11/0.6/1.2/0.7
20APMV/CPM	233.3	518.1/517.0	724.4	402.3	31/69	4/96	2.1/11/0.4/1.1/0.8
40APMV/CPM	233.3	518.1/516.9	724.3	402.7	56/44	6/94	2.0/11/0.8/1.0/1.0
APMV	233.4	518.2/516.9	-	402.5	61/39	9/91	0/11/0.8/1.2/1.4
After reaction							
10APMV/CPM	233.1	518.1/517.0	724.3	-	8/92	0/100	3.5/11/0.4/1.1/0.3
20APMV/CPM	233.3	518.1/516.9	724.3	403.3*	24/76	1/99	1.5/11/0.8/1.1/0.3
40APMV/CPM	233.2	518.1/517.0	724.3	402.4	29/71	3/97	1.5/11/0.7/1.1/0.7
APMV	233.3	518.1/516.9	-	402.3	50/50	6/94	0/11/1/1.1/1.1

In addition to the migration of V from the surface to the bulk, one can also state an increased amount of caesium on the surface of the spent catalyst containing 10 wt.% of APMV. This effect may be driven by the aforementioned migration of vanadium from the surface to the bulk, meaning that a cross-transfer of Cs from the bulk to the surface and V in the opposite direction took place. On the other hand, the enrichment of Cs on the surface may also be explained by the partial decomposition of the active phase (APMV) which consisted of the release of NH_3 and the subsequent removal of protons from the catalyst. Thereby cation vacancies were generated which can then be compensated by the migration of Cs^+ cations, whereby the caesium content at the surface increased.
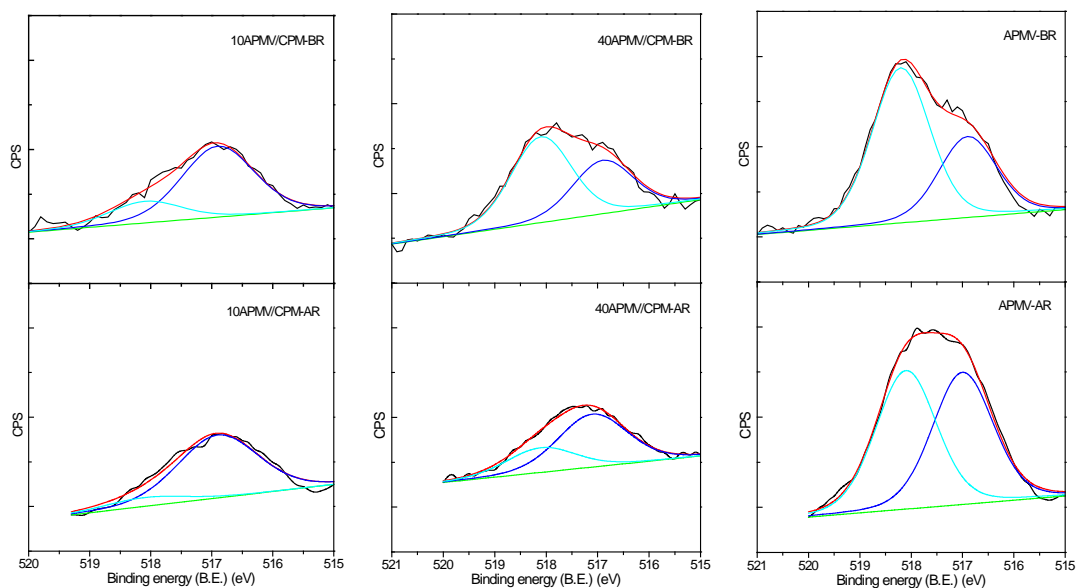
Figure 3-10 V2p$_{3/2}$ spectra of the samples before and after reaction

(here: BR=before reaction, AR=after reaction)

The wide peak assigned to vanadium (V2p$_{3/2}$) at *ca.* 517.5 eV was decomposed to show the presence of both V^{5+} and V^{4+} at *ca.* 518 and 517 eV, respectively (Figure 3-10). The substitution of Mo by a V atom in Keggin unit to modify the redox property, made the initial abstraction of a H$^-$ species at tertiary C atom be easier over V=O sites [25], as a result the V^{5+} cations was reduced. The strong acidic site on the surface played the role of catalyst to promote the reduction, although it may be slowly lost because of the partial decomposition under the reaction conditions. The V^{5+}/V^{4+} ratio was calculated according to the area of corresponding peaks, and it put in evidence that the oxidation state of vanadium changed after catalytic reaction. In the calcined samples, the V^{4+} cations existed in considerable amount as a result of structure evolution during the thermal treatment, which may be probably caused by the loss and oxidation of lattice oxygen to O$_2$ in presence of H$^+$ in the catalyst [26]. The concentration of V^{4+} was strongly depended on the content of APMV, in good agreement with the TG results (*cf. section 3.2.2.1*), as the catalysts with lower APMV content displayed lower thermal stability.

Similar trends could be also observed for the used catalysts. After reaction, V^{5+}/V^{4+} was significantly decreased. It can be assumed that this reduction was caused by the reaction with isobutane during the reaction. Furthermore, it was also stated that the reducibility of V^{5+} was

increased with decreasing amount of APMV. For instance, more than 60% V^{5+} were reduced to V^{4+} in 10APMV/CPM *vs.* only half of V^{5+} in 40APMV/CPM after catalytic experiment. Indeed, the elimination of V from the Keggin structure may facilitate the reduction from V^{5+} to V^{4+} leading thus to the variation of V^{5+}/V^{4+} ratio.
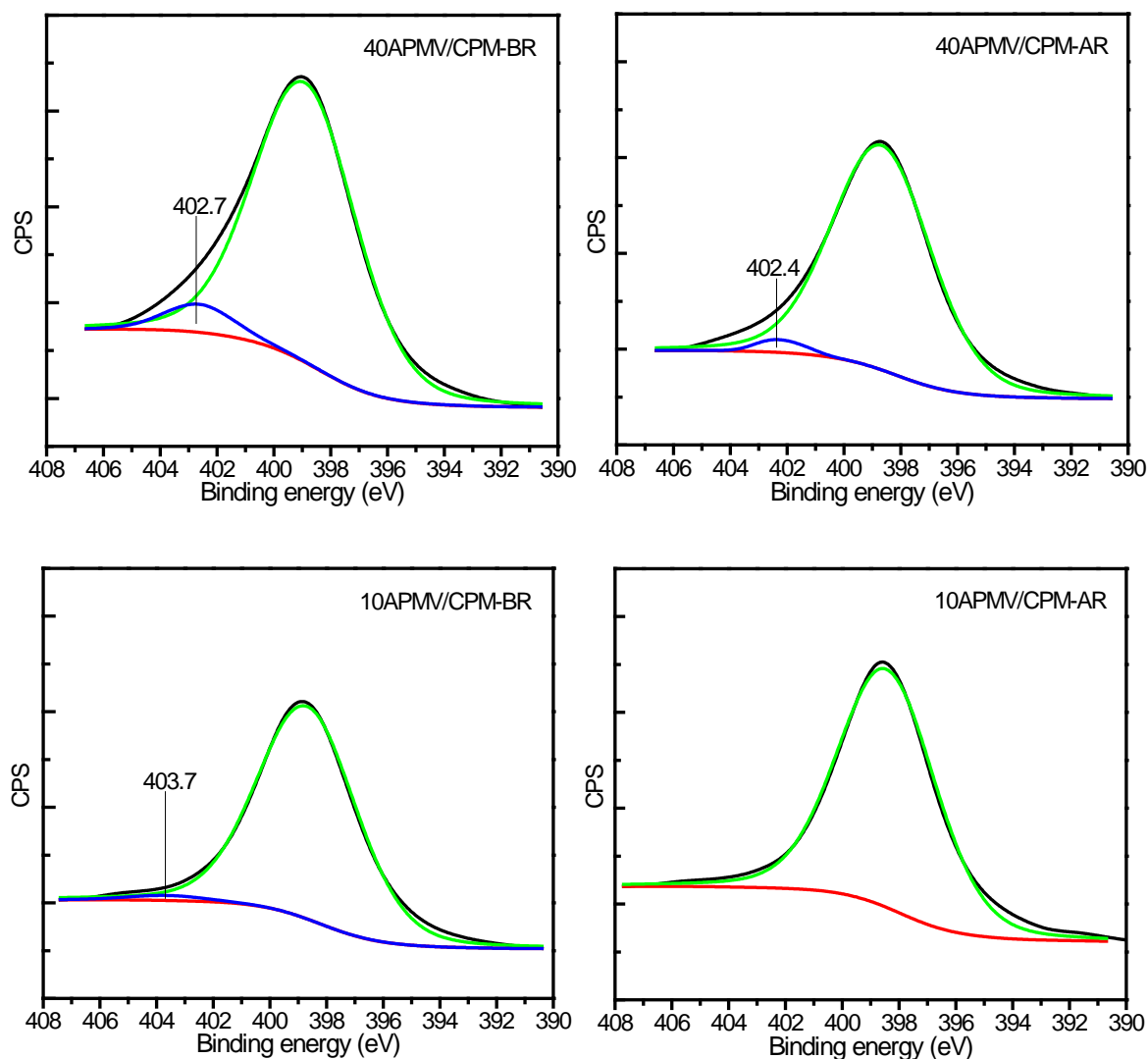
Figure 3-11 N1s spectra of the samples 40APMV/CPM and 10APMV/CPM
(here: BR=before reaction, AR=after reaction)

Another notable changes were from the N element. The spectra of N1s of the samples 40APMV/CPM and 10APMV/CPM were shown in Figure 3-11. Apparently the N signal originated from the ammonium cations. The intense changes of attached N1s in proportion to the main Mo3p$_{3/2}$ (shown in Figure 3-11) implied the effects of the support and the possible structural evolution under the reaction conditions. On the one hand, it decreased as the

decrease of APMV loading from 9/91 for APMV to 2/98 for 10APMV/CPM. On the other hand, it decreased after the reaction even the N1s spectra could not be found any more for the sample with the lowest loading of APMV.

These results thereby suggested that the vanadium was eliminated from the primary structure and then reduced by isobutane under the reaction environment. The partial decomposition of the active phase APMV was unavoidably observed for the all samples as the loss of ammonium cations, but its extent was determined significantly by the loading of APMV. Higher loading was favoured to stabilize the active phase, on the contrary, the decomposition may occur easily on the low loading catalyst. It was in good accordance with the hypothesis we made previously. The enrichment of caesium and the loss of vanadium on the surface indicated the possible mobility between the surface and bulk phase. The process may be driven by the decomposition as more vacancies were created by removal of ammonium as ammonia gas.

3.2.2.6 Reducibility measurements

The reducibility of fresh and spent xAPMV/CPM catalysts was examined by H_2-TPR measurements. (Figure 3-12). All samples exhibited significant H_2 consumption starting from 550 °C which may be ascribed to the reduction of Mo^{6+} to Mo^{4+} [7]. The broad peaks observed hereby, indicated a rather complex reduction process composed of one or more transition states. The quantitative analysis showed that the H_2 consumption increased with x, meaning that the reduced species originated from the active phase (APMV) and not from the support (CPM).
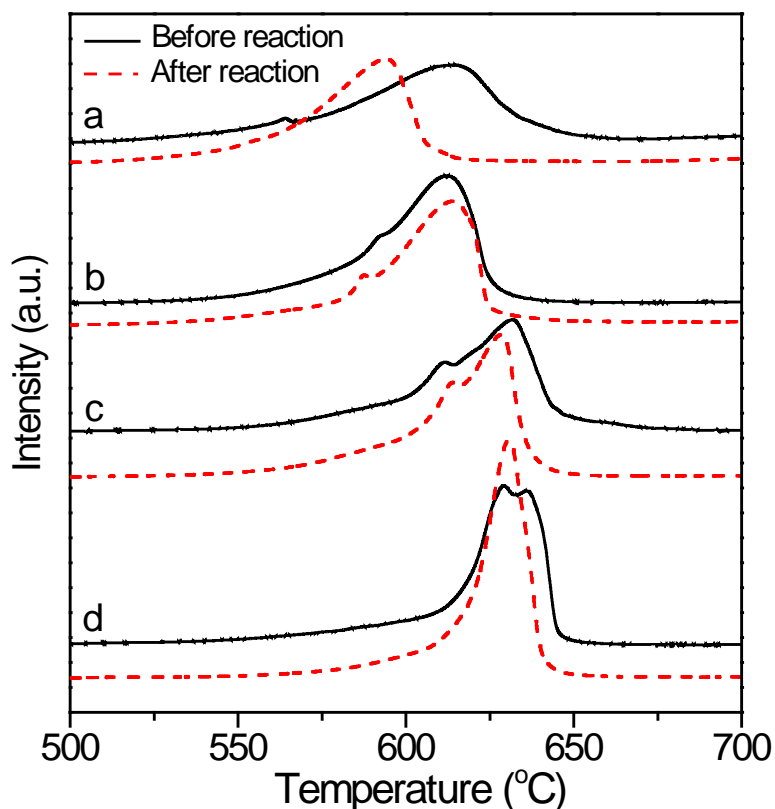
Figure 3-12 TPR profiles of the catalysts
(a: 10APMV/CPM, b: 20APMV/CPM, c: 40APMV/CPM and d: 50APMV/CPM)

The reduction process was further studied by temperature-programmed XRD technique under reducing gas (3 v% H_2/N_2). The results for the sample 40APMV/CPM was shown in Figure 3-13. The changes in diffraction peaks suggested the evolution of the structure as the temperature increased. The diffraction lines from the Keggin-type compounds (the active phases APMV or/and the support CPM) could be still found up to 560 ^{o}C. The line at $2\theta =$ 21.4^o which was considered as characteristic of APMV weakened gradually, indicating its slow disappearance. When the temperature increased to 580 ^{o}C, the XRD pattern changed dramatically: the characteristic Keggin diffraction lines disappeared and gave rise to those of reduced molybdenum oxide, MoO_2 (strong lines at $2\theta =$ 26.0°, 36.6°, 36.8°, 37.1°, 52.7°, 52.9° and 53.4°, *etc*.). The remaining lines at $2\theta =$ 25.2°, 26.0° and 26.5^o were probable due to non-reduced MoO_3. As the temperature continued going up to 600 ^{o}C, the new diffraction peaks at $2\theta =$16.1^o, 19.8^o, 28.1^o and 43.5^o appeared but were ill-defined. In consequence the Keggin units collapsed as the temperature was higher than 580 ^{o}C, which was in excellent

agreement with the TG results (*cf. section 3.2.2.1*). It was also noteworthy that in the pattern obtained at 560 $^{\circ}$C two shoulder peaks at $2\theta = 37.2°$ and 53.5° originated from MoO_2 phases, which demonstrated that the Keggin unit started to decompose and that the generated MoO_3 was afterward reduced by hydrogen. As a result the diffraction features of Keggin-type compounds and MoO_2 phases could be simultaneously observed in this XRD pattern, and the hydrogen consumption starting from 560 $^{\circ}$C could be also detected in TPR profile of sample 40APMV/CPM.
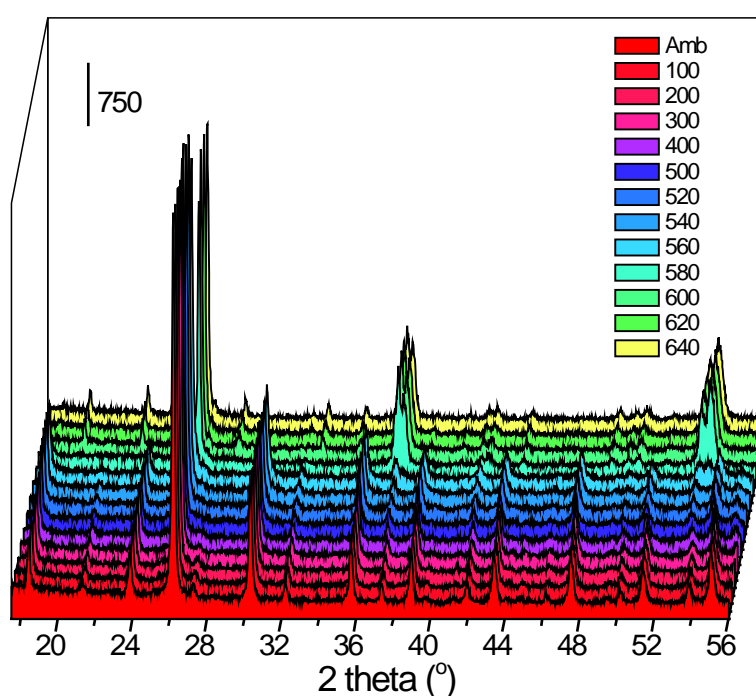
Figure 3-13 Temperature-programmed XRD results over 40APMV/CPM catalyst in hydrogen flow

As far as the vanadium species were concerned, no evident diffraction line assigned to whatever for V^{5+} or V^{4+} species was found by XRD technique. Its low content in the catalyst may take the major responsibility, but the transition state of reduced V^{5+} species by hydrogen may exist [27], which was difficult to detect because of their low content as well.

The reduction peak area can reflect the H_2 consumption during the TPR measurement. The H_2 consumption as a function of APMV loading for the catalysts before and after reaction were depicted in Figure 3-14. It revealed clearly a linearly increase as the increased loading

whatever for the calcined or spent samples. It can be seen simultaneously the spent catalyst consumed less hydrogen compared to the corresponding calcined one, meaning that the spent catalyst exhibited lower content of reducible species. Like aforementioned the reduction of molybdenum species from Mo^{6+} to Mo^{4+} was responsible for the major hydrogen consumption, and the vanadium species can be expelled from Keggin unit, one can speculate that the degraded metal oxides were more difficult to reduce than the Mo-V-O complex compounds. It also proved that the partial decomposition of APMV took place under the reaction conditions.
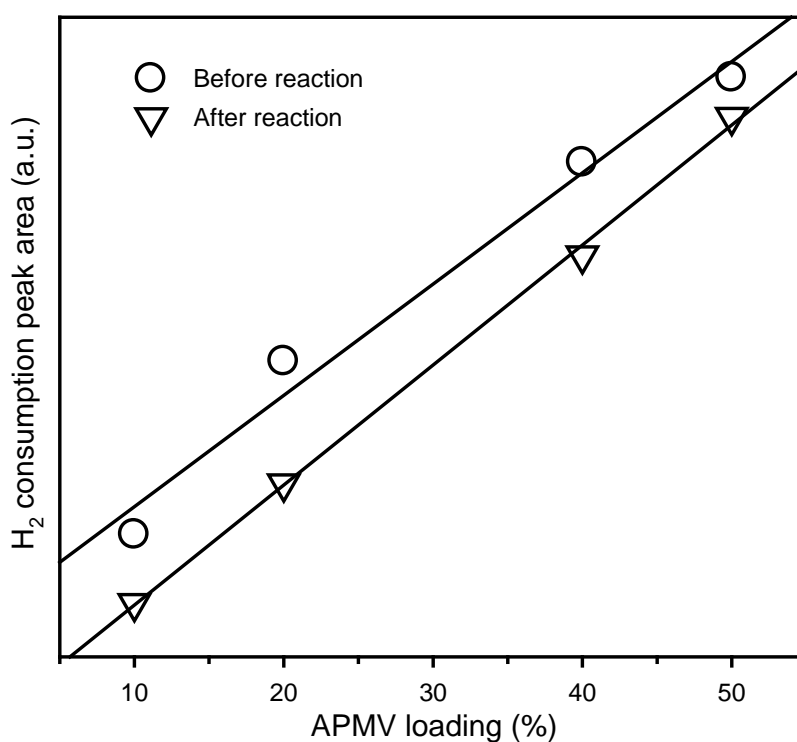
Figure 3-14 H_2 consumption as a function of APMV loading for the samples before and after catalytic reaction

3.2.2.7 Quantification and strength of the acid sites

The NH_3-TPD profiles observed for the CMP-supported catalysts are shown in Figure 3-15 and the quantitative results for the NH_3 uptake are listed in Table 3-10. As NH_3 may also originate from the decomposition of the active phases (APMV) when the temperature

overpassed 350 °C (*cf. section 3.2.2.1*), all values were corrected by eliminating the corresponding amount.

For fresh catalysts, the amount of acid sites increased with x, the amount of active phase: for x = 10, the ammonia uptake was 0.08 mmol/g, *vs.* 1.80 mmol/g for x = 40. However, a further increase to 50 wt.% APMV resulted in a decreased amount of acid sites, which was ascribed to the overloading with active phase due to the low surface area (*cf. section 3.2.2.2*) leading therefore to non-accessible sites. As before (*cf. section 3.1.2.5*) four acid strength ranges were used. All four catalysts exhibited rather similar desorption behaviour below 450 °C, which was assigned to the desorption of NH_3 from weak and medium strength acidic sites. A significant different behaviour was observed for strong and very strong sites, their amount and especially their strength increased with the loading of APMV. The 30% very strong acid sites and 20% strong sites for 20APMV/CPM increased to 50% and 36% respectively for 50APMV/CPM. The highest amount of these strong and very strong sites was observed for 40APMV/CPM (1.54 mmol/g *vs.* 1.42 mmol/g for 50APMV/CPM).
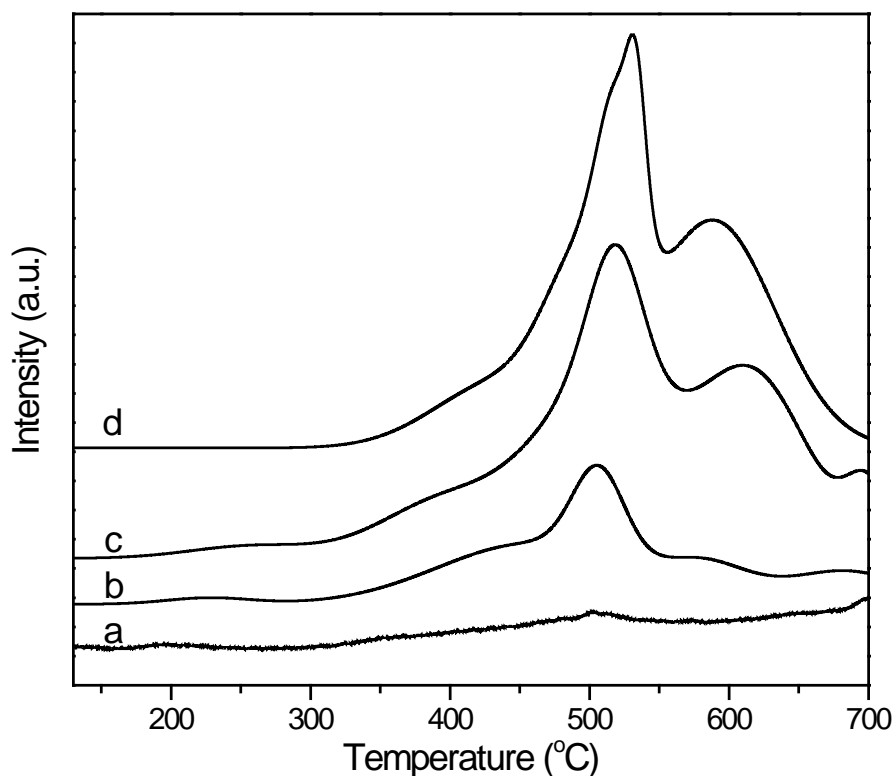

Figure 3-15 NH_3-TPD profiles for: a: 10APMV/CPM, b: 20APMV/CPM,
c: 40APMV/CPM and d: 50APMV/CPM.

Table 3-10 Distribution of acidic sites and their quantity

Catalyst	Acidity, NH$_3$ uptake, mmol/g cat.				Total acidity, mmol/g$_{cat.}$ (μmol/m^2)
	130-300 weak	300-450 medium	450-560 strong	560-700 ^{o}C Very strong	
10APMV/CPM	0.01	trace	0.02	0.05	0.08 (3)
20APMV/CPM	0.02	0.33	0.14	0.21	0.69 (36)
40APMV/CPM	0.05	0.21	0.89	0.65	1.80 (106)
50APMV/CPM	trace	0.25	0.60	0.82	1.67 (144)

3.2.3 Conclusions

The amount of APMV loaded on the CPM support had a significant influence on the properties of the APMV/CPM catalysts. Catalysts containing high amounts of APMV exhibited increased stability against thermally induced structural alteration. These alterations during reactions were caused by (i) sintering of the active phase, which was implied from XRD and nitrogen-physisorption experiments, ii) elimination of the NH$_4^+$ cations from the active phase as shown by FT-IR analysis and, (iii) cross-transfer of V atoms from the surface to the bulk and Cs in the opposite direction, as evidenced by XPS and FT-IR analysis. The latter notably proposed the elimination of the vanadium from the primary structure (Keggin anion) to the secondary structure, leading thus to an increased mobility of V. Most significant decomposition occurred over the catalyst with low amount of active phase (10APMV/CPM).

Furthermore, the vanadium species exhibited increased tendency to be reduced under reaction conditions as found by XPS. Nevertheless, the reduction of vanadium could not be observed neither by TPR nor by XRD, which was supposedly explained by the difference of the techniques that were either specific for the surface (XPS) or for the bulk (XRD and TPR). On the other hand, the two latter clearly demonstrated that decomposition of the Keggin unit took place at increased temperature (also evidenced by thermogravimetry) and yielded MoO$_3$ in the first step, which was then reduced to MoO$_2$ under the employed conditions.

3.3 Mixed-salts catalysts $Cs_x(NH_4)_{3-x}HPMo_{11}VO_{40}$

3.3.1 Introduction

In section 3.1, we have seen that it is possible to obtain high surface area catalysts when supporting the active phase APMV on mesoporous silica materials. Unfortunately the structural stability was degraded at the same time as it became easier to decompose the active phase dispersed as monolayer or sub-monolayer on the high surface silica. We have seen then in section 3.2 that multilayer dispersion of APMV on CPM support allows some improvement of the properties of the catalytic system. In this context, it was found that the amount of APMV loaded on the support has a critical influence on the structural, textual, acidic and redox properties. For instance, the distribution of the surface elements revealed considerable differences, depending strongly on the loading of APMV. Changes were observed after the catalytic reaction as well. The enrichment of caesium on the surface and the loss of vanadium may indicate that these elements cross-diffuse under stream between the surface and the bulk phase of catalyst. Moreover the partial decomposition of the active phases under calcination and reaction conditions may promote the process as more vacancies are created when ammonium cations are decomposed.

Although the microstructure of $(NH_4)_3PW_{12}O_{40}$ [28], $Cs_xH_{3-x}PW_{12}O_{40}$ [29], $Cs_x(NH_4)_{3-x}PW_{12}O_{40}$ [30] and $Cs_x(NH_4)_{3-x}PMo_{12}O_{40}$ [20] have been reported, none of them was applied to catalyse the isobutane oxidation for the production of MAC and MAA. In this part, we will focus on the preparation of the mixed caesium-ammonium salts of 1-vanado-11-molybdophosphoric acid with various caesium/ammonium ratios. The textural, structural stability, structural feature, crystalline phase, acidity and redox properties will be studied by N_2 adsorption/desorption, TGA, spectroscopies (FT-IR and Raman), XRD, NH_3-TPD and TPR techniques, respectively. The aim of this work is to try to establish a

correlation between the catalytic properties and the quantity of introduced cations. The mixed salts $Cs_x(NH_4)_{3-x}HPMo_{11}VO_{40}$ (x=3, 2.5, 1.7, 1.5, 0.5 and 0) were prepared by a precipitation method described in Chapter 2. The prepared samples were noted as $Cs_x(NH_4)_{3-x}H$ in the following text.

3.3.2 Characterization: Result and discussion

3.3.2.1 Structural evolution of the fresh solids

TGA analyses were carried out in an air flow for the $(Cs_{1.7}(NH_4)_{1.3}H)$ and $(Cs_3(NH_4)_0H)$ samples to study the structural evolution that may occur under calcination conditions (Figure 3-16). A continuous weight loss was observed from room temperature up to 450 ^{o}C. Below 100 ^{o}C the physisorbed water was removed. In the case of $Cs_{1.7}(NH_4)_{1.3}H$, crystal water was lost from 100 ^{o}C to 205 ^{o}C, whereas no loss was detected in this temperature range for $Cs_3(NH_4)_0H$, suggesting that it was initially anhydrous. However a broad peak between 175 and 500 ^{o}C was observed and attributed to the loss of the protons as constitutional water [4]. The weight loss of 0.49% observed for this step was in excellent agreement with the theoretical value of 0.48%.

The $Cs_{1.7}(NH_4)_{1.3}H$ sample displayed several peaks during the thermal decomposition from 205 to 430 ^{o}C. The difference between the two samples was explained by the presence of NH_4^+ in this case. The total weight loss of 1.9%, indicated by TG curve, was in good agreement with the theoretical value of 2.0%, which was calculated based on the complete loss of protons and ammonium cations resulting in generation of $Cs_{1.7}PMo_{11}VO_{38.85}$. As already found in our previous work [17], the total decomposition of the ammonium cations leads to the release of NH_3 to yield residual acidic protons and further loss of these residual protons as constitutional water. Then, the Keggin-type compounds with oxygen vacancies $Cs_{1.7}PMo_{11}VO_{38.85}$ and $Cs_3PMo_{11}VO_{39.5}$ were formed from $Cs_{1.7}(NH_4)_{1.3}H$ and $Cs_3(NH_4)_0H$, respectively, started to collapse to form simple oxides at 630 ^{o}C and at 654 ^{o}C, respectively.
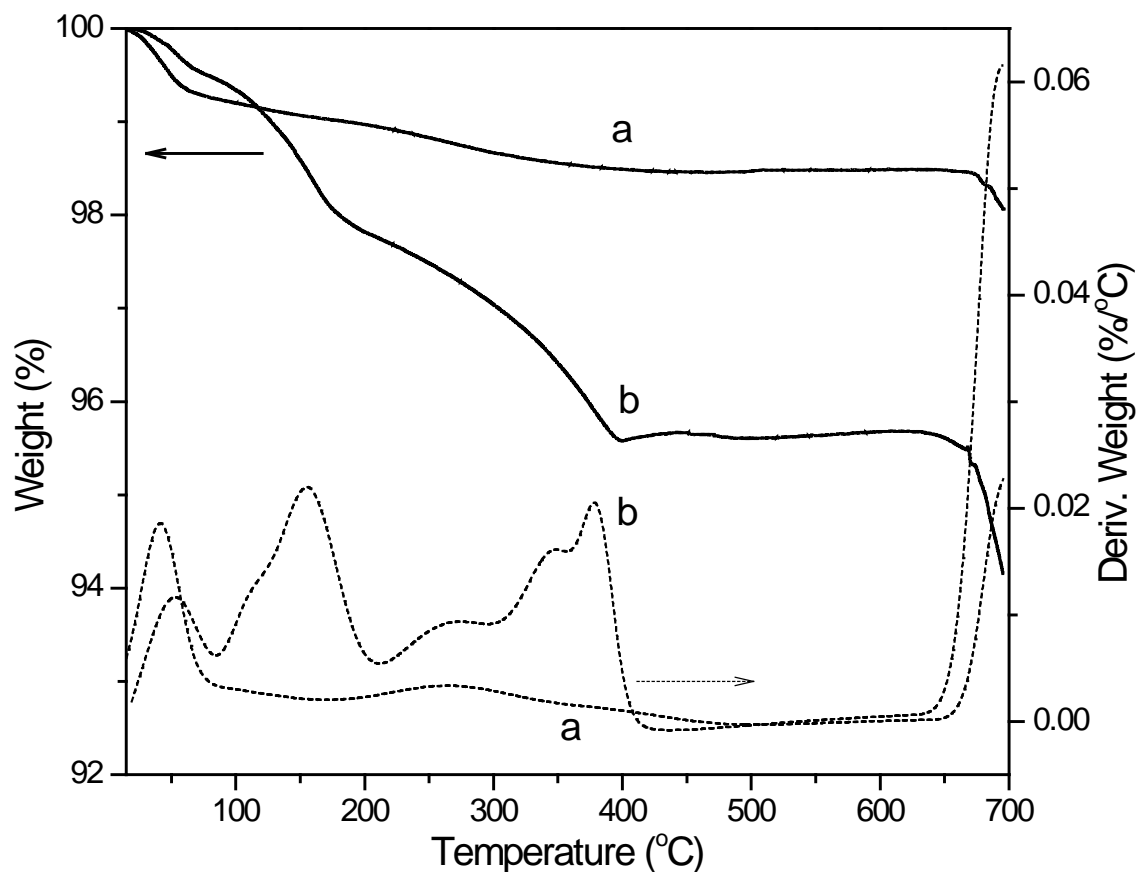
Figure 3-16 Thermogravimetric (TG, solid lines) and derivative thermogravimetic analysis (dash lines) for: a: $Cs_3(NH_4)_0H$, b: $Cs_{1.7}(NH_4)_{1.3}H$

3.3.2.2   Textural property of the calcined sample

The specific surface area (S_{BET}), total pore volume (V) and average pore diameter (D) of calcined samples were reported in Table 3-11. It can be seen that the textural properties were strongly influenced by the presence or absence of ammonium and by the Cs^+/NH_4^+ ratio. The surface area of $Cs_0(NH_4)_3H$ (APMV) was found very low (4 m^2/g), indicative of a non-porous material. As NH_4^+ was replaced by Cs^+ the surface area increased as the number x of Cs^+ cations increased. An increase from 0.5 to 2.5 Cs^+ resulted in a 10-fold increase of the specific surface area from 6 to 59 m²/g. The maximum value of 88 m²/g, 22 times more than the bulk APMV, was observed for $Cs_3(NH_4)_0H$.

Table 3-11 Textural properties of the mixed salts $Cs_x(NH_4)_{3-x}HPMo_{11}VO_{40}$

x	Formula	Ref.	S_{BET}, m^2/g	V, cm^3/g	D, nm
0	$(NH_4)_3HPMo_{11}VO_{40}$	$Cs_0(NH_4)_3H$ (APMV)	4	0.020	23
0.5	$Cs_{0.5}(NH_4)_{2.5}HPMo_{11}VO_{40}$	$Cs_{0.5}(NH_4)_{2.5}H$	6	0.014	11
1.5	$Cs_{1.5}(NH_4)_{1.5}HPMo_{11}VO_{40}$	$Cs_{1.5}(NH_4)_{1.5}H$	8	0.018	7
1.7	$Cs_{1.7}(NH_4)_{1.3}HPMo_{11}VO_{40}$	$Cs_{1.7}(NH_4)_{1.3}H$	16	0.033	7
2.5	$Cs_{2.5}(NH_4)_{0.5}HPMo_{11}VO_{40}$	$Cs_{2.5}(NH_4)_{0.5}H$	59	0.040	4
3	$Cs_3HPMo_{11}VO_{40}$	$Cs_3(NH_4)_0H$	88	0.035	5
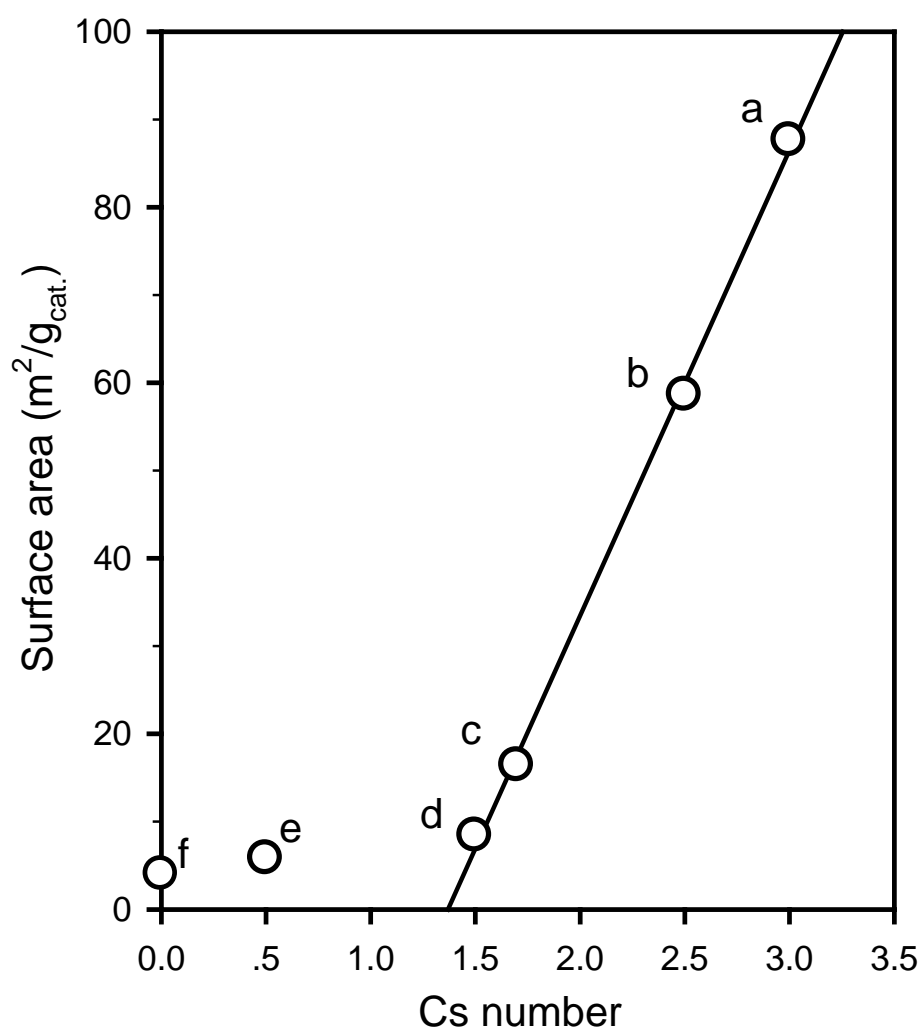
Figure 3-17 Relationship between the surface area and the number of Cs$^+$ in caesium-ammonium catalysts
(a: $Cs_3(NH_4)_0H$, b: $Cs_{2.5}(NH_4)_{0.5}H$, c: $Cs_{1.7}(NH_4)_{1.3}H$, d: $Cs_{1.5}(NH_4)_{1.5}H$, e: $Cs_{0.5}(NH_4)_{2.5}H$, f:APMV)

The relationship between the surface area and the Cs atom number in the catalysts was reported in Figure 3-17. The specific surface area of the catalysts increased linearly as the Cs

number increased from 1.5 to 3.0, while for x = 0.5 (6 m^2/g) the point did not fit the line. As the Cs-free sample Cs$_0$(NH$_4$)$_3$H (APMV) showed a very low surface area, these results showed that it was possible to improve the textural properties by introducing some caesium cations in the catalyst.

The isotherms and pore size distribution of the prepared materials were shown in Figure 3-18 and Figure 3-19, respectively. Whereas the APMV sample exhibited a Type III isotherm according to the IUPAC classification [31], which is the characteristic of non-porous materials. The slight substitution of NH$_4^+$ by equal mole of Cs$^+$ for Cs$_{0.5}$(NH$_4$)$_{2.5}$H did not modify its porosity significantly, though average pore diameter of D=2 nm was seen from the pore size distribution curve. The other solids exhibit either a Type IV or a Type I isotherm characteristic of mesoporous or microporous materials, respectively. The samples with 1.5 and 1.7 Cs atoms [Cs$_{1.5}$(NH$_4$)$_{1.5}$H and Cs$_{1.7}$(NH$_4$)$_{1.3}$H] showed Type IV isotherms with H3 type hysteresis loops, suggesting the pores evolution towards mesopores (D = 4 nm). The H3 type hysteresis loop is usually found in materials with layer structure or slit [32], its appearance in both samples may be related to the precipitation method of preparation.

The samples containing more than 2.5 Cs atoms [i.e. Cs$_{2.5}$(NH$_4$)$_{0.5}$H and Cs$_3$(NH$_4$)$_0$H] exhibited Type I isotherms which is characteristic for microporous materials. As the desorption branch and the adsorption branch formed a narrow hysteresis loop, few mesopores should be present. The pore size distribution curves of both samples shifted to lower pore diameter compared to those of the Cs$_{1.5}$(NH$_4$)$_{1.5}$H and Cs$_{1.7}$(NH$_4$)$_{1.3}$H samples. However the raw data could not be correctly interpreted by the BJH model [32] and no pore-distribution could be obtained.

In conclusion, increasing the substitution of ammonium cations by caesium led to the generation of porosity and to a progressive transition from a mesoporous to a microporous structure.

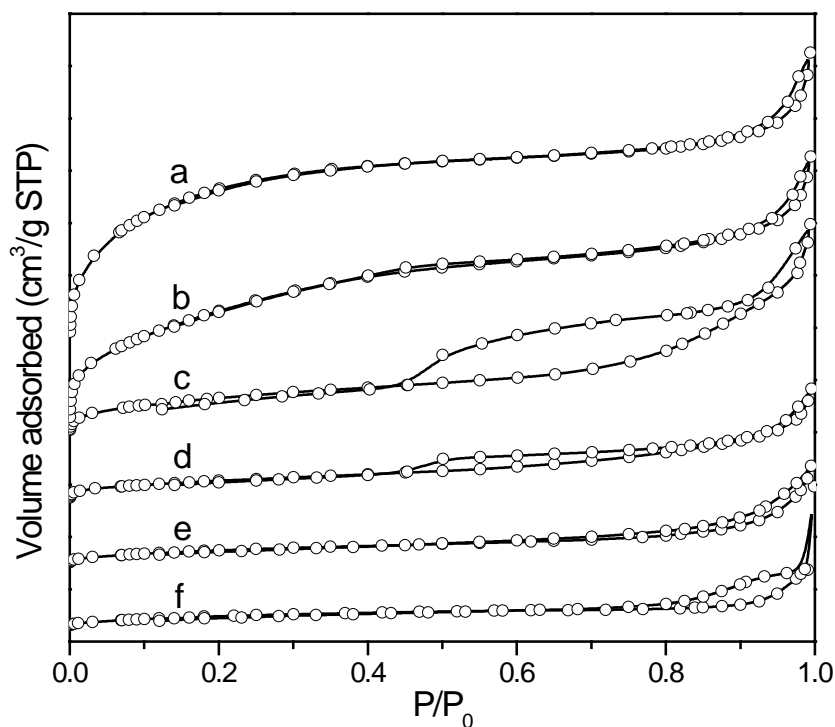Figure 3-18 Isotherms of mixed salts catalysts

(a: $Cs_3(NH_4)_0H$, b: $Cs_{2.5}(NH_4)_{0.5}H$, c: $Cs_{1.7}(NH_4)_{1.3}H$, d: $Cs_{1.5}(NH_4)_{1.5}H$, e: $Cs_{0.5}(NH_4)_{2.5}H$, f: APMV)
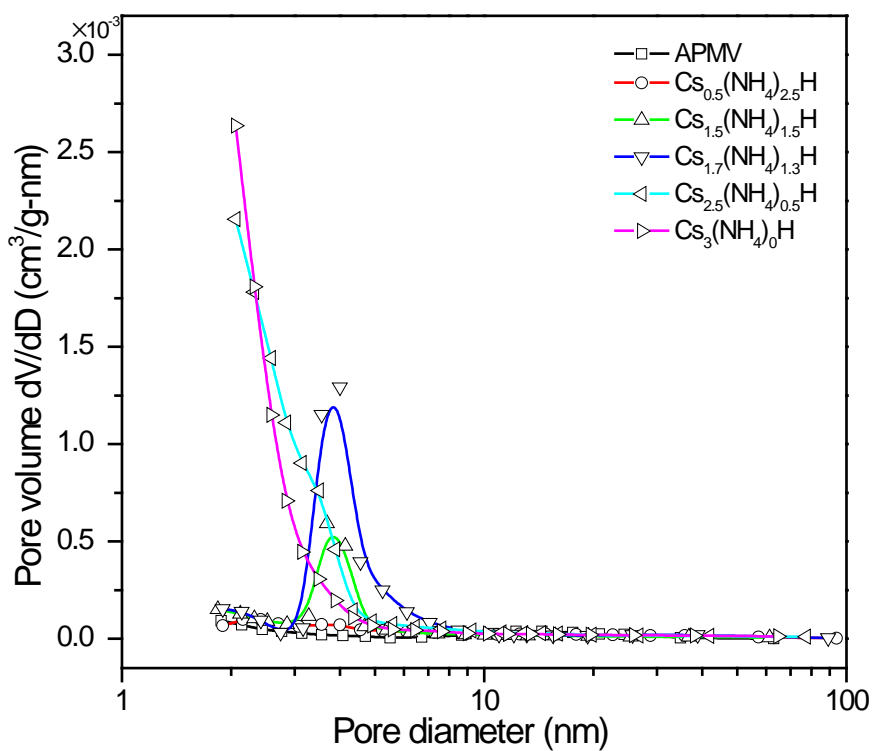

Figure 3-19 Pore size distribution of the different mixed-salt samples

3.3.2.3 Vibrational spectroscopy

The FT-IR spectra of the calcined catalysts were gathered in Figure 3-20. As previously, the bands at 1061, 963, 865 and 788 cm^{-1} were attributed to v_{as} P-O, v_{as} Mo=O_t, v_{as} M-O_b-M and v_{as} M-O_c-M [6, 33, 34], respectively. In addition, three visible shoulders at 1080, 1045 and 996 cm^{-1} were exhibited in $Cs_3(NH_4)_0H$ (Figure 3-20a) and $Cs_{2.5}(NH_4)_{0.5}H$ (Figure 3-20b). They were characteristic of the substitution of Mo by V atom in Keggin anion, the splitting being about 20 cm^{-1} [35], due to the weak distortion of the PO_4 tetrahedron. Therefore, the shoulders at 1080 cm^{-1} and 1045 cm^{-1} were assigned to the asymmetric stretching mode of P-O, while the shoulder band at 996 cm^{-1} was ascribed to the asymmetry stretching mode of Mo=O.

The other samples with lower Cs contents (x = 1.7, 1.5, 0.5) did not show these three shoulders (Figure 3-20c-f). Instead a new peak appeared at 1034 cm^{-1}, which was assigned to the v V=O band of V_2O_5 [36]. The characteristic N-H band could be observed at 1415 cm^{-1} in all ammonia containing samples (b-f), except $Cs_{2.5}(NH_4)_{0.5}H$. This exception could be explained by the quite low content of NH_4^+ and its further removal as NH_3 during the calcination. In all spectra a band at 595 cm^{-1} was attributed to MoO_3 [10], thus suggesting the partial decomposition during calcination. The band at 1384 cm^{-1} was attributed to residual nitrates (NO_3^-) which were not removed during calcination [20].

In conclusion, for high Cs content (x = 3 and 2.5) the structural V-substituted Keggin anion was clearly identified. With decreasing Cs amount (until x = 0 in APMV), the structural feature of V_2O_5 are detected. This observation suggested thus the elimination of V from the primary structure with decreasing amount of caesium, or in other words that the caesium helped to stabilize the primary Keggin structure.
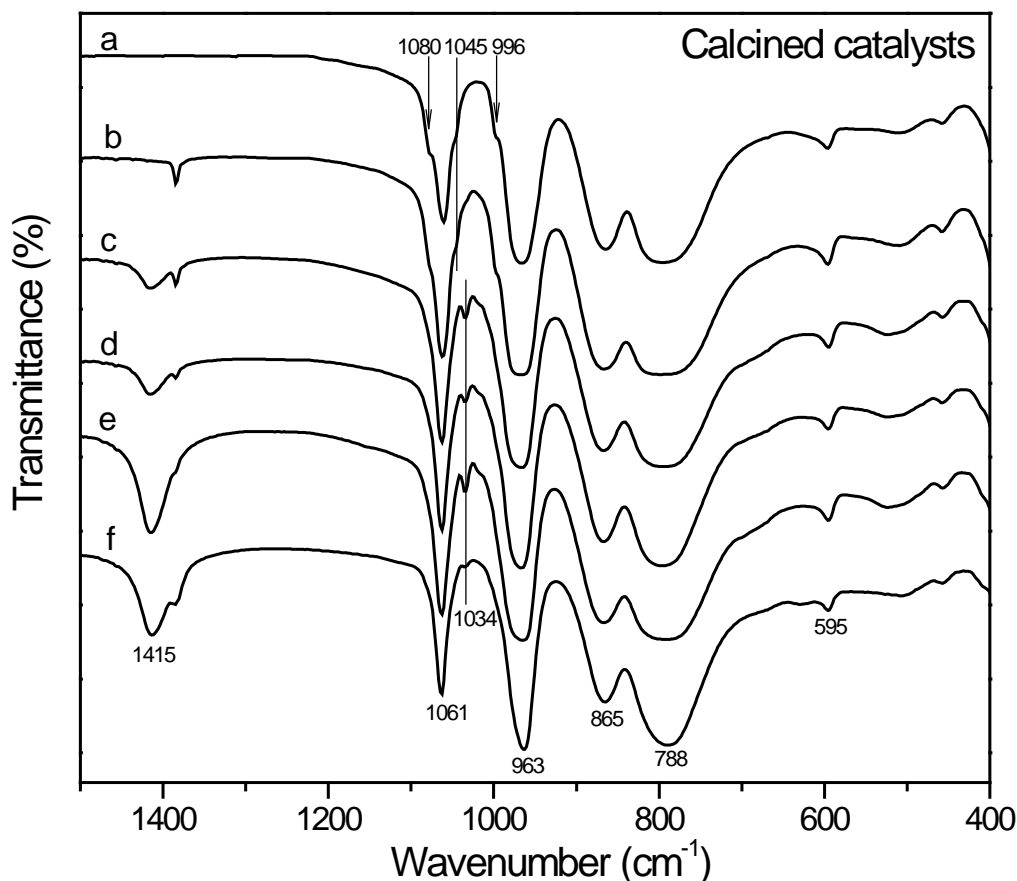
Figure 3-20 FT-IR spectra of the calcined mixed salt catalysts

(a: $Cs_3(NH_4)_0H$, b: $Cs_{2.5}(NH_4)_{0.5}H$, c: $Cs_{1.7}(NH_4)_{1.3}H$, d: $Cs_{1.5}(NH_4)_{1.5}H$, e: $Cs_{0.5}(NH_4)_{2.5}H$, f: APMV)

Compared with those of the fresh catalysts, the bands assigned to the Keggin (v_{as} P-O, v_{as} M=O_t, v_{as} M-O_b-M and v_{as} M-O_c-M) were shifted to higher wavenumbers for used catalysts (Figure 3-21), at 1063, 966, 865 and 795 cm^{-1}, respectively. The shoulders caused by the substitution of V in primary structure also shifted towards low wavenumbers (1077 cm^{-1}) and became less intense for the samples $Cs_3(NH_4)_0H$ and $Cs_{2.5}(NH_4)_{0.5}H$ after reaction. However it must be noted that all shifts were within the accuracy of the technique (spectral resolution of 4 cm^{-1}). A slight decrease of v V=O was found, that could be explained by the partial reduction of $V^{5+}O_x$ by the isobutane reactant [9]. It was further worth to note that a new band appeared at 629 cm^{-1} in all samples, except $Cs_3(NH_4)_0H$. This last-mentioned result in combination with the MoO$_3$ band (595 cm^{-1}), suggested the reduction of MoO$_3$ – originating from the partial decomposition – to MoO$_2$ by isobutane under reaction conditions [19, 20]. Since the intensity

of this band increased as the number of Cs atoms decreased, it seemed that the introduction of Cs stabilized the Keggin structure – as already suggested for the fresh catalyst. The band due to NH_4^+ shifted slightly to lower wavenumber side and its intensity was strongly determined by the number of NH_4^+ in the catalyst.
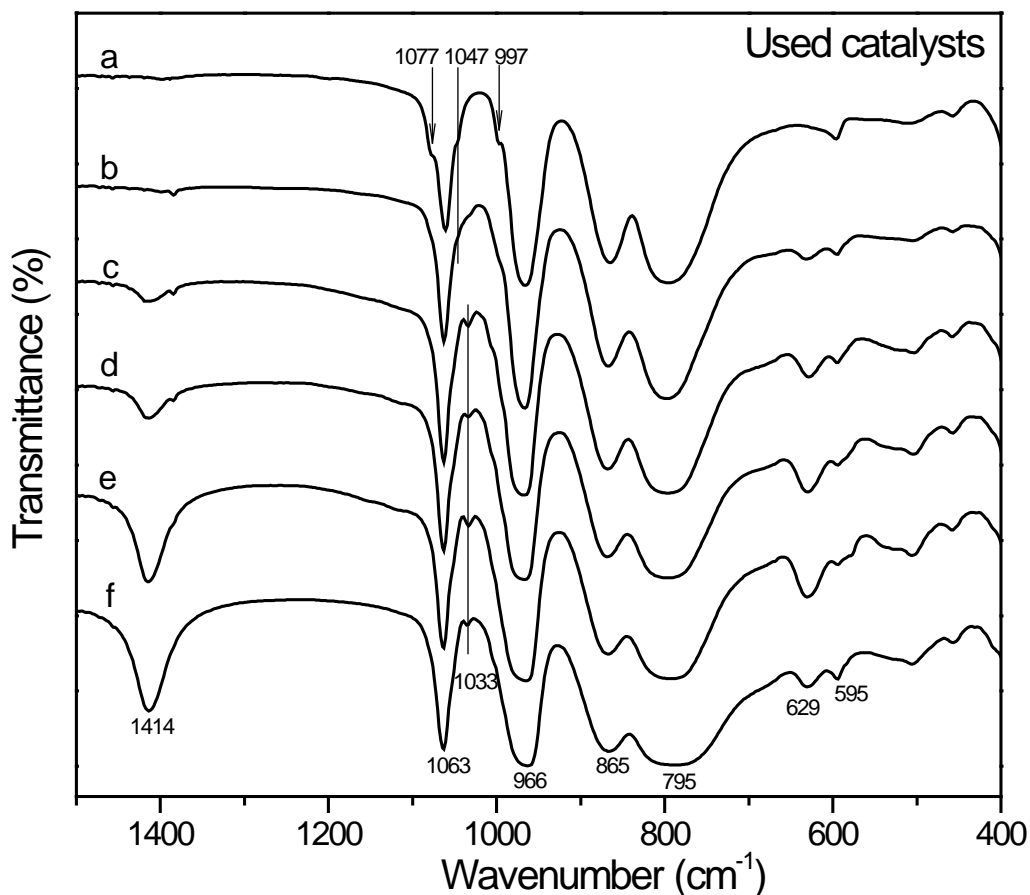
Figure 3-21 FT-IR spectra of the used catalysts
(a: $Cs_3(NH_4)_0H$, b: $Cs_{2.5}(NH_4)_{0.5}H$, c: $Cs_{1.7}(NH_4)_{1.3}H$, d: $Cs_{1.5}(NH_4)_{1.5}H$, e: $Cs_{0.5}(NH_4)_{2.5}H$, f: APMV)

The Raman spectra of the calcined catalysts (Figure 3-22) clearly displayed the characteristic Raman bands from Keggin units. The vibrations at 987, 972, 958, 875 and 600 cm^{-1} were assigned to the v_s Mo=O_d, v_{as} Mo=O_d, v_{as} P-O, v_{as} Mo-O_b-Mo and v_{as} Mo-O_c-Mo [11], respectively.

Evident changes could be observed in the Raman spectra of the spent samples. Firstly the spectrum for each used sample became less intense compared to the fresh one. Secondly the

peak shape became much broader especially for the bands from 930 to 1050 cm^{-1}, which was caused by the reorganization of the structure yielding defective Keggin units. These changes were finally confirmed by additional bands at 817, 660 and 537 cm^{-1} attributed to MoO_3.

Again, the samples with increased amount of caesium [$Cs_3(NH_4)_0H$ and $Cs_{2.5}(NH_4)_{0.5}H$] did not exhibit these three additional bands, suggesting again that high caesium amount (x=3 and 2.5) stabilized the primary structure, which was in agreement with the IR results. On the other hand, no information on the V species and reduction of MoO_3 was obtained by Raman analysis.
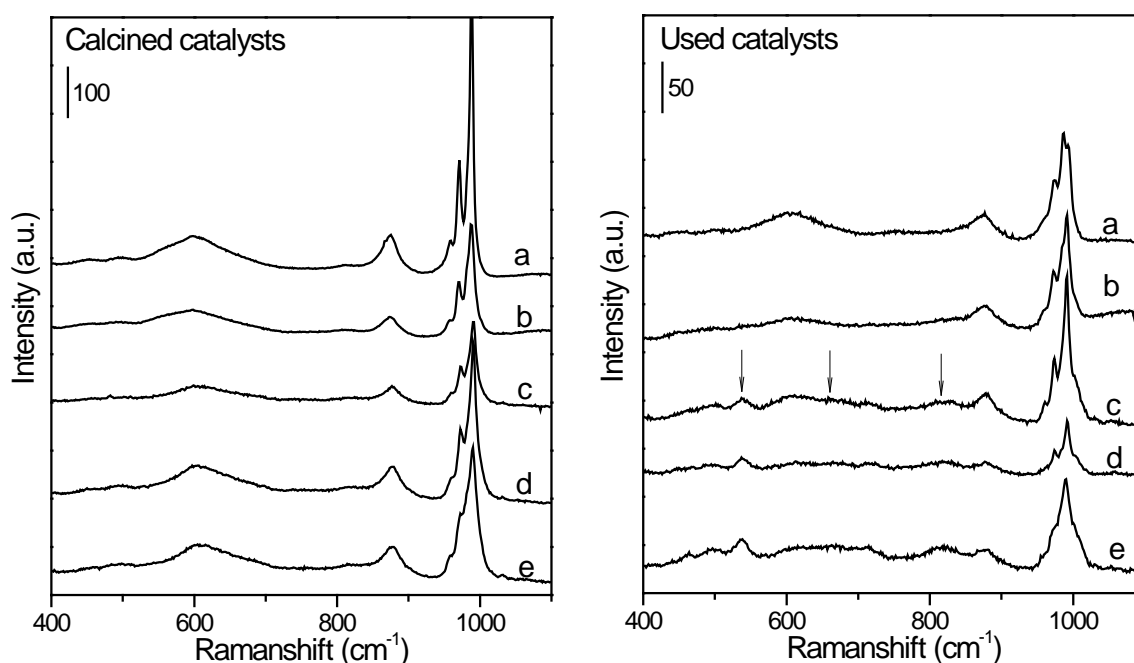
Figure 3-22 Raman spectra of calcined (left) and used catalysts (right)
(a: $Cs_3(NH_4)_0H$, b: $Cs_{2.5}(NH_4)_{0.5}H$, c: $Cs_{1.7}(NH_4)_{1.3}H$, d: $Cs_{1.5}(NH_4)_{1.5}H$, e: $Cs_{0.5}(NH_4)_{2.5}H$)

3.3.2.4 Crystalline phases analysis by XRD

The patterns of the mixed salts $Cs_x(NH_4)_{3-x}H$ (x = 0-3) for the calcined and used catalysts are presented in Figure 3-23 and Figure 3-24, respectively. For calcined APMV (Figure 3-23f) the three strongest diffraction peak were at $2\theta= 26.4^o$, 10.6^o and 36.0^o (not shown here), corresponding to the reflection planes of (222), (110) and (332), respectively, which were

characteristic for Keggin-type compounds [2]. The introduction of Cs into the formula led to a shifting trend to lower angles, ascribed to d-spacing increase when the NH_4^+ cations were substituted by Cs^+ cations. As a matter of fact, the interplanar spacing was then expanded as Cs^+ had a larger ionic radius than NH_4^+. The d-spacing values were significantly dependent upon the number of Cs cations. For example, the d-spacing of the (222) plane increased from 0.3377 nm for the Cs free sample (APMV) to 0.3416 nm for $Cs_{2.5}(NH_4)_{0.5}H$. On the other hand, the fully Cs substituted sample exhibited a slight decrease which was ascribed to the presence of a single pure phase. The detailed results were listed in Table 3-12.

As expected, the two diffraction peaks at $2\theta = 15.1^\circ$ and 21.4° appeared only for the ammonium containing catalysts, and – again as expected – their intensities weakened as the number of NH_4^+ cations decreased, becoming non-detectable in $Cs_3(NH_4)_0H$. Therefore, the two diffraction lines could be considered as characteristic lines for the NH_4^+ containing heteropolycompounds.

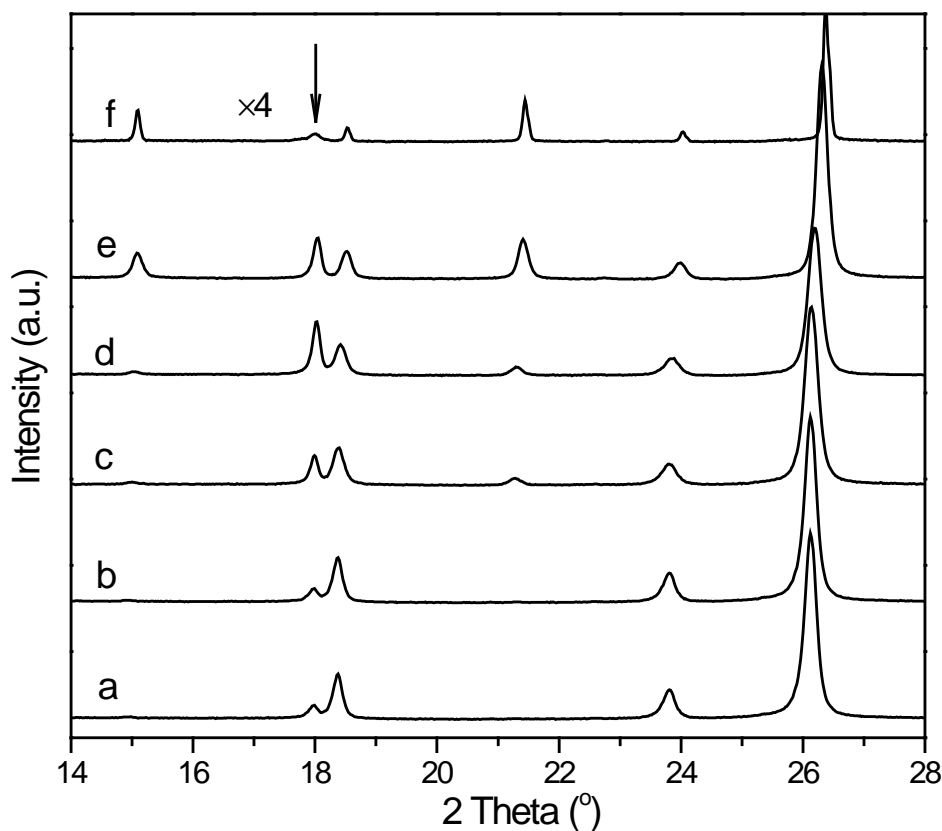Figure 3-23 XRD patterns of the different catalysts before reaction

(a: $Cs_3(NH_4)_0H$, b: $Cs_{2.5}(NH_4)_{0.5}H$, c: $Cs_{1.7}(NH_4)_{1.3}H$, d: $Cs_{1.5}(NH_4)_{1.5}H$, e: $Cs_{0.5}(NH_4)_{2.5}H$, f: APMV)

Arrow indicated the line from the Teflon holder.

For the used catalysts (Figure 3-24), the main diffraction lines from the Keggin-type compounds could still be found, indicating that the structure was maintained under reaction conditions. As far as the intensities of the characteristic diffraction peaks of NH_4^+ containing solids are concerned, a significant decrease was stated for $2\theta= 21.4^o$ and the signal at $2\theta= 15.1^o$ completely vanished for used $Cs_{2.5}(NH_4)_{0.5}H$, $Cs_{1.7}(NH_4)_{1.3}H$ and $Cs_{1.5}(NH_4)_{1.5}H$ catalysts.

On the other hand, a similar shifts as for the fresh catalyst could be observed, corresponding to the change in d-spacing (Table 3-12). For APMV, the d-spacing decreased from 0.3377 to 0.3372 after reaction, which might be explained by two factors: i) V was eliminated from the primary structure leading to the formation of $(NH_4)_3PMo_{12}O_{40}$ (PDF#43-0315) which exhibited d-spacing of 0.3370; ii) the partial release of NH_4^+ as NH_3 to give the acid type species (PDF#52-1117 with a d-spacing of 0.3190)

Additionally, the samples containing less amount of caesium like $Cs_{0.5}(NH_4)_{2.5}H$ and $Cs_{1.5}(NH_4)_{1.5}H$ exhibited increased d-spacing after reaction. This was ascribed to the removal of NH_4^+ cations in the form of NH_3 and water. The resulting vacancies could be rapidly refilled with the peripheral Cs atoms, which has bigger atomic radius. The rest caesium contained samples had the opposite changes, because the removal of NH_4^+ make the catalyst composition evaluate towards to the salt $Cs_4PMo_{11}VO_{40}$ (PDF#46-0481 with d-spacing of 0.3393).

Finally, the influence of Cs on the crystallite size were also investigated using Scherrer's equation [29, 37]. APMV showed the largest crystallite size (>100 nm) whatever for the calcined or spent ones. The introduction of Cs into the catalyst was favourable for obtaining smaller crystallite size [> 100 nm for APMV vs. 45.7 nm for $Cs_{0.5}(NH_4)_{2.5}H$], whereby the latter could be controlled by varying the Cs^+/NH_4^+ ratio. From the values obtained for the spent catalysts, one can see that sintering was limited as the crystallite size was rather unchanged after reaction.
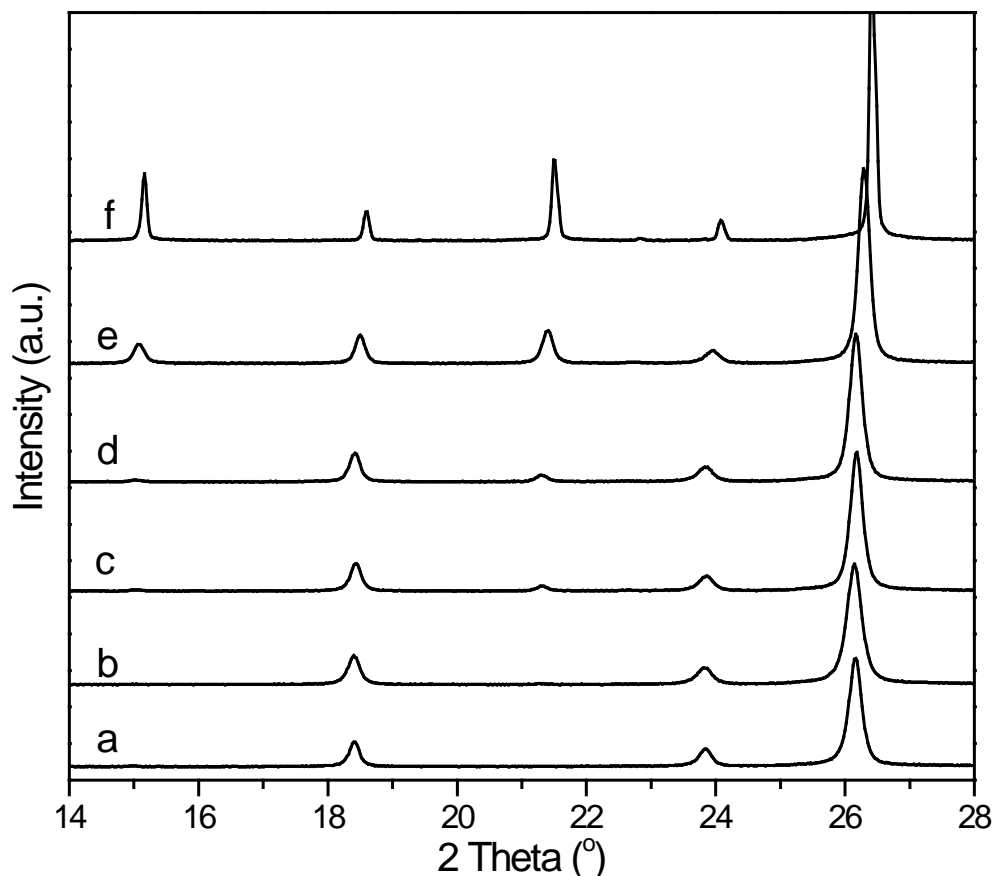
Figure 3-24 XRD patterns of the different catalysts after reaction

(a: $Cs_3(NH_4)_0H$, b: $Cs_{2.5}(NH_4)_{0.5}H$, c: $Cs_{1.7}(NH_4)_{1.3}H$, d: $Cs_{1.5}(NH_4)_{1.5}H$, e: $Cs_{0.5}(NH_4)_{2.5}H$, f: APMV)

Table 3-12 Comparative results of XRD for the catalysts before and after catalytic reaction

Sample	Before reaction			After reaction		
	2 theta at hkl (222)	d(222), nm	Average Crystallite size, nm	2 theta at hkl (222)	d(222), nm	Average Crystallite size, nm
$Cs_0(NH_4)_3H$ (APMV)	26.37	0.3377	>100	26.41	0.3372	>100
$Cs_{0.5}(NH_4)_{2.5}H$	26.29	0.3387	45.7	26.27	0.3390	47.2
$Cs_{1.5}(NH_4)_{1.5}H$	26.18	0.3400	39.4	26.14	0.3406	42.2
$Cs_{1.7}(NH_4)_{1.3}H$	26.12	0.3408	38.8	26.16	0.3403	42.3
$Cs_{2.5}(NH_4)_{0.5}H$	26.06	0.3416	36.9	26.12	0.3408	44.9
$Cs_3(NH_4)_0H$	26.10	0.3411	41.9	26.14	0.3406	46.4

The d(222) values for $(NH_4)_3PMo_{12}O_{40}$ (PDF#43-0315), $Cs_4PMo_{11}VO_{40}$ (PDF#46-0481) and $H_4PMo_{11}VO_{40}$ (PDF#52-1117) are 0.3370, 0.3393 and 0.3190 nm, respectively.

3.3.2.5   Acidic properties determined by NH_3-TPD technique

The acidic properties of the prepared catalysts where studied by temperature programmed desorption of ammonia. The corresponding profiles were collected between 130 to 700 $^{\circ}$C and gathered in Figure 3-25. Strong differences of strength and amount of acid sites could be observed. The flat profile exhibited by $Cs_3(NH_4)_0H$ sample, meaning that no acid sites were present. Despite the fact that a proton was theoretically still present in this sample, the TGA analysis showed that it was easily eliminated under calcination conditions (*cf. section 3.3.2.1*). In the other cases, the ammonia uptake and the main desorption temperature increased with the increase of ammonium ions, and only a broad peak between 130 and 470 $^{\circ}$C was found with $Cs_{2.5}(NH_4)_{0.5}H$. For the remaining three samples the desorption peak area and the temperature increased with the increase of NH_4^+ cations, indicating larger amount of NH_3 uptake and stronger acidic strength. The desorption peak temperature for $Cs_{1.7}(NH_4)_{1.3}H$, $Cs_{1.5}(NH_4)_{1.5}H$ and $Cs_{0.5}(NH_4)_{2.5}H$ catalysts was centred at 435, 445 and 470 $^{\circ}$C, respectively. The quantitative determination of the acidic sites was reported in Table 3-13, whereby the values were corrected by the ammonia resulting from the decomposition of the ammonium at T > 370 $^{\circ}$C (*cf. Annex section 6.3 for details*).

No catalyst exhibited super strong acidic sites, and strong acidic sites were only detected for catalysts having low Cs content [$Cs_{0.5}(NH_4)_{2.5}H$, 1.16 mmol/g_{cat}] which also exhibited the highest amount of acidic sites (1.84 mmol/$g_{cat.}$). As expected, the total acidity displayed a decreasing trend as the Cs atoms increased, whereby medium acidic sites were in majority. The proportion of medium sites increased with decreasing number of Cs atoms, from 59% for $Cs_3(NH_4)_0H$ to 99% for $Cs_{1.5}(NH_4)_{1.5}H$. Thus, the introduction of Cs into the catalysts not only affected the amount but also the strength of the acidic sites. The surface acidic sites density based on the surface was also given. The highest surface acid density of 317 µmol/$m^2_{cat.}$ was obtained over [$Cs_{0.5}(NH_4)_{2.5}H$], which was notably due to its rather low surface area of 6 m²/g. As far as the acidity – in terms of NH_3 uptake – was concerned, an inversed linear relationship with the number of Cs atoms could be observed (Figure 3-26).
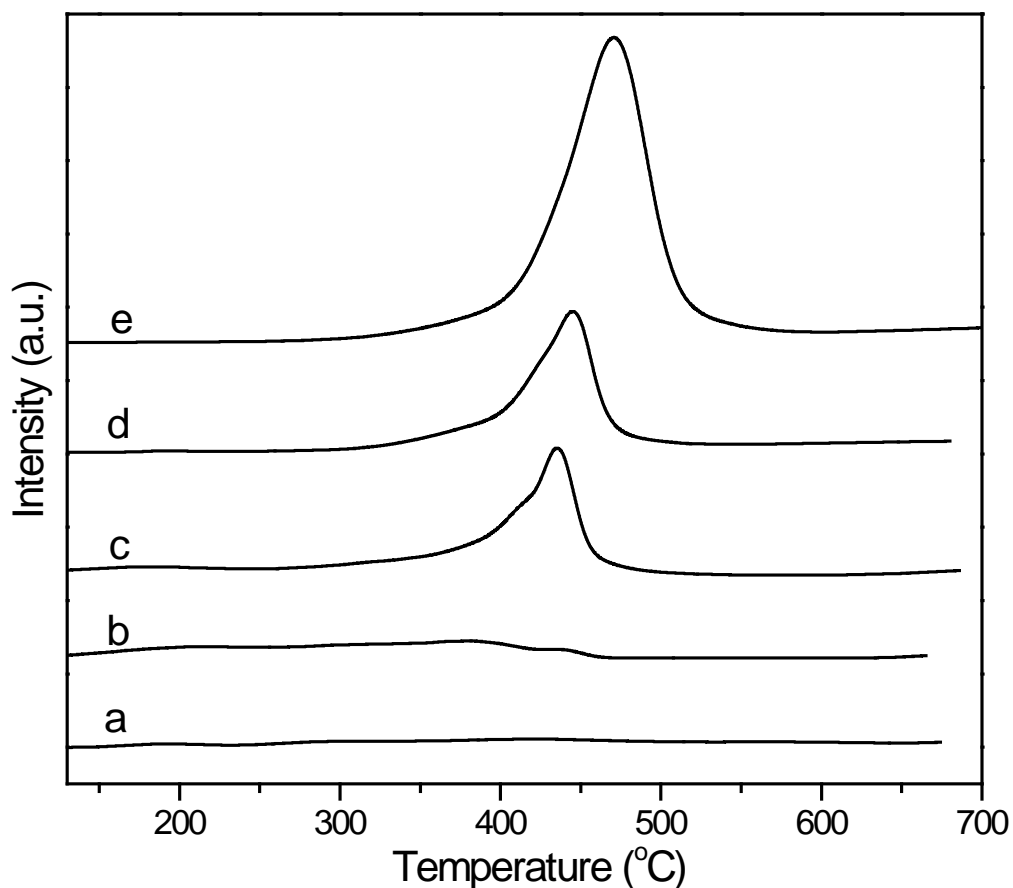
Figure 3-25 NH$_3$-TPD profiles of the mixed salts

(a: Cs$_3$(NH$_4$)$_0$H, b: Cs$_{2.5}$(NH$_4$)$_{0.5}$H, c: Cs$_{1.7}$(NH$_4$)$_{1.3}$H, d: Cs$_{1.5}$(NH$_4$)$_{1.5}$H, e: Cs$_{0.5}$(NH$_4$)$_{2.5}$H)

Table 3-13 The amount of acidic sites and their strength distribution

Catalyst	Acidity, NH$_3$ uptake, mmol/g cat.				Total acidity mmol/g$_{cat.}$ (μmol/m$^2_{cat.}$)	
	130-300 weak	300-450 medium	450-560 strong	560-700 ^{o}C super strong		
Cs$_3$(NH$_4$)$_0$H	0.07	0.10	-	-	0.17	(2)
Cs$_{2.5}$(NH$_4$)$_{0.5}$H	0.07	0.23	-	-	0.30	(5)
Cs$_{1.7}$(NH$_4$)$_{1.3}$H	0.02	0.71	-	-	0.72	(44)
Cs$_{1.5}$(NH$_4$)$_{1.5}$H	0.01	0.89	-	-	0.90	(107)
Cs$_{0.5}$(NH$_4$)$_{2.5}$H	0.00	0.68	1.16	-	1.84	(317)
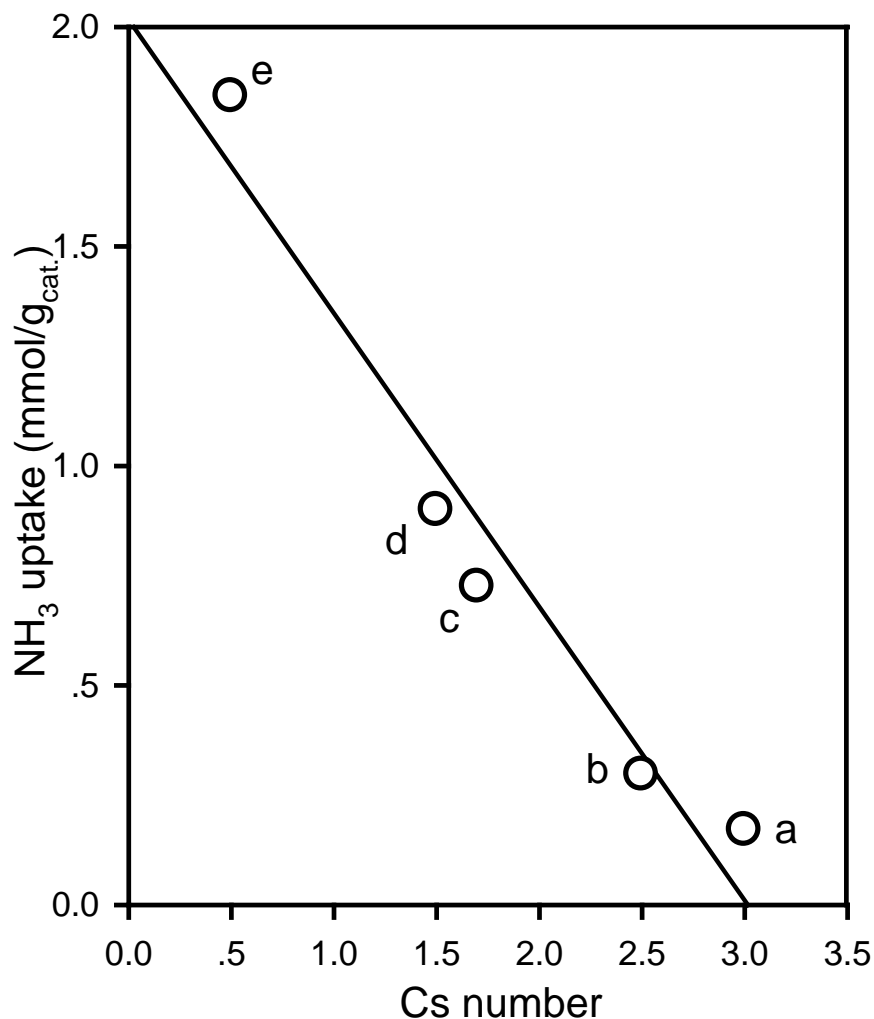
Figure 3-26 NH$_3$ uptake as a function of Cs number in the catalyst
(a: Cs$_3$(NH$_4$)$_0$H, b: Cs$_{2.5}$(NH$_4$)$_{0.5}$H, c: Cs$_{1.7}$(NH$_4$)$_{1.3}$H, d: Cs$_{1.5}$(NH$_4$)$_{1.5}$H, e: Cs$_{0.5}$(NH$_4$)$_{2.5}$H)

3.3.3 Conclusions

Mixed-salts Cs$_x$(NH$_4$)$_{3-x}$HPMo$_{11}$VO$_{40}$ (x=0~3) samples were prepared by precipitation method and their properties such as texture, crystalline phases, acidity and reducibility were successfully controlled by varying the ratio of Cs$^+$/NH$_4^+$ during the preparation. The APMV displayed the features of non-porous materials, the introduction of Cs was favourable to create the meso- and/micro-pores, resulting in changes in specific surface area, pore volumes and pore size distribution, which was strongly determined by the Cs number. XRD results showed clearly the main characteristic diffraction peaks attributed to the Keggin type compounds for

both the calcined and used catalysts. The increase of the crystallite size of the used samples indicated some aggregation during reaction. On the other hand, minor decomposition may occurred under the reaction conditions as attested by the observation of characteristic bands of MoO_3 in FT-IR and Raman spectroscopies, especially for the samples with lower Cs content like $Cs_{1.7}(NH_4)_{1.3}H$, $Cs_{1.5}(NH_4)_{1.5}H$ and $Cs_{0.5}(NH_4)_{2.5}H$. But the decomposition process was too weak to be detected by XRD, and Cs element was also helpful to limit the evolution of primary structure. Besides the effects on the textural properties, the ratio Cs^+/NH_4^+ also affected the acidity of the catalysts as evaluated by NH_3-TPD. The stronger acidic sites and better reducibility could be obtained over the catalysts with the lower Cs content. For a surface type reaction, the catalytic performances should be significantly influenced by the aforementioned properties. This will be studied in the next chapter.

References

[1]   I. V. Kozhevnikov, K. R. Kloetstra, A. Sinnema, H. W. Zandbergen, H. Van Bekkum, J. Mol. Catal. A: Chem. 114 (1996) 287.

[2]   N. Mizuno, M. Tateishi, M. Iwamoto, J. Catal. 163 (1996) 87.

[3]   C. Marchal-Roch, N. Laronze, N. Guillou, A. Tézé, G. Hervé, Appl. Catal. A: Gen 199 (2000) 33.

[4]   I. Kozhevnikov, J. Mol. Catal. A: Chem. 305 (2009) 104.

[5]   M. Kanno, T. Yasukawa, W. Ninomiya, K. Ooyachi, Y. Kamiya, J. Catal. 273 (2010) 1.

[6]   M. Sultan, S. Paul, M. Fournier, D. Vanhove, Appl. Catal. A: Gen 259 (2004) 141.

[7]   M. Sun, J. Z. Zhang, C. J. Cao, Q. H. Zhang, Y. Wang, Appl. Catal. A: Gen 349 (2008).

[8]   C. Rocchiccioli-Deltcheff, M. Fournier, R. Franck, R. Thouvenot, Inorg. Chem. 22 (1983) 207.

[9]   A. Brückner, G. Scholz, D. Heidemann, M. Schneider, D. Herein, J. Catal. 245 (2007) 369.

[10]   N. Ballarini, F. Candiracci, F. Cavani, H. Degrand, J. L. Dubois, Appl. Catal. A: Gen 325 (2007) 263.

[11]   Q. Huynh, A. Selmi, G. Corbel, P. Lacorre, J. Millet, J. Catal. 266 (2009) 64.

[12]   G. Mestl, T. Ilkenhans, D. Spielbauer, M. Dieterle, O. Timpe, Appl. Catal. A: Gen 210 (2001) 13.

[13]   K. M. Parida, S. Rana, S. Mallick, D. Rath, J. Colloid Interface Sci. 350 (2010) 132.

[14]   S. Park, D. R. Park, J. H. Choi, T. J. Kim, Y.-M. Chung, J. Mol. Catal. A: Chem. 332 (2010) 76.

[15]   S. Paul, V. LeCourtois, D. Vanhove, Ind. Eng. Chem. Res. 36 (1997) 3391.

[16]   S. Paul, W. Chu, M. Sultan, E. Bordes-Richard, Sci. China, Ser. B: Chem 53 (2010) 2039.

[17]   F. Jing, B. Katryniok, E. Bordes-Richard, S. Paul, Catal. Today http://dx.doi.org/10.1016/j.cattod.2012.03.028 (2012).

[18]   C. Marchal-Roch, N. Laronze, N. Guillou, A. Tézé, G. Hervé, Appl. Catal. A: Gen 203 (2000) 143.

[19]   C. Marchal-Roch, C. Julien, J. F. Moisan, N. Leclerc-Laronze, F. X. Liu, Appl. Catal. A: Gen 278 (2004) 123.

[20]   C. Marchal-Roch, N. Laronze, R. Villanneau, N. Guillou, A. Tézé, J. Catal. 190 (2000) 173.

[21]   K. Mohan Reddy, N. Lingaiah, P. Nagaraju, P. Sai Prasad, I. Suryanarayana, Catal. Lett. 122 (2008) 314.

[22]   Q. Huynh, Y. Schuurman, R. Delichere, S. Loridant, J. M. M. Millet, J. Catal. 261 (2009) 166.

[23]   F. Cavani, R. Mezzogori, A. Pigamo, F. Trifiro, E. Etienne, Catal. Today 71 (2001) 97.

[24]   F. Cavani, F. Trifiro, Catal. Today 51 (1999) 561.

[25]   G. Busca, F. Cavani, E. Etienne, E. Finocchio, A. Galli, J. Mol. Catal. A: Chem. 114 (1996) 343.

[26]   J. K. Lee, V. Russo, J. Melsheimer, K. Kohler, R. Schlogl, Phys. Chem. Chem. Phys. 2 (2000) 2977.

[27]   S. Besselmann, C. Freitag, O. Hinrichsen, M. Muhler, Phys. Chem. Chem. Phys. 3 (2001).

[28]   K. Inumaru, T. Ito, M. Misono, Microporous Mesoporous Mater. 21 (1998) 629.

[29]   T. Okuhara, H. Watanabe, T. Nishimura, K. Inumaru, M. Misono, Chem. Mater. 12 (2000) 2230.

[30]   J. S. Santos, J. A. Dias, S. C. L. Dias, F. A. C. Garcia, J. L. Macedo, Appl. Catal. A: Gen 394 (2011) 138.

[31]   K. Katsumi, J. Membr. Sci. 96 (1994) 59.

[32]   F. Rouquerol, J. Rouquerol, K. Sing, Adsorption by Powders and Porous Solids, Academic Press, London. 1 (1999).

[33]   X.-K. Li, J. Zhao, W.-J. Ji, Z.-B. Zhang, Y. Chen, J. Catal. 237 (2006) 58.

[34]   C. Knapp, T. Ui, K. Nagai, N. Mizuno, Catal. Today 71 (2001) 111.

[35]   C. Rocchiccioli-Deltcheff, M. Fournier, J. Chem. Soc., Faraday Trans. 87 (1991).

[36]   N. Mizuno, D. J. Suh, W. Han, T. Kudo, J. Mol. Catal. A: Chem. 114 (1996) 309.

[37]   F. Jing, Y. Zhang, S. Luo, W. Chu, H. Zhang, J. Chem. Sci. 122 (2010) 621.

4 Catalytic performances in the selective oxidation of isobutane

4.1 APMV-based catalysts supported on various carriers

4.1.1 Catalytic performance

The catalytic performance of the catalysts discussed in section 3.1 was evaluated for the selective oxidation of isobutane to MAC and MAA in the same conditions (Table 4-1). The lowest IBAN conversion (X_{IBAN} = 2.5%) was reached for the bulk APMV sample. This low conversion was related to the rather low surface area (4 m^2/g) of the catalyst. After supporting the APMV, the catalytic activity increased to different extents, depending on the support. The best performance (yield MAC+MAA = 8 mol.%; X_{IBAN} = 13%) was obtained for the APMV/CPM catalyst, and it was higher than the values currently reported in the open literature (yield = 7 mol%; X_{IBAN} = 10%) [1]. The selectivity to MAA was also found to be strongly dependent on the nature of the support, and it was the highest for bulk APMV (34.3%) and APMV/CPM (42%). Consequently the best yield in the desired products MAC+MAA (8.0 mol.%) was obtained with APMV/CPM whereas it reached no more than 3.1, 0.7 and 1.4 mol% over CARiACT®-silica, zirconia-modified SBA-15 and SBA-15, respectively. The low selectivity in the desired products observed for the silica-based catalysts was due to the formation of large amounts of different by-products. In the case of APMV/SBA-15 and APMV/SiO_2, a lot of acetic acid was formed, whereas the catalyst supported on zirconia-modified SBA-15 exhibited a high selectivity to CO_x (>60%). The strong tendency to total oxidation was confirmed when calculating the ratio of the reactants conversions X_{O2}/X_{IBAN}. The lowest values (*ca.* 4:1) were found for APMV and AMPMV/CPM, while APMV/SBA-15 and APMV/ZrO_2/SBA-15 exhibited rather high values of 10:1 and 14:1, respectively, meaning thus an over-stoichiometric consumption of oxygen with regard to the selective oxidation reaction equation. The significant difference in selectivity between the catalysts could be correlated to the possible presence of MoO_3 (*cf. sections 3.1.2.3 and 3.1.2.4*). Physicochemical analyses showed that the active phase was less stable when

supported on silica-based materials (*cf. section 3.1.2.1*). As a consequence, APMV was partially decomposed to metal oxides – notably MoO_3 – which was claimed to be unselective in IBAN oxidation since it yielded mainly acetic and acrylic acids and carbon oxides (CO_x) [2-5]. Moreover, the uncovered surface of silica when sub-monolayer of APMV was dispersed on the silica support did not help the catalyst improve the catalytic activity as the no conversion of isobutane was found in the blank reaction.

As an intermediate conclusion, one can state that the decreased performance over silica-based catalysts was ascribed to the partial decomposition of the active phase during the catalyst preparation, calcination and under stream, leading (i) to a decreased amount of selective Keggin-type compounds and (ii) to the formation of unselective oxides like MoO_3 favouring the total oxidation of IBAN.

Table 4-1 Catalytic performance in the oxidation of isobutane of bulk APMV and supported catalysts

Catalyst	Conversion [a], %		Selectivity, %				$Y_{(MAC+MAA)}$, %	Carbon balance, %
	O_2	IBAN	MAC	MAA	CO_x	Others		
APMV	10.7	2.5	20.4	34.3	35.8	9.5	1.4	99.7
APMV/SBA-15	50.2	5.0	18.0	9.7	42.0	30.3	1.4	99.6
APMV/ZrO$_2$/SBA-15	91.4	6.6	9.6	1.6	63.5	25.3	0.7	102.0
APMV/SiO$_2$	51.8	11.3	14.7	12.7	42.9	29.7	3.1	100.0
APMV/CPM	61.6	15.3	10.0	42.0	30.7	17.3	8.0	99.3

[a] Reaction conditions: Temperature 340 °C, atmospheric pressure, contact time 4.8 s, Molar ratios: IBAN/O_2/H_2O/inert = 27/13.5/10/49.5. IBAN: isobutane, MAC: methacrolein, MAA: methacrylic acid; Others include acetic acid and acrylic acid.

4.1.2 Relationship between acidity and catalytic activity

The results presented above showed that the specific surface area was not the primary factor accounting for the catalytic activity when different types of supports were used. Indeed, the APMV/CPM catalyst presenting the lowest surface area (namely 17 m²/g) exhibited the

highest IBAN conversion (i.e. 15.3%) of the series. Therefore, a correlation between catalytic activity and acidity was attempted.

On one hand, the activity was here defined as follows:

$$Activity = \frac{F_{IBAN}^{inlet} \times X_{IBAN}}{S_{BET} \times m_{catal.}}$$

where F_{IBAN}^{inlet} is the isobutane molar flowrate feed to the reactor, X_{IBAN} the isobutane conversion, S_{BET} the surface area and m_{cata} the mass of catalyst. On the other hand, the acidity of the catalysts was represented by their TPD NH_3 uptake.

On plotting the so-defined activity *vs.* surface acid density a linear relationship ($R^2 = 0.999$) was obtained (Figure 4-1). Bulk APMV was not added to this graph because the calculated value of acid site density was far higher (550 $\mu mol/m^2_{cat.}$) than those of other catalysts because of its very low surface area. The point for the bare CPM support (0, 0) were reported, as it was inactive and did not exhibit any acidic sites.

This correlation demonstrated that the activation of the isobutane molecule depended above all on the acidic properties of the catalysts. Indeed, the activation of a methyl C-H bond to form a C=C double bond by oxidative dehydrogenation has been shown to be the rate-determining step of the mechanism [6] and it obviously depends mainly on the acidic properties of the catalyst. In addition, these acidic properties also favour the desorption of acidic products like methacrylic acid [7]. As the most acidic catalyst was APMV/CPM, it was at the end not so surprising that the highest conversion of IBAN (15.3%) was obtained for this sample as well as the highest yield in desired products (8.0%).
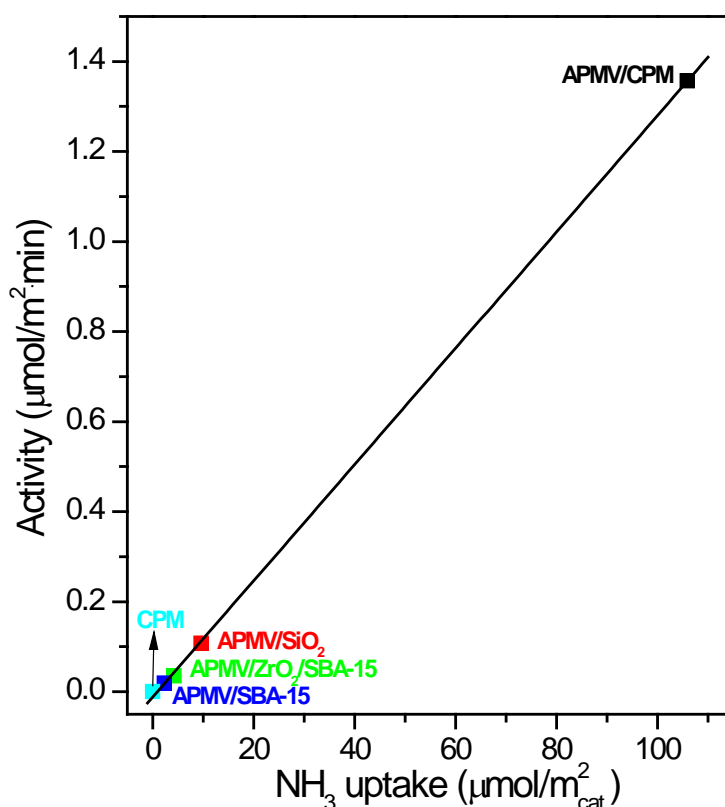
Figure 4-1 Correlation between the activity in isobutane oxidation and the acidity
of catalysts measured by NH_3-TPD

4.2 Optimization of the CPM-supported catalyst

4.2.1 Influence of the amount of APMV active phase

As the CPM-supported catalyst exhibited the best performance, further experiments were carried out with different APMV loadings on the CPM support (namely from 10 to 50 wt.%). The results obtained for this series were summarized in Table 4-2. For the catalyst with 10 wt.% APMV, there was no activity at all. For the other catalysts containing 20 to 50 wt.% APMV, the catalytic activity was in the range of 14 to 15.3% whereby the lowest IBAN conversion was observed for the catalyst containing 50 wt.% APMV. The yield in MAC and MAA was found to increase with the amount of active phase, which was directly linked to the decreased formation of carbon oxides (CO_x) and acetic acid (AA).

Table 4-2 Catalytic performance for IBAN oxidation over APMV/CPM catalysts with different loadings

Catalyst	Conversion[a], %		Selectivity, %					$Y_{(MAC+MAA)}$, %	Carbon balance
	O_2	IBAN	MAC	AA	ACA	MAA	CO_x		
10APMV/CPM	0	0	/	/	/	/	/	/	/
20APMV/CPM	79.3	14.7	9.1	16.4	3.1	33.4	38	6.2	0.995
40APMV/CPM	61.6	15.3	10.0	14.1	3.2	42.0	30.7	8.0	0.993
50APMV/CPM	53.7	14.0	11.4	12.3	3.0	46.6	26.7	8.1	0.994

a Reaction conditions: Temperature=340 °C, atmospheric pressure, contact time=4.8 s.

Here IBAN=isobutane, MAC=methacrolein, AA=acetic acid, ACA=acrylic acid and MAA=methacrylic acid.

On one hand, it was shown in the previous section that the primary important factors for activating the isobutane molecules were the acidity of the catalyst and its surface area. On the other hand, the nature of the active phase was highly influent on the selectivity and the Keggin structure had to be kept to form the desired products. Therefore the combination of the decreasing of the acidity and of surface area for the 50APMV/CPM sample explained the decreased activity observed for this sample whereas the selectivity for MAC and MAA overpasses 58%.

In fact, infrared spectroscopy and IR-Raman evidenced the partial decomposition of APMV during the catalytic test (*cf. section 3.2.2.5*), leading thus to the formation of metal-oxides that were non-selective in the oxidation of IBAN. But the extent of this decomposition process was also found to be strongly correlated to the amount of APMV dispersed on the CPM surface. The catalysts containing low amounts of APMV (10-20 wt.%) were actually found less stable *(cf. section 3.2.2.1)*, explaining therefore the increased formation of products from the oxidative degradation such as acetic acid and CO_x over those catalysts. Increasing the amount of active phase leads to a better stabilization of the Keggin structure and therefore to the reduction of by-products formation.

As seen from the NH_3-TPD (*cf. section 3.2.2.7*), the 10APMV/CPM sample exhibited no acid sites, notably due to its decomposition as attested by XRD, XPS and FT-IR (*cf. sections 3.2.2.3, 3.2.2.4 and 3.2.2.5*). This explains its absence of activity in the isobutane oxidation.

As a matter of fact, it is well known that the first step of the isobutane oxidation mechanism involves the initial abstraction of a H⁻ at the tertiary C atom of the alkane [5, 6]. The acidic sites on the surface can effectively promote the hydrocarbon activation and lead to the C=H bound formation by oxidative dehydrogenation, the resulting alkenes then transforming into methacrolein and methacrylic acid by oxidation, which was found 500 times faster that its formation [8, 9]. This may be the reason why the intermediate isobutene was gotten rid of the reaction mechanism in early publications [5, 10, 11]. Combining the modification of reducibility by introduced-V for the oxidation step and the profound influence of acidity and surface area on catalytic activity (first step of the mechanism), the reaction route for isobutane oxidation over V-substituted bifunctional heteropolycompounds catalysts was proposed in Figure 4-2 [5-8, 12, 13].
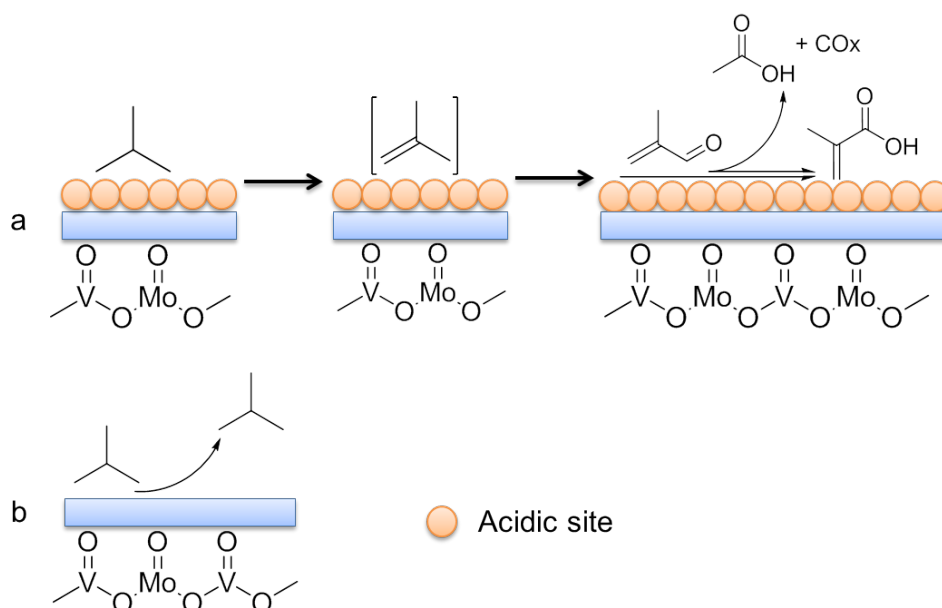
Figure 4-2 Reaction route of isobutane oxidation over V-substituted bifunctional heteropolycompounds catalysts [5-8, 12, 13].

(a: Reaction route on the acidic surface, b: Reaction route on the catalyst surface without acidic sites)

4.2.2 Influence of surface acid density on catalytic activity

It was shown in section *4.1.2* that the density of acidic sites on catalyst surface played a determinable role in the activation of isobutane molecules. Therefore this correlation was also

tested here for the xAPMV/CPM series (Figure 4-3). It did not respect anymore the linear relationship observed previously when the content of APMV increased. The activity displayed actually a sharp leap from 0 to 1.2 $\mu mol/m^2 \cdot min$ as the content of APMV changed from 10 to 20 wt.%, correspondingly the surface acid density changed from 3 to 36 $\mu mol/m^2_{cat.}$. The increasing rate became lower then. However, the activity still increased with the increasing of the surface acid density which emphasized again the importance of these acidic sites and of a minimum of surface area, which were indispensable for reaching high isobutane conversion levels.
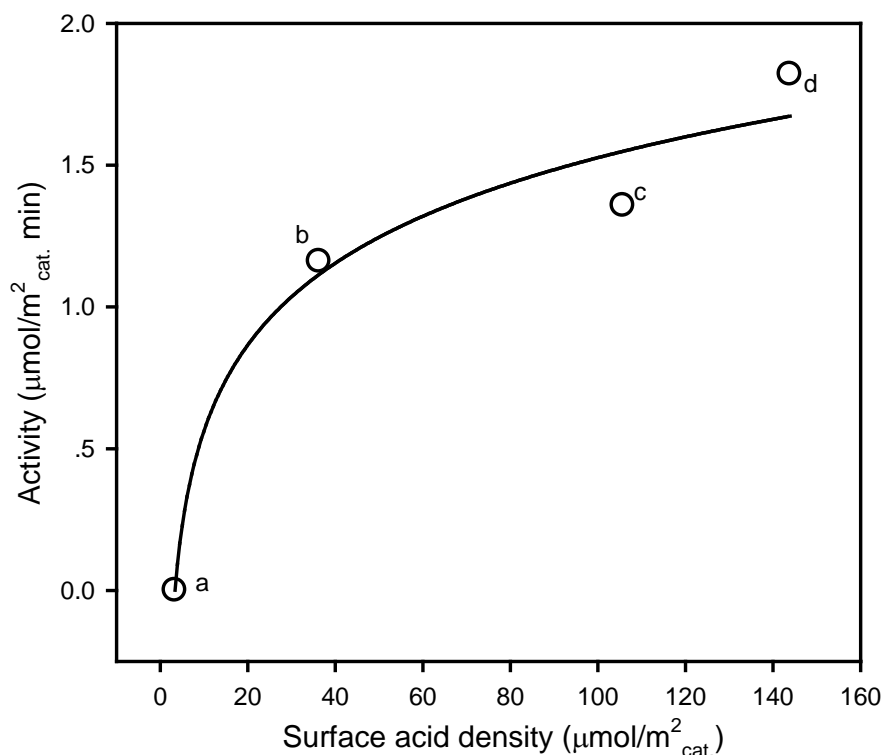
Figure 4-3 Relationship of the activity and the surface acid density
(a: 10APMV/CPM, b: 20APMV/CPM, c: 40 APMV/CPM and d: 50 APMV/CPM)

4.2.3 Effect of reaction temperature

In order to investigate the influence of the reaction conditions on the catalytic performance, the sample 40APMV/CPM was chosen for further study. Firstly the reaction was carried out at different temperatures with a constant contact time of 4.8 s. All the other

operating conditions were the same as above. The corresponding results were shown in Figure 4-4. It can be seen that the IBAN conversion increased linearly as the reaction temperature increased from 280 to 350 °C. It reached a maximum value of 16.3% at 350 °C. As observed from Figure 4-4 the yield in MAC+MAA also followed an increasing linear relationship with temperature. The maximum yield of the desired products (MAC+MAA) was obtained at 350 °C with a value of 8.7%.
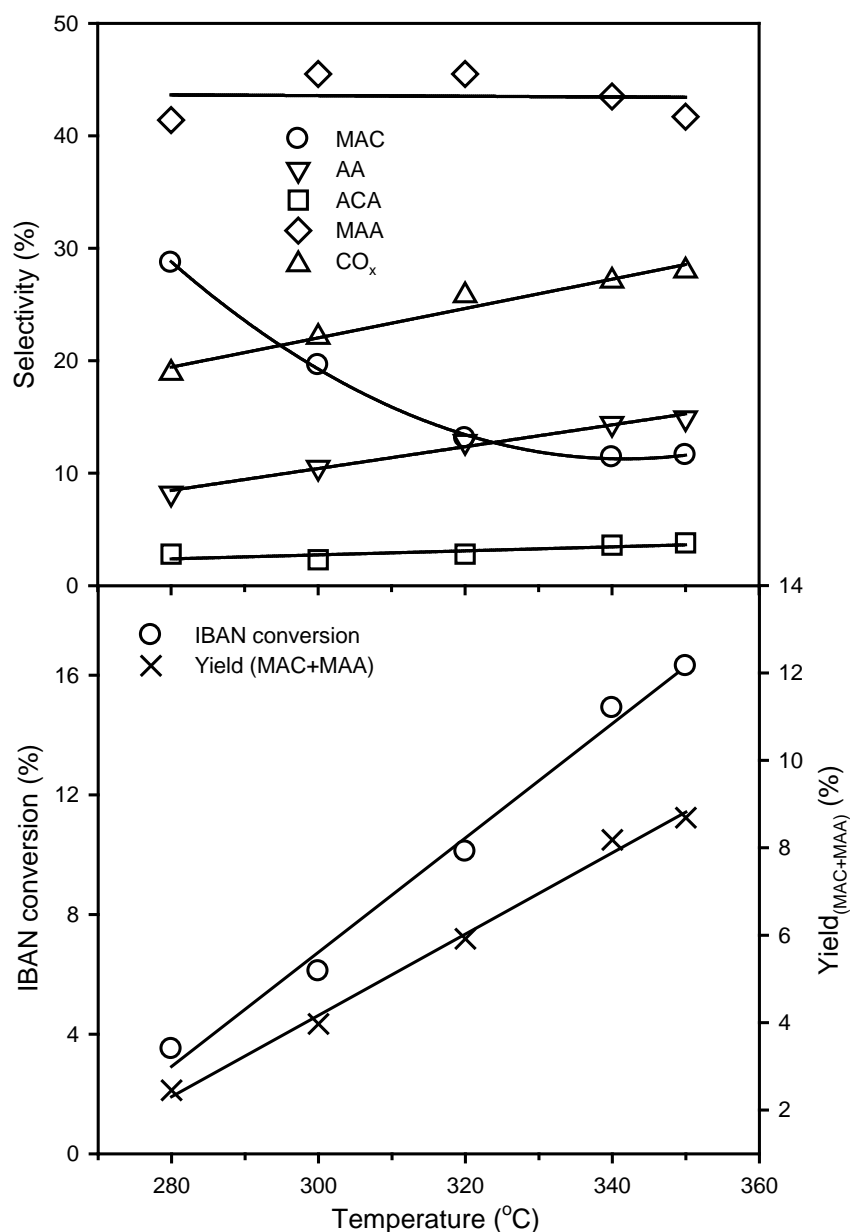
Figure 4-4 Effects of reaction temperature on catalytic performances

IBAN=isobutane, MAC=methacrolein, AA=acetic acid, ACA=acrylic acid and MAA=methacrylic acid.

As far as the products distribution was concerned, it was interesting to note that the selectivity in MAA was kept roughly stable. In reality, a very slight decrease was observed when increasing the temperature. This results indicated that the selectivity to MAA was not deeply affected by the reaction temperature, which was in good agreement with our previous observations [5]. As a matter of fact, in Paul *et al.*'s preliminary work, the catalytic reaction was carried out from 300 ^{o}C to 350 ^{o}C, and the fact that the desired products MAC+MAA demonstrated steady state in selectivity was already referred.

On the other hand, low reaction temperature, i.e. 280 ^{o}C, were found rather favourable in terms of selectivity to the intermediate MAC as the formation of acetic acid (AA), acrylic acid (ACA) and CO_x (products of degradation) was significantly limited. In reverse, increased reaction temperature (350 ^{o}C) lead to significant decrease in MAC selectivity (11.6%), which was in good agreement with its role of intermediate in the reaction mechanism.

Finally one can assume that at the higher temperature more MAA was formed by MAC oxidation but that more by-products were also formed because of the oxidative degradation of MAA and MAC. Therefore even if temperatures superior to 350 °C were not tested in this work one can imagine that the yield in interesting products would finally reach a maximum because of the predominating role of the oxidative degradation.

4.2.4 Effect of contact time

A series of experiments was performed to study the effect of contact time on the catalytic selective oxidation of isobutane at a constant reaction temperature of 340 ^{o}C. The results are reported in Figure 4-5.

The IBAN conversion increased from 13.1, 14.7, 17.1 to 20.2% with contact time of 3.6, 4.8, 6.0 and 7.2 s, respectively, suggesting thus that, as expected, longer contact times are favourable for the activation of the hydrocarbon.

However, the product distribution was also profoundly affected by the change in contact time. Actually, if just a slight increase in acrylic acid formation was observed when the

contact time was increased, the selectivity to MAC and MAA decreased significantly, giving rise to degradation products (i.e. AA and CO_x) at the same time.
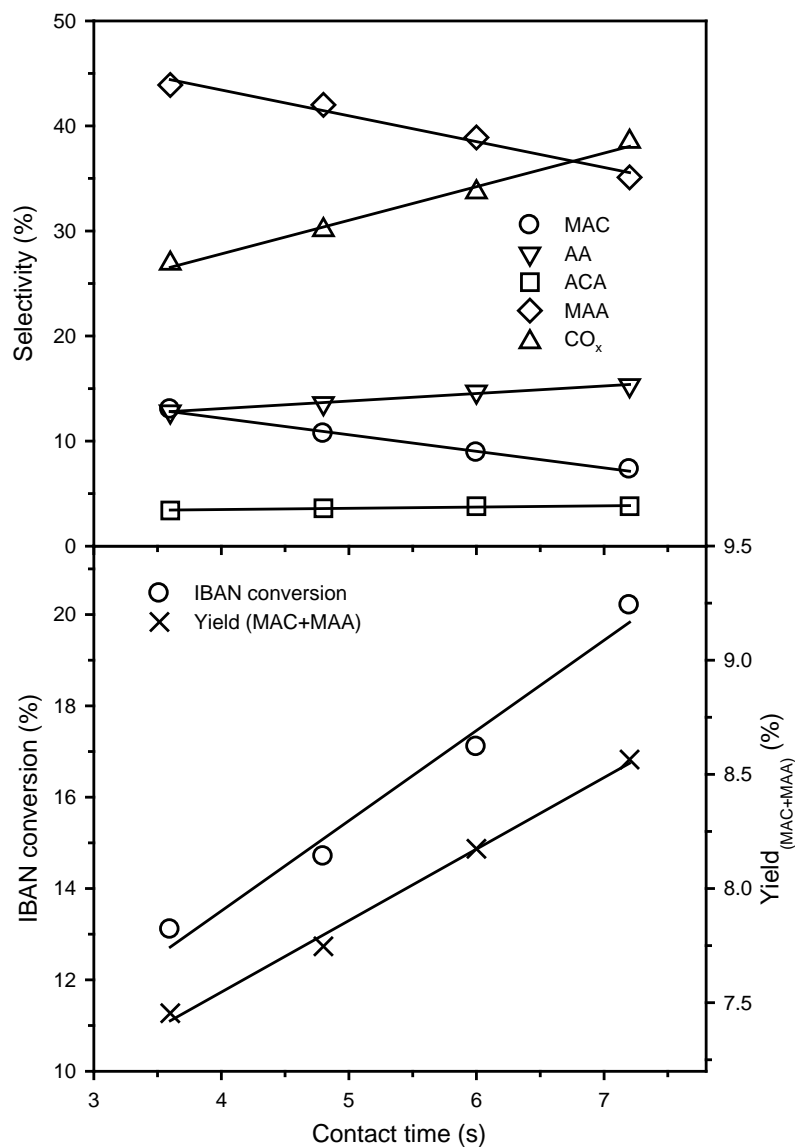
Figure 4-5 Effect of contact time on catalytic performances

IBAN=isobutane, MAC=methacrolein, AA=acetic acid, ACA=acrylic acid and MAA=methacrylic acid.

Starting from isobutane the MAA can be synthesized by a direct and an indirect way *via* MAC as intermediate as shown previously [5]. The kinetic study pointed out that the rate constants for converting MAC into MAA and degradation of MAC to CO_x+AA were 23.4 and 28.7 at the reaction temperature of 350 ^{o}C [5], respectively. The close values implied that the two pathways were competitive reactions and even that the degradation reaction of MAC was

a bit favoured, which can explain the observed inverse trend in the formation of MAC and CO_x/AA.

Moreover, increasing the contact time to high value was detrimental to the control of the isothermicity of the reactor. Hot spots could actually be observed. This may of course be the cause of local degradation of the active phase and of the further decomposition of the Keggin structure then leading to unselective species. The catalytic results observed are consistent with this hypothesis.

4.2.5 Correlation between conversion and selectivity for 40APMV/CPM catalyst

The results obtained in the previous series of tests encouraged us to study the correlation between the selectivities in each product and the conversion of isobutane. Therefore 40APMV/CPM was used as catalyst whereby the conversion was varied by changing either the reaction temperature or the contact time. The reaction conditions and obtained results are gathered in Table 4-3, furthermore the correction was shown in Figure 4-6. One can see that at low conversion (3.5%), both MAC and MAA exhibited high selectivity of 28.7 % and 41.4 % respectively. With increasing conversion, the selectivity in MAC decreases rapidly reaching a constant final value of 11.5%. This can be explained by the different reaction pathways leading to these products. As known from previous studies [5], MAA may be formed either by the direct oxidation of isobutane or *via* the indirect oxidation with MAC as intermediate (Figure 4-2a). According to the kinetic data of Paul *et al.* – obtained for the same type of catalyst– the rate constant for the direct oxidation of isobutane to MAA was rather low compared to the one observed for the indirect oxidation pathway [5]. Therefore, one can explain the decrease in the selectivity of MAC due to its role as intermediate.

From the catalytic results one can see that indeed the selectivity to MAA was rather stable whereas the selectivity in AA and CO_x increased rapidly. As described above, the two reactions starting from MAC were competitive but the degradation reaction of MAC to CO_x was promoted due to its higher rate constant.

Table 4-3 Catalytic results under variable reaction conditions

Run	Reaction temperature, °C	Contact time, s	IBAN conversion, %	Selectivity, %				
				MAC	AA	ACA	MAA	CO$_x$
1	280	4.8	3.5	28.7	8.2	2.8	41.4	18.9
2	300	4.8	6.1	19.6	10.5	2.3	45.5	22.1
3	320	4.8	10.1	13.1	12.8	2.8	45.5	25.8
4	340	3.6	13.1	13.0	12.8	3.4	43.9	26.9
5	340	4.8	14.9	11.4	14.4	3.6	43.5	27.1
6	350	4.8	16.3	11.6	14.9	3.8	41.7	28.0

The sample 40APMV/CPM was used for the catalytic reactions. Feed: IBAN/O$_2$/H$_2$O/inert = 27/13.5/10/49.5. Here: IBAN=isobutane, MAC=methacrolein, AA=acetic acid, ACA=acrylic acid and MAA=methacrylic acid.
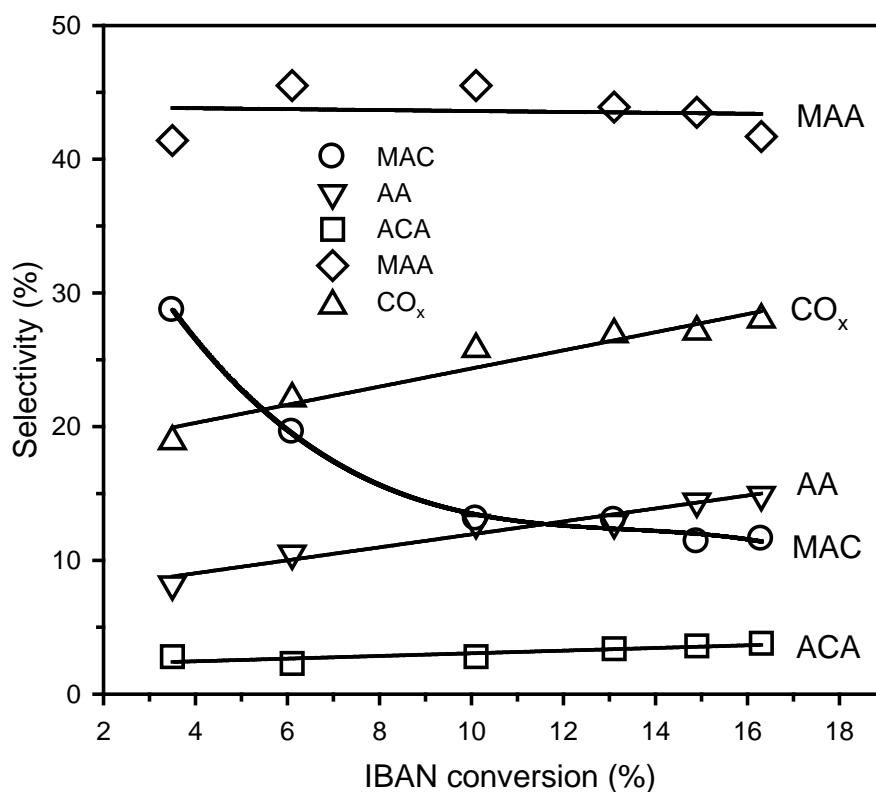
Figure 4-6 Correlation between selectivity and IBAN conversion on 40APMV/CPM sample

4.2.6 Long-term performances of 40APMV/CPM sample

Finally, the long-term catalytic performance was evaluated for the 40APMV/CPM catalyst in the same standard operating conditions used above. From the results (Figure 4-7)

one can see that the catalyst exhibited quite stable performance during 132 h under stream. Only a slight deactivation of the catalyst was observed which was evidenced by the decrease in the conversion of isobutane from 12.5 to 11.5%. This may be due to the sintering of the catalyst as suggested by nitrogen physisorption and XRD showing a decrease in specific surface after test due to the formation of larger crystallites. Meanwhile, the selectivity in the desired products MAA remained stable over the time at 39% whereas the MAC selectivity was slightly increasing at the expense of CO_x.

Figure 4-7 Catalytic stability test over the sample 40APMV/CPM

4.3 The mixed-salts $Cs_x(NH_4)_{3-x}HPMo_{11}VO_{40}$ catalysts

4.3.1 Catalytic performance over various mixed-salts

The catalytic performance of the mixed-salt catalysts was evaluated in the selective oxidation of isobutane to MAC and MAA. Based on the results obtained over silica-supported catalysts, e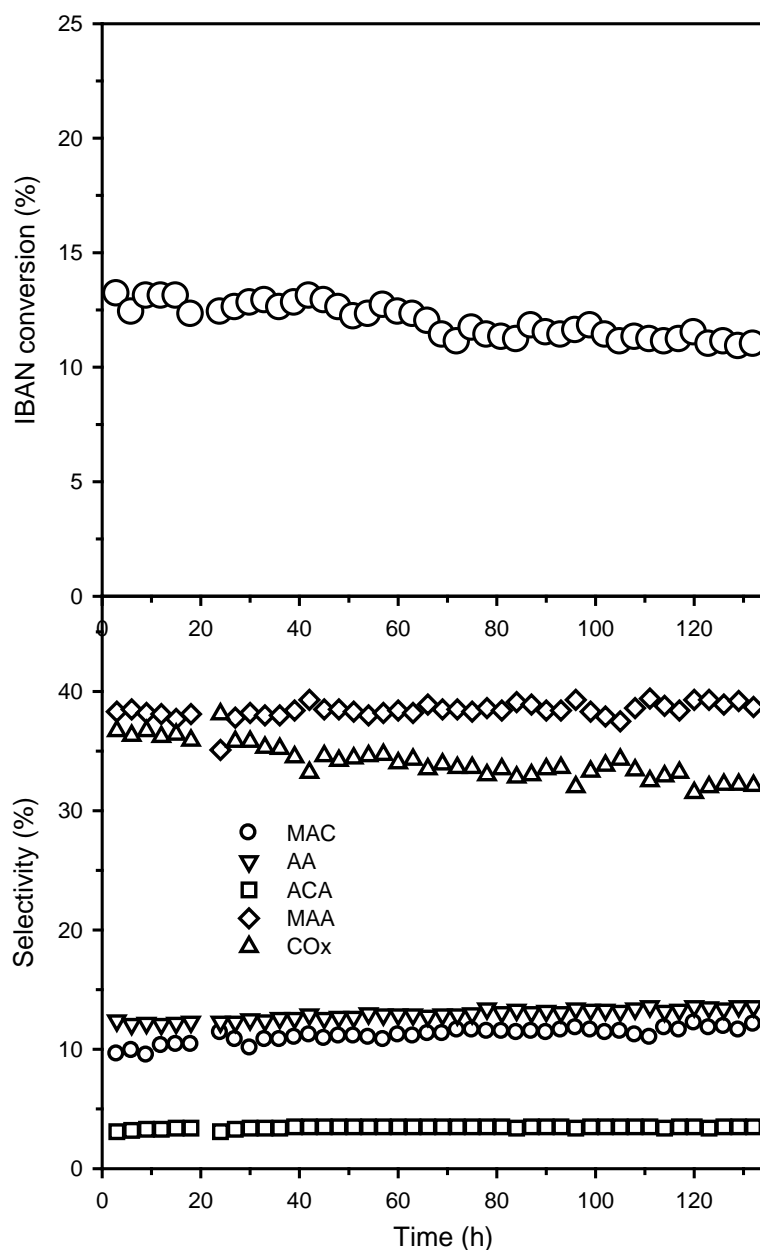xhibiting no benefits over CPM-supported catalyst, a more detailed study for mixed-salts of caesium/ammonia HPAs was performed. Therefore, a series of catalysts based on the $PMo_{11}VO_{40}^{4-}$ anion with different NH_4^+/Cs^+ ratios of counter-cations was prepared. Particularly the sample having the same ratio of Cs^+/NH_4^+ as the supported 40APMV/CPM catalyst ($Cs^+/NH_4^+=1.7$) was included in the series for comparison. The results obtained for the selective oxidation of isobutane into MAC and MAA, carried out in the same conditions, as above are shown in Table 4-4.

The caesium-free catalyst (APMV) exhibited very low conversions in both oxygen and isobutane (10.4% and 2.0%, respectively). In reverse, the introduction of Cs into the catalysts had positive effects on the conversion of reactants and on the products distribution. Over the catalyst with the lowest Cs content [$Cs_{0.5}(NH_4)_{2.5}H$], the conversion of isobutane was 2 times higher than over the caesium-free sample (APMV), and the yield of the desired products (MAC+MAA) also increased from 0.9 to 2.9. When the number of Cs continued to increase to 2.5, the maximum conversion of isobutane (9.9%) and complete oxygen consumption was stated. The highest yield of (MAC+MAA) (5.5%) was obtained over the sample $Cs_{1.7}(NH_4)_{1.3}H$, corresponding to a isobutane conversion of 9.6% and an oxygen conversion of 52.7%. In fact, the two catalysts with 2.5 and 1.7 caesium atoms exhibited similar activity for the isobutane oxidation, but the products distribution were rather different. Whereas $Cs_{1.7}(NH_4)_{1.3}H$ displayed high selectivity for both MAC (13.7%) and MAA (43.4%), and relative lower selectivity for CO_x (25.6%), the $Cs_{2.5}(NH_4)_{0.5}H$ catalyst showed a high selectivity in the latter (namely 53.1%), which was responsible for its low yield in MAA+MAC of 2.9%. This was further indicated by the high oxygen/isobutane conversion

ratio of 10/1, whereas as the other catalysts generally exhibited values around 5/1, which was rather close to the theoretical stoichiometric value. One can therefore state that $Cs_{2.5}(NH_4)_{0.5}H$ promoted the degradation reaction of MAC to COx instead of the selective oxidation of MAC to MAA. As shown before, the surface caesium concentration may play a profound role in affecting the products distribution, which will be further characterized. $Cs_3(NH_4)_0H$ sample gave the lowest activity as a consequence of the poor acidity (*cf. section 3.3.2.5*), resulting in difficulty for activating the C-H bond of the alkane.

Table 4-4 Catalytic performances for IBAN selective oxidation

Catalyst	Conversion, %		Selectivity, %					$Y_{(MAC+MAA)}$, %	Carbon balance
	O_2	IBAN	MAC	AA	ACA	MAA	CO_x		
$Cs_3(NH_4)_0H$	6.2	1.2	16.2	19.9	9.0	31.9	23.0	0.6	0.996
$Cs_{2.5}(NH_4)_{0.5}H$	100.0	9.9	9.7	15.5	2.6	19.1	53.1	2.9	0.998
$Cs_{1.7}(NH_4)_{1.3}H$	52.7	9.6	13.7	13.4	3.9	43.4	25.6	5.5	0.997
$Cs_{1.5}(NH_4)_{1.5}H$	29.2	5.8	22.1	10.7	3.3	44.8	19.1	3.9	0.997
$Cs_{0.5}(NH_4)_{2.5}H$	17.1	4.1	29.3	9.3	3.1	41.5	16.8	2.9	0.995
$Cs_0(NH_4)_3H$ (APMV)	10.4	2.0	11.5	11.9	6.2	32.9	37.5	0.9	0.992

Reaction conditions: Temperature=340 °C, atmospheric pressure, contact time=4.8 s.
Here IBAN=isobutane, MAC=methacrolein, AA=acetic acid, ACA=acrylic acid and MAA=methacrylic acid.

4.3.2 Dependence of activity on acidity

The influence of acidity on the catalytic activity was reported in Figure 4-8. The sample $Cs_3(NH_4)_0H$ having lowest acidity (0.17 mmol/g NH_3 uptake) displayed the lowest activity (1.81 umol/$g_{cat.}$·min). As the acidity increased a little bit to 0.30 mmol/g NH_3 uptake, corresponding to the sample $Cs_{2.5}(NH_4)_{0.5}H$, the activity for isobutane oxidation increased sharply to 14.92 umol/$g_{cat.}$.min. The catalyst $Cs_{1.7}(NH_4)_{1.3}H$ had higher acidity of 0.72 mmol/g NH_3 uptake but a similar activity as $Cs_{2.5}(NH_4)_{0.5}H$. The increased acidity for the samples

$Cs_{1.5}(NH_4)_{1.5}H$ and $Cs_{0.5}(NH_4)_{2.5}H$ did not improve the activity anymore, which may be related to their low surface area as selective oxidation of isobutane over heteropolycompounds catalysts was classified to surface-type reaction [14].
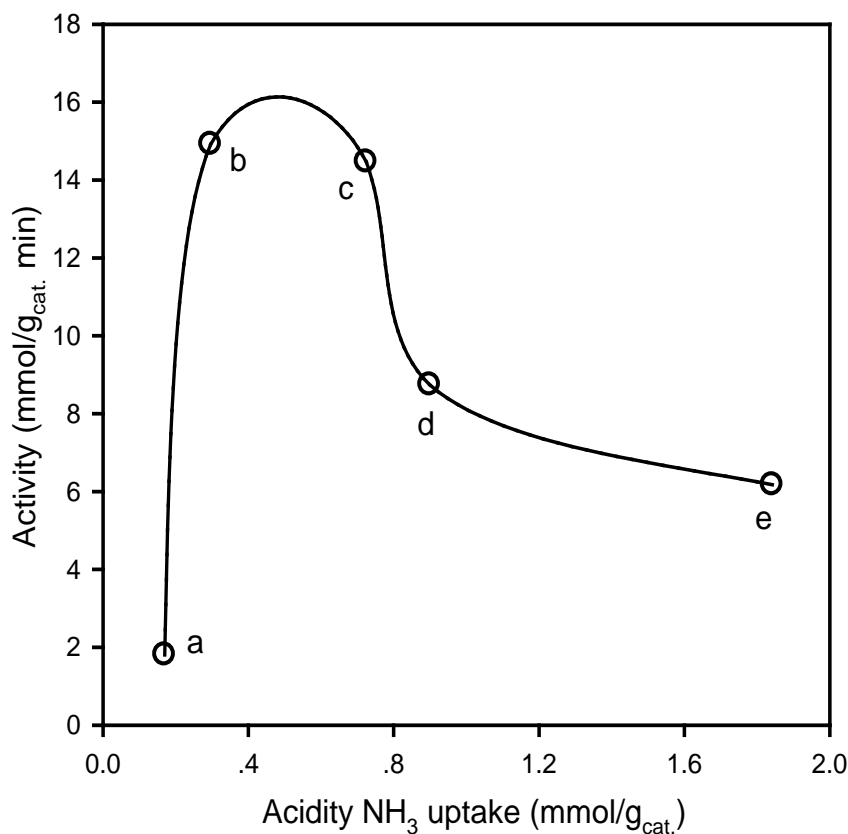
Figure 4-8 Correlation between the catalytic activity and acidity

(a: $Cs_3(NH_4)_0H$, b: $Cs_{2.5}(NH_4)_{0.5}H$, c: $Cs_{1.7}(NH_4)_{1.3}H$, d: $Cs_{1.5}(NH_4)_{1.5}H$, e: $Cs_{0.5}(NH_4)_{2.5}H$)

On the other hand, it has been proved that the mechanism of isobutane oxidation involved an oxidative dehydrogenation step to give isobutene [8, 9, 12], which converted into MAC and MAA 500 times as fast as its formation. The C-H bond activation was considered as the rate-limiting step and was promoted by the surface acidic sites [5, 6]. The sharp increase in activity corresponding to the ammonium-free catalyst to the one containing 0.4 NH_4^+ cations per Keggin unit indicates the importance of the acidic sites in activating the reaction. But it was not the unique determinable factor for the activity, the quite low surface area also restricted the conversion of isobutane such as for the $Cs_{1.5}(NH_4)_{1.5}H$ and $Cs_{0.5}(NH_4)_{2.5}H$

catalysts in spite of the fact that they had a relative high acidity. That was the reason why a decreasing trend was observed when the Cs number was lower than 1.7 (Figure 4-8). The best activity was obtained neither over the catalyst with strongest acidity nor over the catalyst with biggest surface area. Since the surface area and acidity had the opposite trend as varying the Cs amount, thus it became crucial to find the "key point" in order to gain the appropriate acidity and surface area, which seemed to appear between 2.5 and 1.7 according to our results.

4.4 Effect of various preparation techniques on the catalytic performances

In this section we investigated the influence of the preparation method on the catalytic activity and products distribution of the $Cs_{1.7}(NH_4)_{1.3}H$ catalyst. The latter was prepared by adding Cs_2CO_3 and $(NH_4)_2CO_3$ solutions simultaneously to an aqueous solution of HPA (*cf. section 2.3.3*). Besides this catalyst, the sample denoted as APMV/CPM-m was prepared by mechanically mixing the support and the active phases. The catalysts noted $Cs_{1.7}(NH_4)_{1.3}H$-CN and $Cs_{1.7}(NH_4)_{1.3}H$-NC were synthesized by precipitation method with different senses of addition for Cs_2CO_3 and $(NH_4)_2CO_3$ respectively. In fact, –CN meant that in the first step the Cs_2CO_3 solution was added into the HPA solution and then, in the second step, the $(NH_4)_2CO_3$ solution was added. Correspondingly, –NC indicated the opposite order. All samples exhibited the same Cs^+/NH_4^+ ratio as that presented in the supported 40APMV/CPM catalyst. The catalytic performance obtained for these solids are shown in Table 4-5.

From the results one can see that the supported catalyst APMV/CPM displayed the best catalytic performance with a yield in MAC+MAA of 8.0% (15.3% conversion of IBAN). On the other hand, the mechanically mixed sample APMV/CPM-m exhibited the poorest performance of no more than 3.5% yield in MAC/MAA (IBAN conversion of 6.0%). For the three samples prepared by precipitation method, the highest yield was achieved over the $Cs_{1.7}(NH_4)_{1.3}H$ (5.5% yield), whereas $Cs_{1.7}(NH_4)_{1.3}H$-CN and $Cs_{1.7}(NH_4)_{1.3}H$-NC exhibited

similar yields of 4.1 and 4.3% respectively but the adding order of the precursors had a considerable influence on the IBAN conversion and the products distribution. The IBAN conversion followed the order $Cs_{1.7}(NH_4)_{1.3}H-NC > Cs_{1.7}(NH_4)_{1.3}H > Cs_{1.7}(NH_4)_{1.3}H-CN$.

Table 4-5 Influence of the preparation methods on the catalytic performances for isobutane oxidation

Catalyst [a]	Conversion, %		Selectivity, %					$Y_{(MAC+MAA)}$, %	Carbon balance
	O_2	IBAN	MAC	AA	ACA	MAA	CO_x		
$Cs_{1.7}(NH_4)_{1.3}H-CN$	40.4	7.2	15.2	13.3	3.2	44.3	24.0	4.3	0.998
$Cs_{1.7}(NH_4)_{1.3}H-NC$	99.0	10.8	9.0	14.9	3.3	28.5	44.3	4.1	0.998
$Cs_{1.7}(NH_4)_{1.3}H$	52.7	9.6	13.7	13.4	3.9	43.4	25.6	5.5	0.997
APMV/CPM-m	35.4	6.0	20.9	9.5	2.7	37.1	29.8	3.5	0.994
APMV/CPM	61.6	15.3	10.0	14.1	3.2	42.0	30.7	8.0	0.993

a The content of active phases APMV was 40 wt.% for both APMV/CPM and APMV/CPM-m catalysts. Reaction conditions: Temperature=340 °C, atmospheric pressure, contact time=4.8 s. IBAN=isobutane, MAC=methacrolein, AA=acetic acid, ACA=acrylic acid and MAA=methacrylic acid.

$Cs_{1.7}(NH_4)_{1.3}H-NC$ and $Cs_{1.7}(NH_4)_{1.3}H$ exhibited rather close values in IBAN conversions (10.8% and 9.6%, respectively), but a significant difference was found in the oxygen ones (99.0% and 52.7%, respectively). The converted reactants ratio of O_2/IBAN for $Cs_{1.7}(NH_4)_{1.3}H-NC$ was almost 10, that was to say around 2 times as much as that of $Cs_{1.7}(NH_4)_{1.3}H$. The high content of caesium cations on the catalyst surface may be responsible for the high conversion of oxygen because of its stronger ability to adsorb oxygen from gas phase. The adsorbed oxygen species promoted the combustion of the products, whereby more CO_x were formed. On the other hand, an equilibrated concentration of ammonium cations was more favourable for methacrylic acid formation.

It seemed that the precipitating order of the cations played an important role in determining the conversion, which was explained by the faster precipitation when using Cs^+ compared to NH_4^+. As a matter of fact the Cs salt has a very low solubility in water.

For the sample $Cs_{1.7}(NH_4)_{1.3}H-NC$ where the Cs^+ was added after NH_4^+, one can assume

that the composition at the catalyst surface was mainly consisting of Cs salt coexisting with small quantity of ammonium salts because of its slower precipitation rate. The probable surface cations distribution could be described as in Figure 4-9a.

On the other hand, when the precursors were added simultaneously the catalyst surface rather exhibited a similar concentration for the two cations like depicted in Figure 4-9b. Finally, when first adding caesium and then ammonium $[Cs_{1.7}(NH_4)_{1.3}H\text{-}CN]$ the surface composition was dominated by ammonium salts with only few caesium salts like shown in Figure 4-9c. In this latter case, the generated ammonium salts did not contribute to the surface area, on the contrary they may block the pore, resulting in a surface decrease (*cf. section 3.3.2.2*) and explaining thus its decreased activity.

On the other hand, the high catalytic performance of the APMV/CPM catalyst was explained as followed: during the preparation, the CPM support was dispersed in the aqueous solution of 1-vanado-11-molybdophosphoric acid. Then the ammonium precursor was added to the slurry. Under these strong acidic conditions, the CPM support may partially disassociate into caesium cations and 12-molybdophosphoric anions, whereby an ammonium rich mixed salt was formed at the catalyst surface (Figure 4-9c).
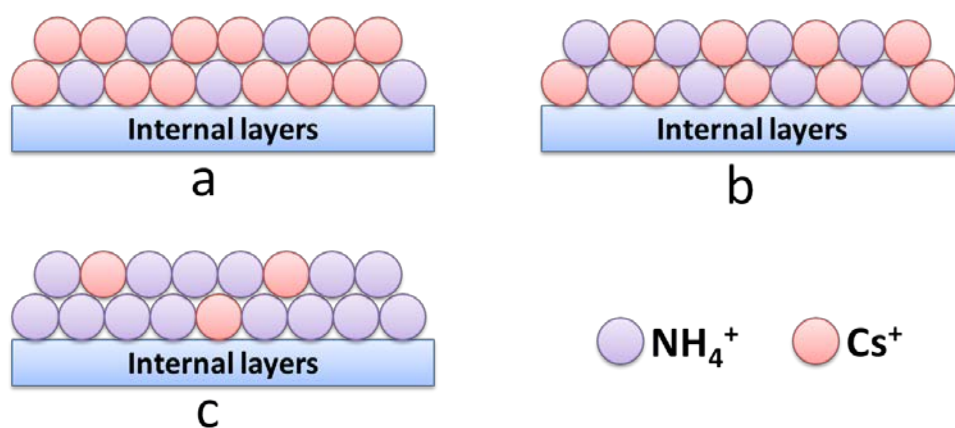
Figure 4-9 Supposed Cs^+ and NH_4^+ surface distribution according to the preparation method

References

[1]   F. Cavani, Catal. Today 157 (2010) 8.

[2]   N. Ballarini, F. Candiracci, F. Cavani, H. Degrand, J. L. Dubois, Appl. Catal. A: Gen 325 (2007) 263.

[3]   M. Kanno, T. Yasukawa, W. Ninomiya, K. Ooyachi, Y. Kamiya, J. Catal. 273 (2010) 1.

[4]   H. Nair, J. T. Miller, E. A. Stach, C. D. Baertsch, J. Catal. 270 (2010) 40.

[5]   S. Paul, V. LeCourtois, D. Vanhove, Ind. Eng. Chem. Res. 36 (1997) 3391.

[6]   G. Busca, F. Cavani, E. Etienne, E. Finocchio, A. Galli, J. Mol. Catal. A: Chem. 114 (1996) 343.

[7]   F. Cavani, Catal. Today 41 (1998) 73.

[8]   G. P. Schindler, T. Ui, K. Nagai, Appl. Catal. A: Gen 206 (2001) 183.

[9]   Q. Huynh, Y. Schuurman, R. Delichere, S. Loridant, J. M. M. Millet, J. Catal. 261 (2009) 166.

[10]   K. Inumaru, A. Ono, H. Kubo, M. Misono, J. Chem. Soc., Faraday Trans. 94 (1998) 1765.

[11]   N. Mizuno, M. Misono, Chem. Rev. 98 (1998) 199.

[12]   L. Jalowiecki-Duhamel, A. Monnier, Y. Barbaux, G. Hecquet, Catal. Today 32 (1996) 237.

[13]   F.   Jing,   B.   Katryniok,   E.   Bordes-Richard,   S.   Paul,   Catal.   Today http://dx.doi.org/10.1016/j.cattod.2012.03.028 (2012).

[14]   N. Mizuno, M. Tateishi, M. Iwamoto, J. Catal. 163 (1996) 87.

5 General conclusions and perspectives

5.1 General conclusions

In this work, the selective oxidation of isobutane into methacrolein and methacrylic acid using Keggin-type heteropolycompounds as catalysts was studied. More precisely the ammonium salt of 1-vanado-11-molybdophosphoric acid (APMV) was used as active phase and the role of silica-based and caesium salt of 12-molybdophosphoric acid (CPM) supports were investigated. The stability, textural properties, structural features, crystal phases, acidity and redox properties of the catalysts were studied using various techniques in a view to try to establish some correlations between the key properties of the samples and their catalytic performance for the desired reaction. Furthermore, the catalyst design and the reaction conditions were optimized.

The isobutane oxidation is claimed to belong to the so-called surface-reaction type [1]. Therefore, the first part of this work aimed at preparing a series of high surface area catalysts by supporting APMV (40 wt.%) on silica-based materials and on CPM. The active phase was found to be hierarchically stacked on the support layer by layer, which number was significantly dependent on the surface area of the supports. The higher the surface area, the lower the number of dispersed layers. It was found that the extent of the stack (and also probably the interactions with the support) determined the thermal stability of the supported catalysts. Hence, the silica-supported catalysts did not lead to the best catalytic performance, even if they presented a high surface area. This was ascribed to the fact that APMV was too easily decomposed under calcination and reaction conditions on this kind of support. As a matter of fact the NH_4^+ and residual H^+ were progressively eliminated in forms of ammonia and water, respectively. Thus the acidity and therefore the activity decreased significantly very rapidly. However, as known from the literature, strong acidic sites are indispensable for the activation of a C-H bond, which is the rate determining step in the studied reaction. Furthermore, the strong acidic sites favour the desorption of the produced methacrylic acid from the catalyst surface. One can thus conclude that the reduced thermal stability explained

the low catalytic performance observed for the silica-supported catalysts, which were not therefore good candidates for the desired reaction.

On the contrary, the CPM support, presenting the most important number of APMV layers stacked on it and having the best chemical compatibility with the active phase, displayed the best ability in stabilizing the APMV active phase. Consequently, even if its surface area was rather low (roughly 15-20 m^2/g), the 40APMV/CPM catalyst led to the best performance with an isobutane conversion of 15.3% and a yield in desired products (MAA+MAC) of 8.0% at 340 °C. This results meant that a minimum of surface area was needed to get a good catalytic performance - which was illustrated by the poor performance of the bulk APMV - but also that the acidity of the catalysts surface was a critical parameter. These acid properties were found to be considerably influenced by the nature of the support. As a matter of fact the silica-supported catalysts showed a rather low total acidity compared to the CPM-supported one. In conclusion an active catalyst must present a well-balanced combination of appropriate textural and acidic properties which were well represented by the notion of surface acid site density. Actually, a direct linear correlation between this characteristic and the activity (i.e. the propensity to convert isobutane) was enlightened. The surface acid site density must therefore be increased in order to obtain high isobutane conversion but, of course, this is not sufficient to get the desired products. Activating the isobutane molecules is the starting point and also the rate-limiting step of the mechanism but orientating the evolution of the intermediate formed on the catalyst surface towards methacrolein and methacrylic is another challenge. To illustrate this point, one can consider the catalyst using zirconia-modified SBA-15 and simple SBA-15 as supports which exhibited close isobutane conversions (5-6%) but completely different products distribution. This results may be related to the oxygen adsorption ability which was improved by introducing the zirconia oxides on SBA-15 surface, resulting in the consecutive oxidation of the aimed products. In addition, the MoO$_3$ generated by the decomposition of the active phase was also detrimental to the selectivity to desired products.

In view of the encouraging results obtained in the first part of the thesis, the work was then focused on CPM-supported catalysts. Samples with APMV active phase contents from

10 to 50 wt.% were prepared. It was shown that using higher contents of active phase - up to a certain extent - limited its partial decomposition. As the surface area did not change a lot within the series, the acidity was here the key point in determining the catalytic activity as shows the poorest conversion of isobutane (0%) obtained over the sample 10APMV/CPM without acidic sites and the best conversion of isobutane (15.3%) obtained over the sample 40APMV/CPM with a high surface site density. Moreover, surface acidity not only affected the activity but also the products distribution as it can enhance the conversion of methacrolein to methacrylic acid and favour the desorption of the generated acid [2, 3]. During a long term (132 h) catalytic test only a slight deactivation was observed. It was ascribed to i) a slow but unavoidable degradation of the APMV active phase forming unselective species and ii) the sintering of the catalyst leading to the aggregation of crystallites under the reaction conditions. The deactivation mechanism of CPM-supported APMV was based i) on the decomposition into simple oxides at high temperature and ii) on the release of ammonia and of residual protons at lower temperature. As a matter of fact, it was supposed that during the process of ammonium cations decomposition caesium cations diffused from the bulk support to the secondary structure, leading to a neutralization of the catalyst surface and hence to a decrease of activity. In order to confirm this theory, the role of caesium cations in the superficial layers of the catalysts was further studied by preparing mixed-salts using different techniques. In fact, when the caesium precursor and then the ammonium precursors were added to the 1-vanado-11-molybdophosphoric acid (HPMV), an APMV rich surface was obtained, whereas the addition in the inverse sense led to a surface enriched in the caesium salt of HPMV. The former can be seen as a model for a fresh APMV/CPM catalyst, where all the APMV was present at the surface, whereas the latter can be seen as a model for a spent catalyst, where the ammonium cations were substituted by caesium from the bulk. As expected, the latter exhibited poor catalytic performance. We thus conclude that on the one hand caesium stabilized the APMV phase, but on the other hand, that the caesium mobility led to a successive deactivation. Therefore the deposition of a multi-layer stack of active phase was necessary to limit the extent of the process of diffusion of caesium cations and hence to

keep good catalytic performance under stream.

Considering the conclusions drawn above it was clear that the preparation method can strongly affect the catalysts properties and therefore the performance by tuning the surface elements redistribution, especially the caesium one. The redistribution of caesium may lead both the acid and redox properties of the catalysts to change, and further affect the catalytic performances. It was also shown that the surface area increased with the caesium content in the mixed-salts. The pore size distribution and the average pore diameter were also significantly affected by the Cs^+/NH_4^+ ratio. They evolved from non-porous material (for x=0.5 and 0) to mesoporous material (for x=3 and 2.5) *via* microporous material (for x=1.7 and 1.5). The structural features determined by spectroscopies showed that the highest caesium contents were favourable to limit the release of V atoms from the Keggin unit. However, the partial decomposition cannot be totally avoided under the reaction conditions, as proved the visible band of MoO_3 from FT-IR and Raman spectra. The amount of acidic sites was also dependent on the number of ammonium cations in the catalysts. It increased with the decrease of caesium number but the super acidic sites were absent of all samples.

In the investigation concerning the reducibility, the XPS and H_2-TPR results have enlightened the different levels of reduction of the metals. By comparing the oxidation states of the elements present on the surface before and after the reaction, the obvious reduction of V^{5+} species could be observed from XPS results, while only evident MoO_3 was reduced according to the combined results of H_2-TPR and H_2-XRD. This discrepancy can be explained by: i) reduced molybdenum oxides were reoxidized by air as the *ex situ* XPS was performed; ii) the rather low content of vanadium in the catalyst make it undetectable for XRD technique. On the other hand, the active sites were reduced by the hydrocarbon under the reaction conditions. This process was promoted by the surface strong acidic sites. The modification of the redox properties of the catalyst by introducing one vanadium atom into the Keggin anion made the V^{5+} species easily reduced under the reaction conditions.

Within all the catalysts tested, the sample 40APMV/CPM led to the highest conversion of isobutane (20.2%) at T = 340 ^{o}C and contact time = 7.2 s, corresponding to a 8.6% yield in

MAC+MAA which is also at the top level by comparing with the results in the open literature up to now.

5.2 Perspectives

From the above conclusions it can be stated that the silica-based materials are not suitable to be used as catalyst carriers for dispersing heteropolycompounds and then for preparing efficient catalysts for the selective oxidation of isobutane. Nevertheless, the low surface and non-porous feature of the bulk heteropolyacid is definitely a major drawback of those materials. Therefore, self-assembly of polyoxometalate nanoparticle with cations, positively charged nanoparticles and intercalated with other materials like layered-double hydroxides (LDH) could be explored to prepare bi-functional samples exposing both the redox and acidity needed at the nano-scale [4-6]. Additionally, mesoporous metal oxides or other nano-materials like carbon nanotubes (CNTs) could also be studied as catalyst supports.

Concerning the catalyst composition, various parameters could be the subject of more detailed studies: As far as the mixed-salts catalysts are concerned, the acidity, the redox properties and the surface area were directly influenced by the number of Cs cations per Keggin unit. Therefore, the latter could be further optimized by investigating the range from 1.7 to 2.5 Cs^+. Another parameter is the nature of the counter-cation itself. In the present study we mainly concentrated on caesium and/or ammonium salts of 1-vanado-11-molybdophosphoric acid. The further modification of Keggin anions could be made by substituting more Mo by V or other transition metal elements like Fe, Nb and Ta, etc. Furthermore, the latters may even be used as counter-cations.

On the other hand, a significant impact of the amount and strength of the acidic sites was found. Whereas the importance of acidic sites was obvious, no attention was paid to the nature of the latter. Thus a further studied should also focus on the influence of the Brönsted and Lewis acid sites.

Concerning the deactivation mechanism and the Cs mobility, a more detailed study notably on the effect of the partial decomposition on the catalyst surface characteristics would be necessary. There are strong hints that the decomposition proceeds via the cleavage of ammonium cations and that during the process Cs ions diffuse from the bulk to the surface, but only in-situ spectroscopy could give a proof of this assumption. This technique would also help for the better understanding of the redox properties notably the role of the V^{5+}/V^{4+} redox couple.

The oxygen species present at the surface, including the adsorbed oxygen and the lattice oxygen, and the understanding of their transformation in one form of the other is also of main importance as the adsorbed oxygen species are more active comparing to the lattice oxygen species. The excess of adsorbed oxygen may play a negative role by promoting the combustion reaction of our desired products.

The catalyst preparation technique has also a profound effect on the catalytic properties. The caesium surface concentration may be a key point for the products distribution. More characterization should be carried out in order to prove this assumption.

Finally, the catalytic test results were obtained under rather standard conditions. Nevertheless, best performance was obtained at relatively high temperature (350 ^{o}C) and increased contact time (7.2 s). In order to further increase the catalytic performances or the catalyst lifetime a parameter optimization using experimental design software would be useful.

References

[1]   N. Mizuno, M. Tateishi, M. Iwamoto, J. Catal. 163 (1996) 87.

[2]   N. Mizuno, M. Misono, Chem. Rev. 98 (1998) 199.

[3]   F. Cavani, Catal. Today 41 (1998) 73.

[4]   K. Zhu, D. Wang, J. Liu, Nano Res. 2 (2009) 1.

[5]   S. Liu, Z. Tang, Nano Today 5 (2010) 267.

[6]   A. M. Douvas, E. Makarona, N. Glezos, P. Argitis, J. A. Mielczarski, ACS Nano 2 (2008) 733.

6 Annexes

6.1 Structure confirmation of the commercial and prepared materials

6.1.1   Amount of crystal water in commercial $H_3PMo_{12}O_{40} \cdot xH_2O$

TGA measurement was carried out to determine the amount of crystal water in the sample. The initial weight loss stage under 150 ^oC (see Figure 6-1) is attributed to the removal of crystal water with a loss of 7.3%. 8 crystallite waters are contained in each molecule of molybdophosphoric acid according to the follow formula:

$$\Delta W\% = \frac{M_{H2O} \times x}{M_{HPC} + M_{H2O} \times x} \tag{6-1}$$
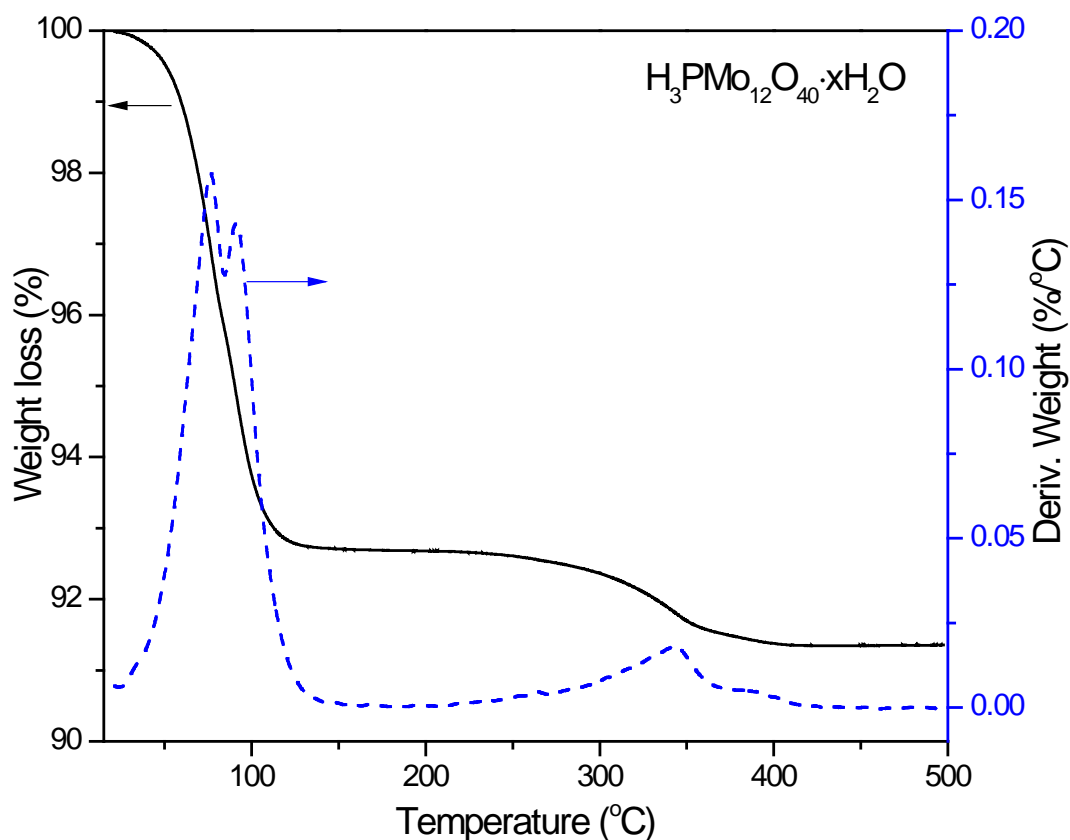
Figure 6-1 Thermogravimetric analysis (TGA) of hydrated $H_3PMo_{12}O_{40}$

6.1.2 Synthesized $H_4PMo_{11}VO_{40} \cdot xH_2O$

6.1.2.1 Structure feature

The structure of the prepared heteropolyacid was checked by IR techniques, and the results are displayed in Figure 6-2. The typical IR characteristic bands of the Keggin-type compounds at 1063, 963, 865 and 782 cm^{-1} were attributed to the asymmetric stretching of the central atom-oxygen (P-O) of PO_4 tetrahedron, the asymmetric stretching of peripheral atoms-terminal oxygen (Mo=O_d) and the stretching of M–O_b–M inter- and M–O_c–M intra-octahedron bridge of trimetallic groups, respectively [1]. Additionally, an evident shoulder could be found at around 1084 cm^{-1}, which was characteristic of the heteropolyacid $H_3PMo_{12}O_{40}$ with one Mo atom substituted by one V atom [2].
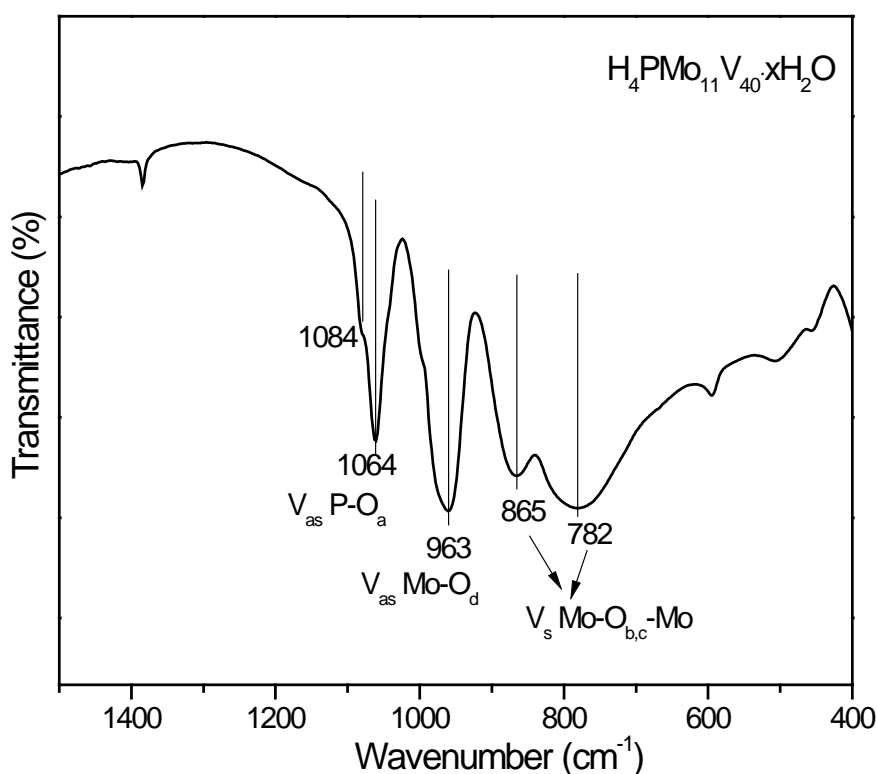
Figure 6-2 IR spectrum of the prepared $H_4PMo_{11}VO_{40} \cdot xH_2O$

6.1.2.2 Amount of crystal water

According to the TGA results presented in Figure 6-3, the number of crystal water is 8.
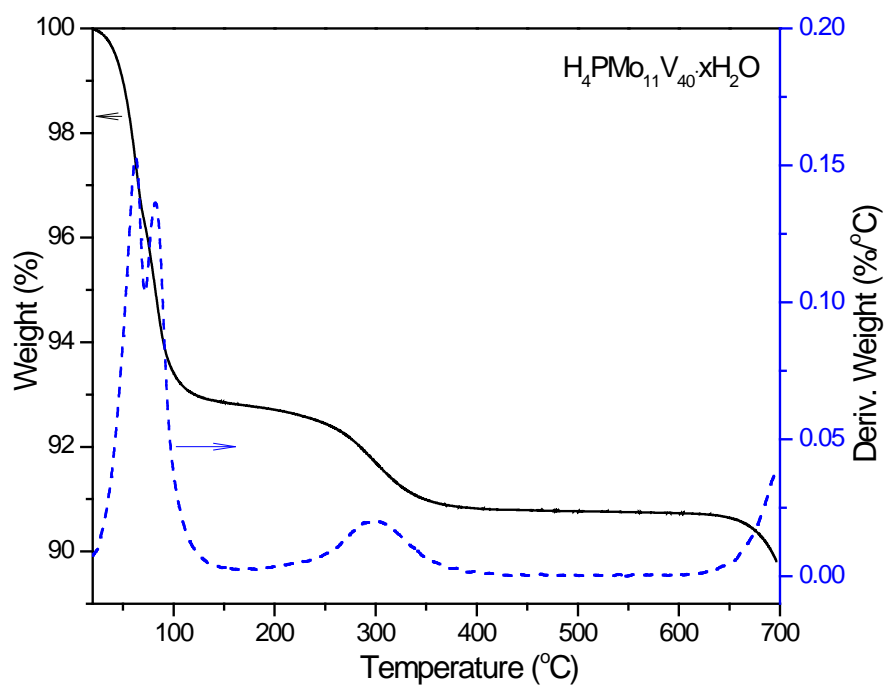

$H_4PMo_{11}V_{40} \cdot xH_2O$

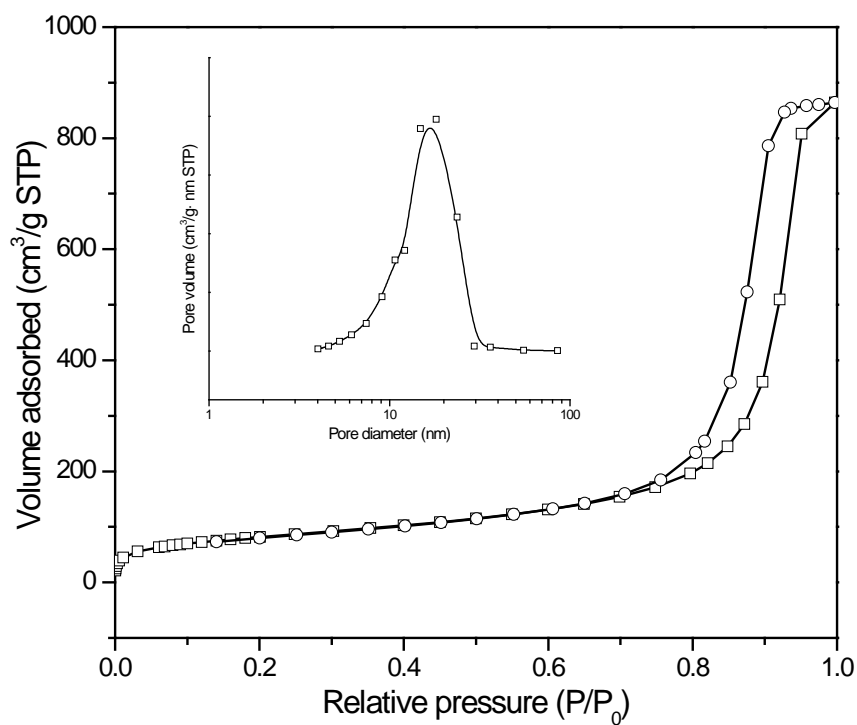Figure 6-3 Thermal decomposition of $H_4PMo_{11}VO_{40} \cdot xH_2O$

Figure 6-4 Adsorption and desorption isotherms and pore size distribution (insert graph) of

CARiACT® SiO_2

6.1.3 Commercial CARiACT® SiO₂

The CARiACT® SiO₂ with a hexagonal structure was commercially acquired from Fuji Silysia Chemical Company. The specific surface area, total volume and average pore diameter are 295 m^2/g, 1.34 cm^3/g and 15 nm, respectively. The isotherm and pore size distribution are shown in Figure 6-4.

6.1.4 Synthesized mesoporous molecular sieve SBA-15

The specific surface area of the material was 632 m^2/g and the porosity including the isotherm and the pore size distribution are shown in Figure 6-5. An obvious characteristic of mesoporous molecular could be observed and a narrow pore diameter distribution (between 4 and 7 nm centred at around 4 nm) was obtained.

Figure 6-5 Adsorption and desorption isotherms and pore size distribution (insert graph)
of the prepared SBA-15

6.1.5   Cs$_3$PMo$_{12}$O$_{40}$ (CPM)

6.1.5.1 Textural properties

The specific surface area of the material was 22 m^2/g which is relatively small although the isotherms exhibit mesoporous features (Type IV) (Figure 6-6). This material displayed a large pore size distribution including both meso- and macro-pores (2<D<50 nm and D>50 nm, respectively) (insert graph).
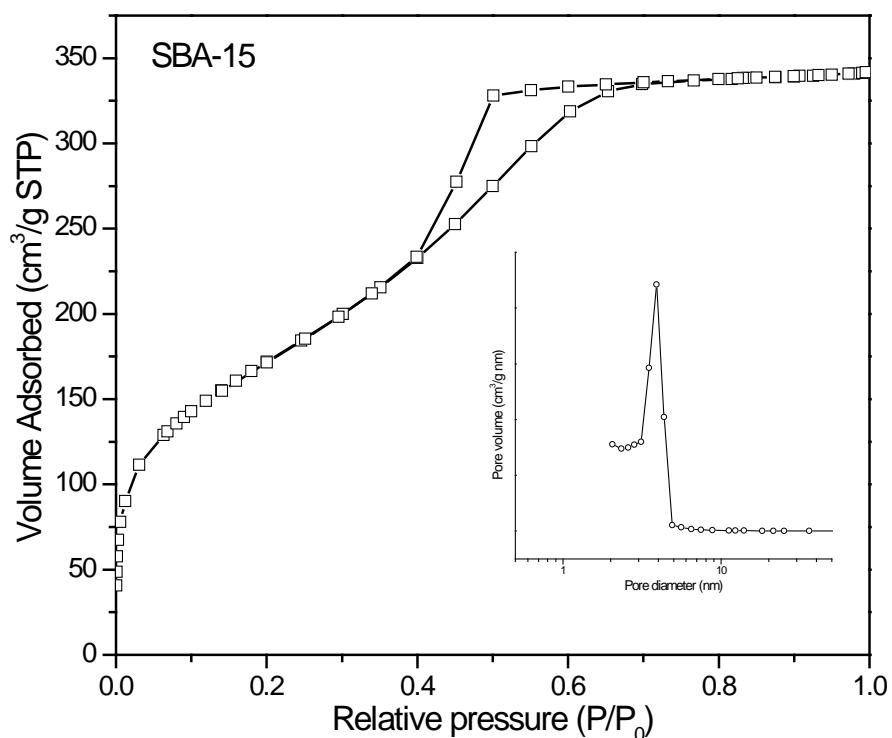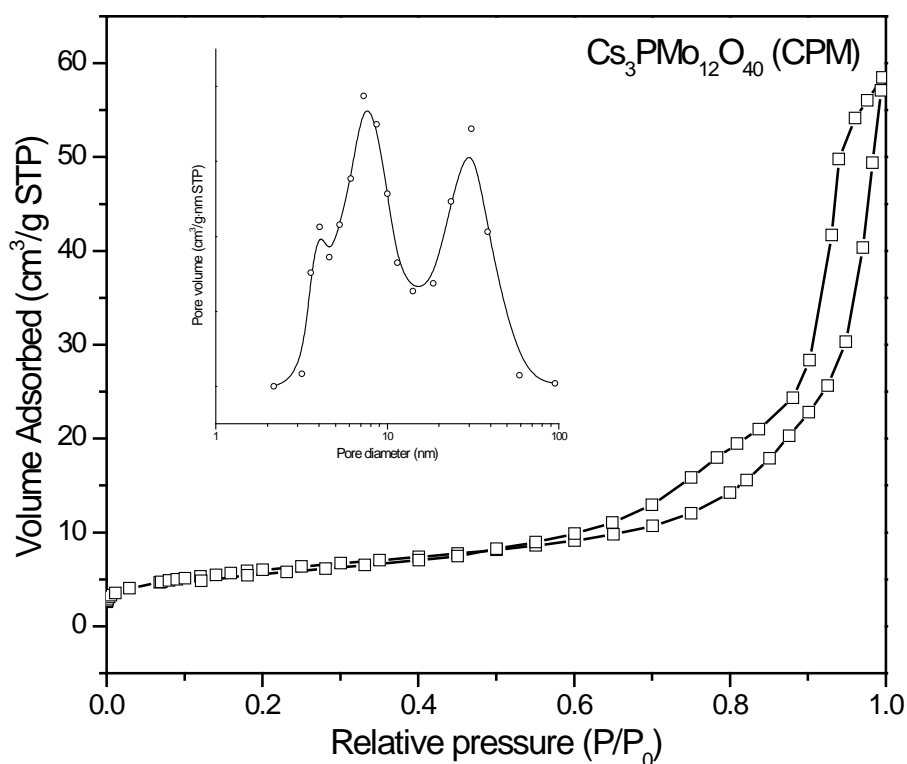

Figure 6-6 Adsorption and desorption isotherms and pore size distribution (insert graph) of the prepared Cs$_3$PMo$_{12}$O$_{40}$ (CPM)

6.1.5.2 Confirmation of the Keggin structure

As expected, infrared spectroscopy confirmed that the characteristic bands of the Keggin structure are present in the spectra (Figure 6-7).
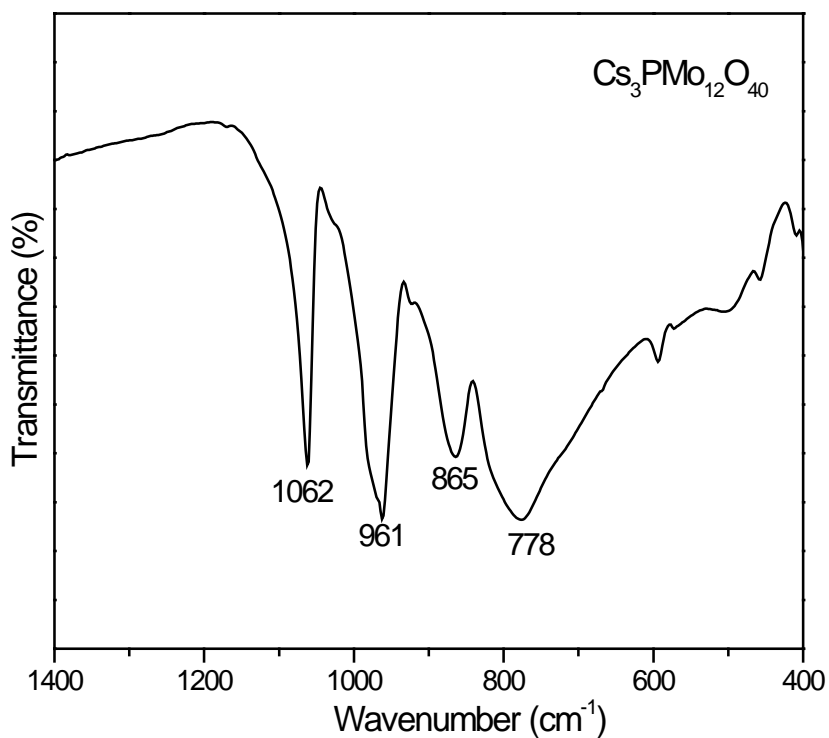
Figure 6-7 FT-IR spectrum of $Cs_3PMo_{12}O_{40}$ (CPM)

References

[1]   M. Sun, J. Z. Zhang, C. J. Cao, Q. H. Zhang, Y. Wang, Appl. Catal. A: Gen 349 (2008).

[2]   C. J. Dillon, J. H. Holles, R. J. Davis, J. A. Labinger, M. E. Davis, J. Catal. 218 (2003) 54.

6.2 Theoretical specific surface area

The support of the catalyst has a known BET surface and pore volume (for example 100 m²/g). The impregnation with APMV (40 wt.%) ideally leads to the formation of a homogenous layer. If this layer does not generate new surface, the BET value decreases proportionally to the amount of introduced active phase (in our example, it must respectively decrease to 60 m²/g). A negative deviation between experimental and calculated values (*i.e.*, a measured value even lower than the corrected calculated value) can be ascribed to the partial plugging of pores, indicating thus the formation of agglomerates. On the other hand, a positive deviation (*i.e.*, a measured value larger than the calculated value) is explained with the creation of new surface due to the deposition of a porous structure.

Table 6-1 Textural properties of bare APMV, bare CPM support and APMV/CPM catalyst

Sample	S_{BET}, m²/g	V_p, cm³/g
APMV	4	0.02
CPM	22	0.09
APMV/CPM	17	0.11

Reference

[1] M. Bonne, S. Pronier, F. Can, X. Courtois, S. Valange, J-M. Tatibouet, S. Royer, P. Marécot, D. Duprez, *Solid State Sci.*, *12 (2010)* 1002.

6.3 Quantitative calculation of NH$_3$-TPD measurement

The NH$_3$-TPD measurements were performed in order to investigate the nature and strength of the acidic sites of the catalysts. Prior to start the temperature-programed desorption the solid was pre-treated at 250 ^{o}C to remove the physisorbed water, then the temperature was cooled down to the NH$_3$ adsorption temperature 130 ^{o}C. After saturation by NH$_3$ the desorption procedure was carried out from 130 to 700 ^{o}C with a ramp of 10 ^{o}C/min. The curve was recorded by a thermal conductivity detector (TCD).

Taking as an example the sample APMV/CPM, the desorption curves was collected as the black thick solid line in the following Figure 6-8. Obviously the origin curve involved several overlapped peaks, which could not be used for quantitative calculation. Therefore the deconvolution treatment was done by using a Gaussian shaped function to obtain the separated peaks, like the peaks shown in Figure 6-8 (thin dashed line).

The quantitative calculation was done as follows and the results for each step are listed in Table 6-2.

Step 1. The peaks and their areas were obtained by Gaussian shaped function

Step 2. Calculation of the amount of NH$_3$ uptake according to the NH$_3$ calibration

Step 3.1. Calculation of the amount of NH$_3$ involved in the active phases APMV using the formula:

$$n, \mu mol = \frac{3 \times m_{cat.}, mg \times X\%}{M_{APMV}, g/mol} \times 1000$$

(6-2)

Where n, $m_{cat.}$, $X\%$ and M_{APMV} are amount of NH$_3$ involved in the active phases, the mass of the catalyst for TPD test (50 mg), the content of the active phases APMV (40%) and the molecule weight of the active phases APMV (1832.26 g/mol), respectively.

Step 3.2. From the TG test results, the NH$_4^+$ was only released as NH$_3$ when temperature was higher than 350 ^{o}C, so the weak acidic sites (<300 ^{o}C) was not included in the correction. The acidic sites strength detected at temperature higher than 300 ^{o}C were recalculated taking

into account the amount of NH_3 potentially released by the decomposition of NH_4^+ cations.

Step 4. Calculation of the density of surface acidic sites using the following formula:

$$D_{acidity}, \mu mol/m^2 = \frac{Acidity, mmol/g_{cat.}}{S_{BET}, m^2/g_{cat.}} \times 1000$$

(6-3)
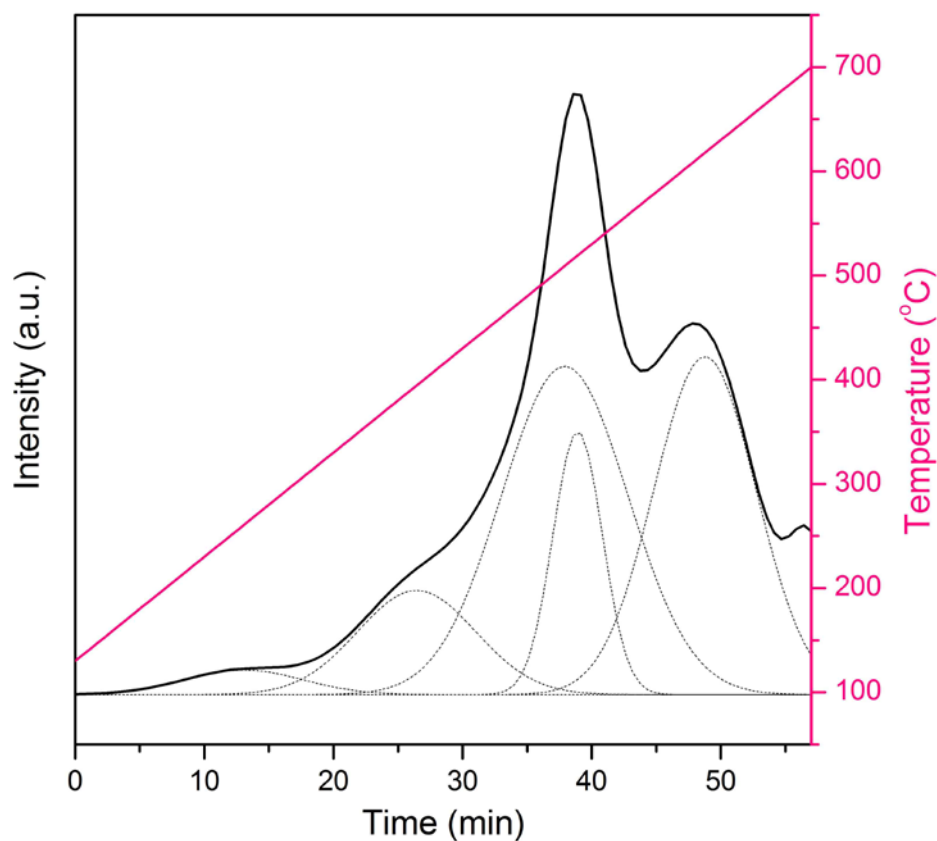
Figure 6-8 NH_3-TPD curve of APMV/CPM sample

Table 6-2 Results of each step of calculation

Catalyst APMV/CPM	Acidic sites distribution				Total acidity
	130-300°C weak	300-450°C medium	450-560°C strong	560-700°C very strong	
Peak area	12.5	53.7	236.3	150.1	473.6
NH_3 uptake before correcting, mmol/g	0.05	0.21	0.91	0.66	1.83
NH_3 uptake after correcting, mmol/g	0.05	0.21	0.89	0.65	1.80
Acidic sites density, $\mu mol/m^2$	2.9	12.4	52.4	38.2	105.9

6.4   Conclusions générale (version française)

Dans ce travail, l'oxydation sélective de l'isobutane en méthacroléine et acide méthacrylique sur catalyseurs hétéropolyanioniques de type Keggin a été étudiée. Plus précisément, le sel d'ammonium de l'acide 1-vanado-11-molybdophosphorique (APMV) a été utilisé comme phase active et le sel de césium de l'acide phospho-molybdique (CPM) ainsi que différentes silices ont été utilisées comme supports. La stabilité, les propriétés texturales, la structure cristallographique, les propriétés acides et redox des catalyseurs ont été examinés en utilisant de nombreuses techniques de caractérisation avec pour objectif d'essayer d'établir des corrélations entre les propriétés clé de ces solides et leurs performances catalytiques. De plus, le mode de préparation du catalyseur et les conditions opératoires de test ont été optimisés.

L'oxydation sélective de l'isobutane est connue comme étant une réaction de surface [1]. Par conséquent, la première partie de ce travail a consisté à préparer une série de catalyseurs présentant des aires spécifiques élevées en support 40% poids d'APMV sur des silices divers ou sur le sel de césium CPM. Il a été montré que la phase active se dépose sous forme de couches superposées à la surface des supports. Le nombre de couche est d'autant plus faible que la surface spécifique du support est élevée. Il a été montré que le nombre de couches superposées (et également probablement les interactions avec le support) conditionnaient la stabilité de la phase active. Ainsi, les supports à base de silice n'ont pas conduit à de bonnes performances catalytiques malgré leur aire spécifique élevée. Ceci s'explique par le fait que la phase active APMV est trop facilement dégradée sur ce type de support dans les conditions de calcination ou de test. En effet, les ions ammoniums et les protons résiduels sont progressivement éliminés sous la forme d'ammoniac et d'eau, respectivement. Ainsi, l'acidité et donc l'activité décroissent significativement très rapidement. Cependant, il est connu de la littérature que des sites acides forts sont nécessaires pour activer la liaison C-H de l'hydrocarbure. Cette activation est l'étape limitante du mécanisme de la réaction étudiée. De

plus la présence de sites acides forts favorise la désorption de l'acide méthacrylique produit à la surface du catalyseur. On peut donc conclure que la stabilité thermique restreinte explique les faibles performances catalytiques obtenues pour les catalyseurs supportés sur silice. Ces catalyseurs ne sont donc pas de bons candidats pour la réaction souhaitée.

Au contraire, le support CPM qui présente le plus grand nombre de couches de phase active superposées à sa surface et la meilleure compatibilité chimique avec l'APMV, a conduit à des catalyseurs plus stables. Conséquemment, même si sa surface spécifique est assez faible (de l'ordre de 15-20 m^2/g), l'échantillon 40APMV/CPM a conduit aux meilleures performances dans les conditions opératoires standard (conversion de l'isobutane=15.2% et 8% de rendement en MAA+MAC. Ce résultat signifie qu'un minimum de surface spécifique est nécessaire pour obtenir de bonnes performances catalytiques – comme l'illustre les piètres performances de l'APMV massique – mais aussi que l'acidité de la surface est un paramètre critique. Ces propriétés acides sont considérablement influencées par la nature du support. En effet, les catalyseurs supportés sur silice présentent une faible acidité comparés aux catalyseurs supportés sur CPM. En conclusion, un catalyseur actif doit présenter une combinaison bien équilibrée de propriétés texturales et acides. Ceci est bien représentée par la notion de densité de sites acides en surface. Une relation linéaire entre cette caractéristique et l'activité (en d'autres termes la conversion de l'isobutane) a été mise en évidence. La densité de site acide doit donc être la plus élevée possible pour obtenir de fortes conversions de l'isobutane mais, bien évidemment, cela n'est pas suffisant pour obtenir les produits désirés. Activer la molécule d'isobutane est le point de départ et l'étape limitante du mécanisme mais l'orientation de l'évolution des intermédiaires vers la méthacroléine ou l'acide méthacrylique est un tout autre challenge. Pour illustrer ce point on peut considérer les catalyseurs supportés sur silice SBA-15 ou sur silice SBA-15 zirconée. Ces 2 catalyseurs présentent des conversions de l'isobutane proches (de l'ordre de 5-6%) mais des distributions de produits totalement différentes. Ce résultat peut être relié à une capacité d'adsorption de l'oxygène exacerbée par le dopage de la silice par la zircone, résultant en l'oxydation totale des produits désirés. De plus, le MoO_3 généré par la décomposition de la phase active contribue lui aussi à la baisse de

sélectivité en produits recherchés.

A la vue des résultats encourageants obtenus dans la première partie de la thèse, les recherches ont été orientées vers l'étude des catalyseurs supportés sur CPM. Ainsi des échantillons contenant de 10 à 50% poids d'APMV ont été préparés. Il a été montré que l'utilisation des quantités les plus importantes d'APMV conduit jusqu'à une certaine limite à une limitation de sa décomposition. Puisque les surfaces spécifiques ne changent pas beaucoup dans la série de catalyseurs préparés l'acidité est devenue la propriété clé comme l'illustre l'activité nulle de l'échantillon 10APMV/CPM qui ne présente aucune acidité et la meilleure conversion obtenue sur l'échantillon 40APMV/CPM (15.3%) qui présente une densité de sites acides en surface élevée. De plus, l'acidité de surface n'affecte pas seulement l'activité mais aussi la distribution des produits en accélérant la conversion de la méthacroléine en acide méthacrylique et la désorption des acides formés en surface [2, 3]. Pendant le test de longue durée (132h) une faible désactivation est observée. Elle a été attribuée à : i) la lente mais inévitable dégradation de la phase active dans les conditions de réaction, ii) le phénomène de frittage du catalyseur conduisant à l'agglomération des cristallites dans les conditions de réaction. Le mécanisme de désactivation des catalyseurs supportés sur CPM est basé : i) sur la décomposition de la phase active en oxydes simples à hautes température et ii) à l'élimination des ions ammoniums et des protons résiduels à plus basse température. En effet, il est supposé que pendant le processus de décomposition des cations ammonium des cations césium diffusent du cœur du catalyseur vers la surface provoquant ainsi sa neutralisation et ainsi la diminution de son activité. Afin de confirmer cette théorie le rôle du césium dans les couches superficielles du catalyseur a été étudié plus avant en préparant par différentes méthodes des sels mixtes césium-ammonium. En fait, quand les précurseurs du césium puis de l'ammonium sont ajoutés à la solution d'acide 1-vanado-11-molybdophosphorique (HPMV) une surface riche en APMV est obtenue. Si on inverse l'ordre d'addition des précurseurs la surface sera riche en sel de césium de HPMV. Le premier peut être vu comme un analogue du catalyseur frais APMV/CPM tandis que le second comme un analogue du catalyseur après test où les ions ammoniums sont substitués par des

cations césium. Comme attendu ce dernier présente de mauvaises performances catalytiques. On peut donc conclure que, d'un côté, le césium permet de stabiliser la phase APMV mais que, d'un autre, la mobilité du césium conduit à sa désactivation lors de l'élimination des ions ammoniums. Ainsi la déposition de nombreuses couches d'APMV est nécessaire pour limiter le processus de diffusion du césium et ainsi pouvoir garder plus longtemps de bonnes performances catalytiques sous flux réactionnel.

En considérant les conclusions tirées ci-dessus il est clair que la méthode de préparation pourra influer fortement sur les propriétés du catalyseur et donc sur ces performances en ajustant la redistribution des éléments en surface, notamment celle du césium. La mobilité du césium conduit à des modifications des propriétés acides mais aussi redox et affecte donc les performances catalytiques. Il a aussi été montré que la surface spécifique augmente avec la teneur en césium dans les sels mixtes. La distribution de la taille des pores et le diamètre moyen des pores sont également impactés significativement par le ratio Cs^+/NH_4^+. La porosité évolue d'un matériau non poreux pour x=0 et 0.5 à un matériau mésoporeux pour x=2.5 et 3 en passant par un matériau microporeux pour x= 1.5 et 1.7. Les analyses structurales montrent en outre que les teneurs les plus fortes en césium permettent de limiter l'éjection du vanadium de la structure primaire. Quoiqu'il en soit la décomposition partielle de la phase active ne peut être totalement évitée dans les conditions de réaction comme le montre la formation de MoO_3 détectée par FT6IR et Raman. Le nombre de sites acides est aussi directement corrélés à la quantité d'ions ammonium (et donc de césium) présents dans le catalyseur. Ils augmentent lorsque la quantité de césium décroit mais les sites superacides sont absent de tous les échantillons de sels mixtes.

Dans les investigations concernant la réductibilité, l'analyse XPS et la RTP sous H_2 mettent évidence les différents degrés de réductions des éléments métalliques. Si on compare les états d'oxydation en surface avant et après test, on constante que seul la réduction du V^{5+} est observée. Pourtant seul le MoO3 est réduit d'après les analyses de RTP sous H_2. Cette incohérence peut être expliquée par les différents mécanismes de réduction. Dans les conditions de réaction, les sites sont réduits par l'isobutane et ce processus est promu par les

sites acides forts. Les modifications apportées aux propriétés redox du catalyseur en introduisant une atome de vanadium dans la structure primaire rend la réduction du catalyseur plus aisée qu'en seule présence de molybdène.

Parmi tous les catalyseurs testés les meilleures performances ont été obtenues sur l'échantillon 40APMV/CPM à 340°C et avec un temps de contact de 7,2s. La conversion de l'isobutane est alors de 20.2% et le rendement en produits recherchés de 8.6% ce qui en fait la meilleure valeur rapportée jusqu'alors dans la littérature.

References

[1]   N. Mizuno, M. Tateishi, M. Iwamoto, J. Catal. 163 (1996) 87.
[2]   N. Mizuno, M. Misono, Chem. Rev. 98 (1998) 199.
[3]   F. Cavani, Catal. Today 41 (1998) 73.

6.5 Publications, communications and training

<u>Articles</u>

Improvement of the catalytic performance of supported $(NH_4)_3HPMo_{11}VO_{40}$ catalysts in isobutane selective oxidation.

Fangli JING, Benjamin KATRYNIOK, Elisabeth BORDES-RICHARD, Sébastien PAUL, **Catalysis Today**, (2012), in press, DOI: 10.1016/j.cattod.2012.03.028

Catalytic selective oxidation of isobutane into methacrylic acid over supported $(NH_4)_3HPMo_{11}VO_{40}$ catalysts

Fangli JING, Benjamin KATRYNIOK, Elisabeth BORDES-RICHARD, Sébastien PAUL, in preparation.

<u>Oral communication</u>

Effect of acidity of supported $(NH_4)_3HPMo_{11}VO_{40}$ catalysts on their performances in the selective oxidation of isobutane

Fangli JING, Benjamin KATRYNIOK, Elisabeth BORDES-RICHARD, <u>Sébastien PAUL</u>, (2012) *15th International Congress on Catalysis*, München, Germany

<u>Posters</u>

Enhance the catalytic performances of selective oxidation of isobutane over supported $(NH_4)_3HPMo_{11}VO_{40}$ catalysts

Fangli JING, Sébastien PAUL, <u>Elisabeth BORDES-RICHARD</u>. (2011) *EuropaCAT X* in Glasgow

Selective oxidation of iso-butane into methacrylic acid over supported heteropolyacid catalysts

Fangli JING, Sébastien PAUL, Elisabeth BORDES-RICHARD. (2010) *Journées Nord-Ouest Européennes des Jeunes Chercheurs*, Villeneuve d'Ascq, France

Training

Characterization in Catalysis Research

(2011) Schuit Institute of Catalysis - Eindhoven University of Technology, The Netherlands